June 10, 2010

Coastal and Ocean Engineering

John Fenton

TU Wien, Institut für Wasserbau und Ingenieurhydrologie
Karlsplatz 13/E222, A-1040 Wien
fenton@kw.tuwien.ac.at

Abstract

This course introduces maritime engineering, encompassing coastal and ocean engineering. It concentrates on providing an understanding of the many processes at work when the tides, storms and waves interact with the natural and human environments. The course will be a mixture of description and theory – it is hoped that by understanding the theory that the practice will be made all the easier. There is nothing quite so practical as a good theory.

Table of Contents

References

Australia, G. (2004), Small threat, but warning sounded for tsunami research, *AusGeo News* **75**(September), 4–7.

Barber, N. F. (1969), *Water Waves*, Wykeham.

Bascom, W. (1964), *Waves and Beaches*, Doubleday.

Benjamin, T. B. & Lighthill, M. J. (1954), On cnoidal waves and bores, *Proc. Roy. Soc. London A* **224**, 448–460.

Bird, E. C. F. (1984), *Coasts: An Introduction to Coastal Geomorphology*, Australian National University Press, Canberra.

Cartwright, D. E. (1999), *Tides: A Scientific History*, second edn, Cambridge.

Dean, R. G. & Dalrymple, R. A. (1984), *Water Wave Mechanics for Engineers and Scientists*, Prentice-Hall.

Dingemans, M. W. (1997*a*), *Water wave propagation over uneven bottoms. Part 1 – Linear wave propagation*, Vol. 13 of *Advanced Series on Ocean Engineering*, World Scientific, Singapore.

Dingemans, M. W. (1997*b*), *Water wave propagation over uneven bottoms. Part 2 – Nonlinear wave propagation*, Vol. 13 of *Advanced Series on Ocean Engineering*, World Scientific, Singapore.

Fenton, J. D. (1979), A high-order cnoidal wave theory, *J. Fluid Mechanics* **94**, 129–161.
URL: *http://johndfenton.com/Papers/Fenton79-A-high-order-cnoidal-wave-theory.pdf*

Fenton, J. D. (1985), A fifth-order Stokes theory for steady waves, *J. Waterway Port Coastal and Ocean Engng* **111**, 216–234.
URL: *http://johndfenton.com/Papers/Fenton85d-A-fifth-order-Stokes-theory-for-steady-waves.pdf*

Fenton, J. D. (1988), The numerical solution of steady water wave problems, *Computers and Geosciences* **14**, 357–368.

Fenton, J. D. (1990), Nonlinear wave theories, *in* B. Le Méhauté & D. M. Hanes, eds, 'The Sea - Ocean Engineering Science, Part A', Vol. 9, Wiley, New York, pp. 3–25.
URL: *http://johndfenton.com/Papers/Fenton90b-Nonlinear-wave-theories.pdf*

Fenton, J. D. (1993), Simulating wave shoaling with boundary integral equations, *in* 'Proc. 11th Australasian Conference on Coastal and Ocean Engng, Townsville', pp. 71–76.

Fenton, J. D. (1999*a*), The cnoidal theory of water waves, *in* J. B. Herbich, ed., 'Developments in Offshore Engineering', Gulf, Houston, chapter 2, pp. 55–100.
URL: *http://johndfenton.com/Papers/Fenton99Cnoidal-The-cnoidal-theory-of-water-waves.pdf*

Fenton, J. D. (1999*b*), Numerical Methods for Nonlinear Waves, *in* P. L.-F. Liu, ed., 'Advances in Coastal and Ocean Engineering', Vol. 5, World Scientific, Singapore, pp. 241–324.

URL: *http://johndfenton.com/Papers/Fenton99Liu-Numerical-methods-for-nonlinear-waves.pdf*

Fenton, J. D. & McKee, W. D. (1990), On calculating the lengths of water waves, *Coastal Engineering* **14**, 499–513.

Gourlay, M. R. (1996), History of Coastal Engineering in Australia, *in* N. C. Kraus, ed., 'History and Heritage of Coastal Engineering', ASCE, New York.

Guo, J. (2002), Simple and explicit solution of wave dispersion equation, *Coastal Engineering* **45**, 71–74.

Hamill, R., Christian, C. D. & Fenton, J. D. (1989), Investigation of beach erosion at Mission Bay, *in* 'Proc. 9th Australasian Conference on Coastal and Ocean Engng, Adelaide', pp. 219–223.

Hedges, T. S. (1995), Regions of validity of analytical wave theories, *Proc. Inst. Civ. Engnrs, Water, Maritime and Energy* **112**, 111–114.

Herbich, J. B. (1999*a*), *Developments in Offshore Engineering: Wave Phenomena and Offshore Topics*, Gulf, Houston.

Herbich, J. B. (1999*b*), *Handbook of coastal engineering*, McGraw-Hill.

Infeld, E. & Rowlands, G. (1990), *Nonlinear waves, solitons and chaos*, Cambridge.

Kajiura, K. & Shuto, N. (1990), Tsunamis, *in* B. Le Méhauté & D. M. Hanes, eds, 'The Sea - Ocean Engineering Science, Part A', Vol. 9, Wiley, New York, pp. 395–420.

Khandekar, M. L. (1989), *Operational Analysis and Prediction of Ocean Wind Waves*, Springer.

Kinsman, B. (1984), *Wind Waves*, Dover, New York.

Kowalik, Z. & Murty, T. S. (1993), *Numerical Modeling of Ocean Dynamics*, World Scientific, Singapore.

Le Méhauté, B. (1976), *An Introduction to Hydrodynamics and Water Waves*, Springer, New York.

Le Méhauté, B. & Hanes, D. M. (1990), *The Sea - Ocean Engineering Science*, Wiley, New York.

LeBlond, P. H. & Mysak, L. A. (1978), *Waves in the Ocean*, Elsevier.

Lighthill, M. J. (1978), *Waves in Fluids*, Cambridge.

MacCamy, R. C. & Fuchs, R. A. (1954), Wave forces on piles: a diffraction theory, Technical Memorandum 69, U.S. Army Corps of Engineers, Beach Erosion Board.

Massel, S. R. (1989), *Hydrodynamics of Coastal Zones*, Elsevier, Amsterdam.

Massel, S. R. (1999), *Fluid Mechanics for Marine Ecologists*, Springer.

Nelson, R. C. (1994), Depth limited design wave heights in very flat regions, *Coastal Engineering* **23**, 43–59.

Nelson, R. C. (1997), Height limits in top down and bottom up wave environments, *Coastal Engineering* **32**, 247–254.

Nielsen, P. (1992), *Coastal Bottom Boundary Layers and Sediment Transport*, World Scientific, Singapore.

on Forces on Inclined, A. T. C. & Structures, V. W. (1995), *Wave Forces on Inclined and Vertical Wall Structures*, ASCE, New York.

Peregrine, D. H. (1972), Equations for water waves and the approximation behind them, *in* R. E. Meyer, ed., 'Waves on Beaches and Resulting Sediment Transport', Academic, New York.

Pond, S. & Pickard, G. L. (1983), *Introductory Dynamical Oceanography*, second edn, Pergamon.

Protection Manual, S. (1975), *Shore Protection Manual*, U.S. Army Coastal Engineering Research Center, Fort Belvoir, Virginia.

Rahman, M. (1995), *Water Waves : relating modern theory to advanced engineering applications*, Oxford.

Sarawagi, T. (1995), *Coastal Engineering – Waves, Beaches, Wave-Structure Interactions*, first etc edn.

Sarpkaya, T. & Isaacson, M. (1981), *Mechanics of Wave Forces on Offshore Structures*, Van Nostrand Reinhold, New York.

Schwartz, L. W. & Fenton, J. D. (1982), Strongly-nonlinear waves, *in* M. Van Dyke, J. V. Wehausen & J. L. Lumley, eds, 'Ann. Rev. Fluid Mech.', Vol. 14, Annual Reviews, Palo Alto, pp. 39–60.
URL: *http://johndfenton.com/Papers/Schwartz82-Strongly-nonlinear-waves.pdf*

Silvester, R. (1974), *Coastal Engineering*, Elsevier.

Simkin, T. & Fiske, R. S. (1983), *Krakatau 1883*, Smithsonian, Washington.

Sleath, J. F. A. (1984), *Sea Bed Mechanics*, Wiley, New York.

Sobey, R. J., Goodwin, P., Thieke, R. J. & Westberg, R. J. (1987), Application of Stokes, cnoidal, and Fourier wave theories, *J. Waterway Port Coastal and Ocean Engng* **113**, 565–587.

Sorensen, R. M. (1997), *Basic Coastal Engineering*, Chapman & Hall, New York.

Stoker, J. J. (1957), *Water Waves*, Academic.

Symons, G. J. (1888), The Eruption of Krakatoa, and Subsequent Phenomena, Report, Krakatoa Committee of the Royal Society, London.

Tricker, R. A. R. (1964), *Bores, Breakers, Waves and Wakes*, Mills and Boon.

Wantanabe, A., Isobe, M. & Kraus, N. (1999), *International Handbook Of Coastal Engineering And Management*, Academic.

Wehausen, J. V. & Laitone, E. V. (1960), Surface Waves, *in* S. Flügge, ed., 'Encyclopaedia of Fluid Mechanics', Vol. 9, Springer.
URL: *http://www.coe.berkeley.edu/SurfaceWaves/*

Wharton, W. J. L. (1888), On the seismic sea waves caused by the eruption of Krakatoa, August 26th and 27th, 1883, *in* 'Symons (1888)', pp. 89–151.

Wiegel, R. L. (1964), *Oceanographical Engineering*, Prentice-Hall.

Williams, J. M. (1981), Limiting gravity waves in water of finite depth, *Phil. Trans. Roy. Soc. London A* **302**, 139–188.

Yokoyama, I. (1981), A geophysical interpretation of the 1883 Krakatau eruption, *J. Volcanology and Geothermal Res.* **9**, 359–378.

List of useful references

Introductory and General Books

Barber (1969)	Simple and interesting
Bascom (1964)	Simple and interesting
Tricker (1964)	Simple and interesting
Gourlay (1996)	History of Australian coastal engineering
Massel (1999)	Readable wide-ranging technical book

Tides, oceanography

Cartwright (1999)	Interesting historical and scientific book on tides
Kowalik & Murty (1993)	Basic computational oceanography
Pond & Pickard (1983)	Basic mathematical oceanography

Water waves – Mathematical Aspects

Infeld & Rowlands (1990)	Interesting book from modern physics point of view
LeBlond & Mysak (1978)	Mathematical treatise on all aspects of waves in the ocean
Lighthill (1978)	Readable, insightful, some mathematics
Peregrine (1972)	Interesting chapter on long wave theories
Stoker (1957)	Interesting mathematical treatment of waves and hydraulics
Wehausen & Laitone (1960)	Classical, mathematical encyclopaedic article on waves

Water waves – Engineering Aspects

Dean & Dalrymple (1984)	Very readable and accessible
Kinsman (1984)	Readable and physical orientation
Le Méhauté (1976)	Readable engineering-orientated book
Massel (1989)	Readable introductory mathematical
Rahman (1995)	Readable application of theory to practice
Wiegel (1964)	Engineering handbook, now dated

Water waves – Computational Aspects

Dingemans (1997*a*), Dingemans (1997*b*)	Mathematical, encyclopaedic
Fenton (1999*b*)	Review article on numerical methods
Schwartz & Fenton (1982)	Dated review article

Steadily progressing waves

Benjamin & Lighthill (1954)	Interesting paper on long waves and hydraulic jumps
Fenton (1985)	Stokes theory
Fenton (1990)	Review article on steady waves
Fenton & McKee (1990)	Calculating the length of waves
Fenton (1999*a*)	Cnoidal theory for long waves
Sobey, Goodwin, Thieke & Westberg (1987)	Review of methods for steady waves

Forces on structures

on Forces on Inclined & Structures (1995)	Recent general work
Sarpkaya & Isaacson (1981)	Classical book

Maritime engineering generally

Herbich (1999*a*)	Practically-orientated handbook
Le Méhauté & Hanes (1990)	Wide-ranging handbook

Coastal engineering and geomorphology

Bird (1984)	Readable book on erosion and coastal processes
Herbich (1999*b*)	Wide-ranging practically-orientated handbook
Nielsen (1992)	Readable, on bed processes
Sarawagi (1995)	Higher level but practical book
Protection Manual (1975)	Simplistic cookbook for coastal engineering
Silvester (1974)	Encyclopaedic book on coastal engineering
Sleath (1984)	Bed processes
Sorensen (1997)	Simplistic readable handbook
Wantanabe, Isobe & Kraus (1999)	

1. Introduction

The most important liquid on Earth is water. It covers 71% of the Earth's surface. Of the Earth's total water content some 97.2% is contained in the oceans, 2.15% is stored in ice sheets and glaciers, 0.62% is groundwater, and only 0.03% is in rivers and freshwater lakes. For major parts of the Atlantic, Pacific and Indian Oceans, the average depth is about $4\,\mathrm{km}$.

1.1 Physical properties of seawater

1.1.1 Density

Water has many unique chemical and physical properties. Unlike most substances which contract when frozen, water expands, allowing ice to float on the surface. The density of pure water ρ is about $1000\,\mathrm{kg\,m^{-3}}$, being 770-890 times that of air at sea level. Pressure has an insignificant effect on the density of water for most applications, unless we consider water at great depths in the ocean. For example, at a depth of $1\,\mathrm{km}$ the density of water is only 0.5% greater than at the surface, and at the deepest point in the earth's oceans, the Marianas Trench, due to pressure effects alone water is about 6% denser than at the surface.

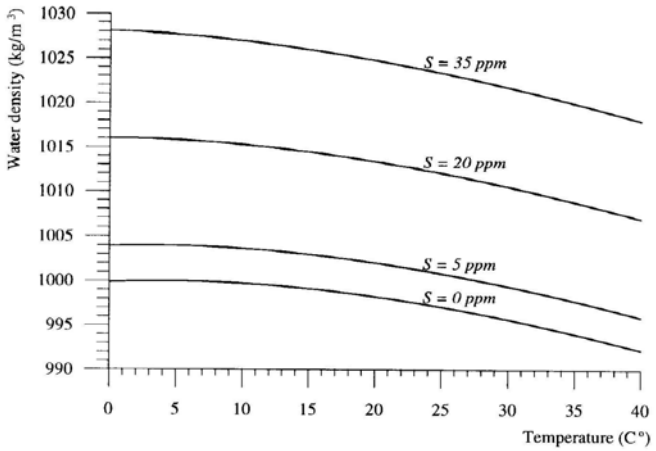

Figure 1-1. The density of fresh and sea water as a function of temperature and salinity (after Massel, 1999)

The density is much more temperature dependent, freshwater density generally decreasing as the temperature increases, with a maximum at about $4°$C. Salinity also influences water density. Away from coasts the salinity of ocean water varies from $32 - 37$ ppm. The variations in salinity result from the differences in the relative rates of precipitation and evaporation from the ocean surface. Ocean water does not show the anomalous thermal expansion of freshwater. The density decreases monotonically with increasing temperature, right from the freezing point, as shown in Figure 1-1. When temperature and pressure are constant, density of sea water increases with salinity. A difference of 1 ppm in salinity has an effect on the density of sea water which is about five times greater than the change caused by $1°$C of temperature. The large scale density structure of the ocean is dominated by variations in temperature, while salinity differences have more effect on smaller scale motions. The densest waters are formed off Greenland and in the Norwegian Sea.

The general dependence of the sea water density on salinity, temperature and pressure is called the equation of state. The expression is rather complicated.

1.1.2 Viscosity

This is a measure of the rapidity with which momentum is diffused through a fluid. The coefficient of dynamic molecular viscosity μ appears fundamentally in the equations of motion relating shear stresses to transverse velocity gradients. In resisting applied forces (such as gravity or pressure) the response of the fluid is proportional to the density ρ:

$$\text{mass} \times \text{ acceleration of fluid particle} = \text{Total net force on fluid particle},$$

so that we can show that the equation of motion looks like

$$\rho \times \text{Acceleration} = \mu \times (\text{ terms involving velocity gradients}) + \text{pressure terms} + \text{body force terms}.$$

Dividing by density ρ shows that in the fundamental equation of motion the viscosity appears in the ratio μ/ρ. This is the kinematic molecular viscosity ν:

$$\nu = \frac{\mu}{\rho}.$$

Typical values for air and water are such that $\mu_{\text{air}}/\mu_{\text{water}} = 1.8 \times 10^{-2}$. However, $\rho_{\text{air}}/\rho_{\text{water}} = 1.2 \times 10^{-3}$, and calculating the ratio of the kinematic viscosities gives:

$$\nu_{\text{air}}/\nu_{\text{water}} = 15.$$

Hence we find that in its effect on the flow patterns, air is 15 times more viscous than water!

The kinematic viscosity for sea water of salinity $S = 35$ ppm and temperature $T = 20°\text{C}$ is $1.064 \times 10^{-6}\,\text{m}^2\,\text{s}^{-1}$.

However, the viscosities of both air and water are small (compared with honey) and are such that viscous effects are usually confined to thin layers adjacent to boundaries. In the body of the flow viscosity is unimportant. In most flows of engineering significance, the effects of turbulence are much greater. Instead of single molecules, finite masses of water move through the flow, redistributing momentum, and generally tending to make flows more uniform.

In geophysical flows such as the oceans, atmosphere, and rivers, eddies and turbulent motions in the flow can be so effective in moving particles among themselves that the effects of molecular diffusion are overwhelmed. For such situations, a turbulent or eddy viscosity is used, which can be thousands of times larger than the molecular viscosity.

When we come to study wave motion, however, the underlying fluid motion is relatively small, and there is no well-developed turbulent flow structure. In this case viscosity can be ignored, which we will do throughout the rest of this course.

1.1.3 Surface tension

This is an important determinant of the exchange processes between the air and the sea, however for the purposes of this course it is not important.

2. Introduction to Oceanography

2.1 Ocean currents

Much of what we observe in the sea is wind-generated surface gravity waves, commonly called water waves, which are more or less periodic in nature. Both everyday observations and measurements provide evidence of a different type of water motion in the ocean which is not periodic – namely relatively slow ocean currents. This persistent water motion is responsible for slowly transporting large volumes of water over vast distances. The nature of flow associated with large-scale ocean currents depends on a few dominant driving mechanisms: wind stress, pressure gradients, water density gradients, and the Coriolis effect.

Numerical modelling of ocean circulation and the coupling of oceanic and atmospheric circulation modelling can mimic observed oceanic features and help in understanding and predicting the global climate system and its impact on life in the oceans. Present models do seem to encompass the major features observed in ocean circulation.

Continental shelf and coastal waters play a specific role for global ocean ecology, linking land masses with the ocean waters. Because of interactions with decreasing depths and coasts, the water circulation and associated chemistry and biology are complex.

2.1.1 Wind patterns on Earth

Local winds may be generated by local atmospheric systems which may last only a few days. However ocean currents in meso- and global scales are driven by average conditions, prevailing for months or years.

The wind field in the vicinity of the Earth's surface is driven by the interaction of pressure gradients and the Coriolis effect. In fact, due to the Coriolis effect, the steady wind field in the vicinity of large high and low pressure systems is not from the high to the low pressure, but roughly parallel to the isobars (to within $15°$). This flow is known as geostrophic flow, and is typical for much of the large-scale flow in the atmosphere. It blows with the area of high pressure on its left in the Southern Hemisphere, and the reverse in the Northern. Hence, as a high-pressure region passes from west to east over southern Australia, ahead of it the wind is from south to north – and is cooler.

Major surface wind patterns: Consider the simplest example of the relationship between wind and

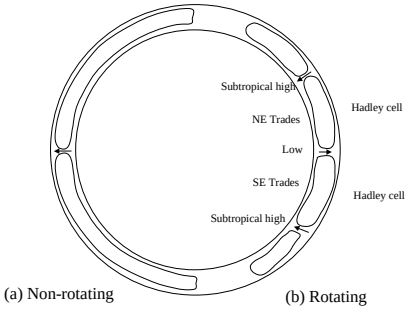

Figure 2-1. (a) Convection cell rotation on a non-rotating uniform Earth, (b) Schematic representation of the Hadley cells either side of the equator, and the resulting other cells, on a rotating earth.

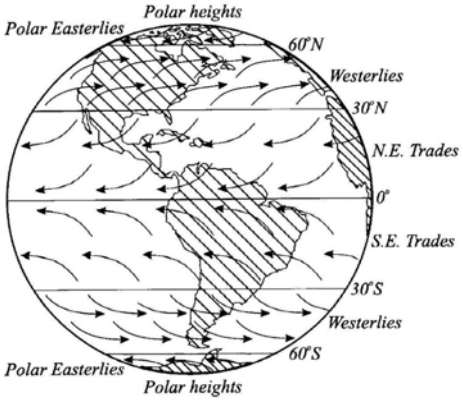

Figure 2-2. Simplified global wind patterns (from Massel, 1999)

pressure gradients, namely the sea breeze and land breeze phenomena on coasts. During the day the temperature of the land surface rises higher than that of the sea surface, resulting in a horizontal pressure gradient from the sea to the land, giving rise to a sea breeze, with a reverse flow at higher levels. In the night the reverse occurs, with a land breeze out to sea. Just as sea and land breezes are the result of horizontal pressure gradients induced by uneven temperature distributions over the land and the sea, the major planetary wind belts are induced by uneven temperature distributions between high and low latitudes, and the Earth's rotation. If the Earth did not rotate and its surface were uniform, the larger heating near the equator would result in air rising there and travelling toward the poles where it would sink again, resulting in two large circulation patterns, one in each hemisphere. Such a situation is shown in Figure 2-1(a). The rotation of the earth changes this. As the air flows towards the poles from the equator, initially it is unaffected by Coriolis acceleration. This is because it, given by $2\Omega \times u$, is of a magnitude $2\Omega_E \sin\lambda U$, where λ is the latitude (zero at the equator), Ω_E is the angular speed of the Earth, and U is the horizontal speed across the Earth's surface. Hence the Coriolis force is small near the equator. Further away, the air is deflected by the sideways Coriolis acceleration, with the net result that a large spiralling cell flow is set up, giving rise to the Trade Winds. These cells are the Hadley Cells, on both sides of the equator. A schematic representation of the global wind pattern on the Earth is given in Figure 2-2.

2.1.2 Wind-driven surface and near-surface currents

Forces driving ocean currents: Ocean currents that flow steadily for longer periods of time (months or years) are the result of the combined action of three main physical mechanisms: wind stress, pressure gradients, and the Coriolis effect. Wind also generates surface gravity waves – we will be dealing with these in depth later.

Wind stress can be represented by the expression

$$\tau_0 = C_{10}\rho_a V_{10}^2, \quad \text{where } C_{10} \text{ is the drag coefficient} \quad C_{10} \approx 0.00075 + 0.000067\, V_{10},$$

in which V_{10} is the wind speed at a height of $10\,\mathrm{m}$, and where ρ_a is the density of air. The actual speed of the ocean current is a small fraction of the wind speed, roughly 3-5%.

The pressure-gradient force is a consequence of horizontal variations in the level of the water surface and the resulting sea surface slope.

The magnitude of the horizontal component of Coriolis acceleration can be written

$$a_C = 2\Omega_E \sin\lambda\, U = fU,$$

where we have introduced f:

$$f = 2\Omega_E \sin\lambda,$$

which has units of T^{-1}, and which is called the Coriolis parameter. In many studies it is considered constant over the region of interest.

Geostrophic flow: Similar to the geostrophic flow in the atmosphere, geostrophic currents under the combined

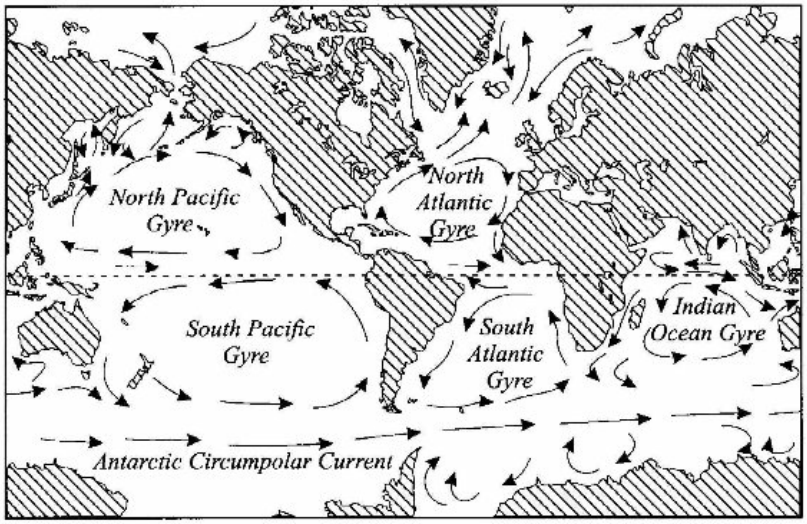

Figure 2-3. Schematic representation of the global surface current pattern (from Massel, 1999)

action of Coriolis and pressure forces generally form large gyres. In the Northern Hemisphere the Westerlies and Trade Winds cause water to flow to the centre of the ocean. This converging flow piles the water up in the ocean centre, generating a pressure gradient. When water begins to flow radially outwards, the Coriolis effect bends the current to the right. The continents interrupt the flow and deflect the westerly flow at the Equator poleward, while the easterly flow at mid latitudes is deflected equatorward, giving closed ocean gyres with clockwise rotation. In the Southern Hemisphere the flow is a mirror image, with anti-clockwise gyres. This geostrophic model of ocean currents agrees well with the observed large-scale circulation, and the geostrophic gyres are shown in Figure 2-3 as a part of the global surface water current pattern.

General patterns of wind-driven ocean circulation: The flow of currents is not uniform and varies substantially in different parts of the gyres. The strongest currents are the Gulf Stream and the Kuroshio Current. Both flow northward as narrow streams along the western edges of the Atlantic and Pacific Oceans respectively. The typical width of these currents is $50 - 75\,\mathrm{km}$ and a typical speed is $1 - 3\,\mathrm{m\,s^{-1}}$. Two main factors contribute

to an intensification of current flow along the western edge of ocean basins. Rotation of the Earth from west to east results in sea water lagging behind the rotating solid ocean bottom, which pushes water against the western side of a basin. Additionally, an equatorial drift induced by the Trade Winds piles large quantities of water against the eastern margins of continents. The resulting mound of water produces a steep poleward pressure gradient causing strong currents away from the equator.

The volume of water transported by such currents is usually measured in Sverdrup units ($1\,\mathrm{Sv} = 10^6\,\mathrm{m}^3\,\mathrm{s}^{-1}$). The Pacific equatorial current is $10 - 70\,\mathrm{Sv}$, the Gulf Stream $50 - 150\,\mathrm{Sv}$, the Antarctic Circumpolar Current $50 - 150\,\mathrm{Sv}$. In addition to such currents the eastern arms are relatively weak, being slow but wide.

On both sides of the equator the Trade Winds generate the North and South Equatorial Currents. Due to complexities of the wind between the Trade Wind belts, there is another surface eastward-flowing current known as the Equatorial Countercurrent and a subsurface eastward current, the Equatorial Undercurrent or Cromwell Current in the Pacific Ocean. Both are weak and change location with the seasons.

2.1.3 Thermohaline circulation

The wind-induced currents are limited to the uppermost levels of the ocean. Ocean waters lying beneath are in motion as well. The important causes for this motion are the differences in temperature and salinity. These affect fluid density. Vertical convection, circulation, and mixing provide the mechanisms for distribution of sea water density differences from the sea surface into the deeper ocean. The horizontal density differences generate subsurface currents known as thermohaline circulation. This is a slow process.

From the equator to approximately 50° latitude there is a surface layer of water, less than $1\,\mathrm{km}$ deep, known as the thermocline, which has temperatures ranging from 5° to 28°C. The salinity in the thermocline also varies, and is highest in the tropics. Temperature decreases with latitude and depth.

The deep and bottom water in the oceans sinks and spreads away with a time scale of years to centuries. This allows oceanographers to trace its path and determine its origin.

In general sea water is homogeneous in terms of temperature and salinity; over 75% of all ocean water has a temperature in the range of $0 - 5^\circ$C and a salinity of $34 - 35$ ppm.

2.2 El Niño, La Niña, and the Southern Oscillation

There are some very interesting and graphical websites which can be used to explore this topic, under the auspices of the US Government Agency, the National Oceanic and Atmospheric Administration:

http://www.cdc.noaa.gov/people/klaus.wolter/MEI/

http://www.pmel.noaa.gov/toga-tao/el-nino/nino-home.html

El Niño (EN) is characterized by a large scale weakening of the trade winds and warming of the surface layers in the eastern and central equatorial Pacific Ocean. El Niño events occur irregularly at intervals of 2-7 years, although the average is about once every 3-4 years. They typically last 12-18 months, and are accompanied by swings in the Southern Oscillation (SO), an interannual see-saw in tropical sea level pressure between the eastern and western hemispheres. During El Niño, unusually high atmospheric sea level pressures develop in the western tropical Pacific and Indian Ocean regions, and unusually low sea level pressures develop in the southeastern tropical Pacific. SO tendencies for unusually low pressures west of the date line and high pressures east of the date line have also been linked to periods of anomalously cold equatorial Pacific sea surface temperatures (SSTs) sometimes referred to as La Niña.

The Southern Oscillation Index (SOI), defined as the normalized difference in surface pressure between Tahiti, French Polynesia and Darwin, Australia is a measure of the strength of the trade winds, which have a component of flow from regions of high to low pressure. High SOI (large pressure difference) is associated with stronger than normal trade winds and La Niña conditions, and low SOI (smaller pressure difference) is associated with weaker than normal trade winds and El Niño conditions. The terms ENSO and ENSO cycle are used to describe the full range of variability observed in the Southern Oscillation Index, including both El Niño and La Niña events.

There has been a confusing range of uses for the terms El Niño, La Niña and ENSO by both the scientific community and the general public. Originally, the term El Niño (in reference to the Christ child) denoted a warm

southward flowing ocean current that occurred every year around Christmas time off the west coast of Peru and Ecuador. The term was later restricted to unusually strong warmings that disrupted local fish and bird populations every few years. However, as a result of the frequent association of South American coastal temperature anomalies with interannual basin scale equatorial warm events, El Niño has also become synonymous with larger scale, climatically significant, warm events. There is not, however, unanimity in the use of the term El Niño. The tendency in the scientific community though is to refer interchangeably to El Niño, ENSO warm event, or the warm phase of ENSO as those times of warm eastern and central equatorial Pacific SST anomalies. Conversely, the terms La Niña, ENSO cold event, or cold phase of ENSO are used interchangeably to describe those times of cold eastern and central equatorial Pacific SST anomalies.

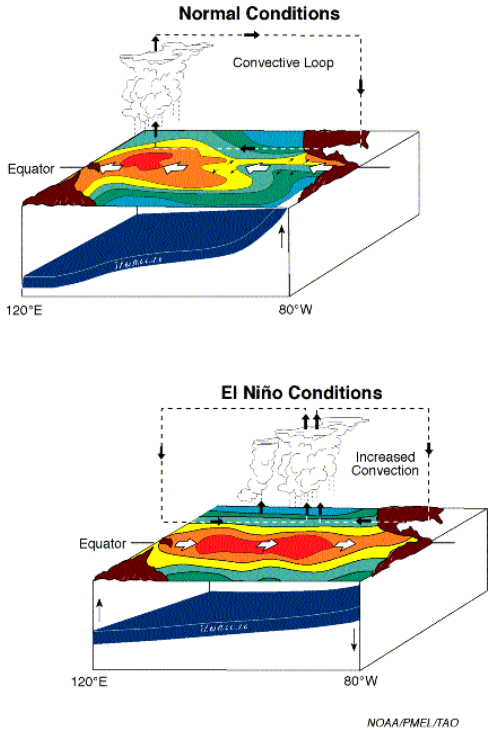

Figure 2-4. Three-dimensional view of Pacific Ocean during normal and El Niño conditions (from NOAA Website).

El Niño is a disruption of the ocean-atmosphere system in the tropical Pacific having important consequences for weather around the globe. Among these consequences are increased rainfall across the southern tier of the US and in Peru, which has caused destructive flooding, and drought in the West Pacific, sometimes associated with devastating bush fires in Australia. Observations of conditions in the tropical Pacific are considered essential for the prediction of short term (a few months to 1 year) climate variations.

In normal, non-El Niño conditions (top panel of Figure 2-4), the trade winds blow towards the west across the tropical Pacific. These winds pile up warm surface water in the west Pacific, so that the sea surface is about 1/2 meter higher at Indonesia than at Ecuador. The sea surface temperature is about $8°\mathrm{C}$ higher in the west, with cool temperatures off South America, due to an upwelling of cold water from deeper levels. This cold water is nutrient-rich, supporting high levels of primary productivity, diverse marine ecosystems, and major fisheries. Rainfall is found in rising air over the warmest water, and the east Pacific is relatively dry. The observations at $110°\mathrm{W}$ show that the cool water (below about $17°\mathrm{C}$, the black band in these plots) is within $50\,\mathrm{m}$ of the surface.

During El Niño (bottom panel of Figure 2-4), the trade winds relax in the central and western Pacific leading to a depression of the thermocline in the eastern Pacific, and an elevation of the thermocline in the west. The observations at $110°\mathrm{W}$ show, for example, that during 1982-1983 the $17°\mathrm{C}$ isotherm dropped to about $150\,\mathrm{m}$ depth. This reduced the efficiency of upwelling to cool the surface and cut off the supply of nutrient rich thermocline water to the euphotic zone. The result was a rise in sea surface temperature and a drastic decline in primary productivity, the latter of which adversely affected higher trophic levels of the food chain, including commercial fisheries in this region. The weakening of easterly tradewinds during El Niño is evident in this figure as well. Rainfall follows the warm water eastward, with associated flooding in Peru and drought in Indonesia and Australia. The eastward displacement of the atmospheric heat source overlaying the warmest water results in large changes in the

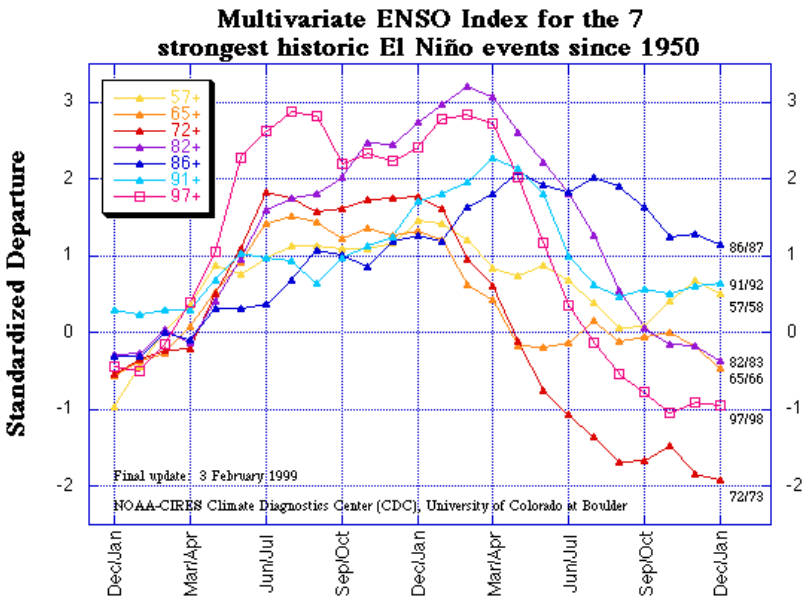

Figure 2-5. ENSO Index for strong El Niño events since 1950 brought back to a common time scale

global atmospheric circulation, which in turn force changes in weather in regions far removed from the tropical Pacific.Figure 2-5 shows a graph of a more general ENSO index for the seven strongest events since 1950. It can be seen that the strongest event was 82/83, which brought a very bad grain harvest and catastrophic bushfires to Victoria. It is interesting that the 97/98 event (shown by squares), was almost as bad, but lasted longer. Figure 2-6 shows a graph of the Index without bringing back to a common reference point. Some famous extreme years in Victoria are easily identified: the very wet year of 1956, and the drought year of 1982-3. Some noteworthy features include:

- the apparent inability of the index to linger about the mean, and
- the remarkable tendency for conditions to be El Niño since 1976!

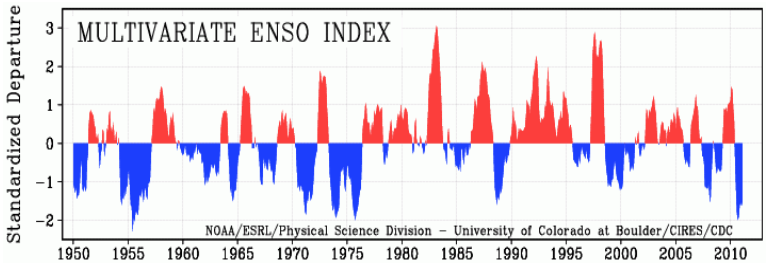

Figure 2-6. Time series of the Multivariate ENSO Index since 1950, showing El Niño events above zero, and La Niña below

2.3 Indian Ocean Dipole

The Indian Ocean Dipole (IOD) is an oceanographic phenomenon affecting climate in the Indian Ocean region. The IOD phenomenon was first identified by climate researchers in 1999. Yet evidence from fossil coral reefs demonstrates that the IOD has functioned since at least the middle of the Holocene period, 6500 years ago. It involves an aperiodic oscillation of sea-surface temperatures, between "positive", "neutral" and "negative" phases. A positive phase sees greater-than-average sea-surface temperatures and greater precipitation in the western Indian Ocean region, with a corresponding cooling of waters in the eastern Indian Ocean—which tends to cause droughts in adjacent land areas of Indonesia and Australia. The negative phase of the IOD brings about the opposite conditions, with warmer water and greater precipitation in the eastern Indian Ocean, and cooler and drier conditions in the west.

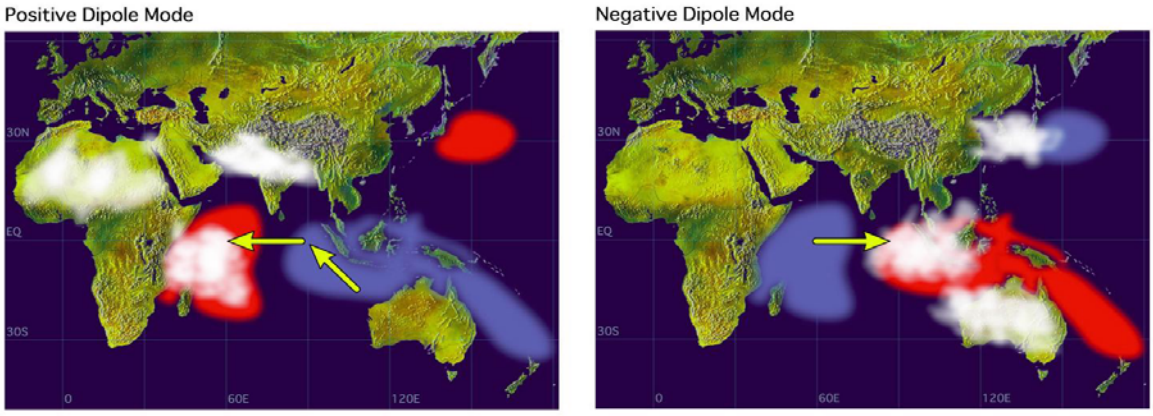

Figure 2-7. (a) Positive IOD event and (b) Negative Photographs: http://www.jamstec.go.jp/frsgc/research/d1/iod/

The IOD also affects the strength of monsoons over the Indian subcontinent. A significant positive IOD occurred in 1997-8, with another in 2006. The IOD is one aspect of the general cycle of global climate, interacting with similar phenomena like the El Niño-Southern Oscillation (ENSO) in the Pacific Ocean.

An average of four each positive/negative IOD events occur during each 30 year period with each event lasting around six months. However, there have been 12 positive IODs since 1980 and no negative events since 1992. The occurrence of consecutive positive IOD events are extremely rare with only two such events recorded, 1913–1914 and the three consecutive events from 2006-2008 which preceded the Black Saturday bushfires. Modelling indicates that consecutive positive events occur twice over a 1,000 year period. The positive IOD in 2007 evolved together with La Niña which is a very rare phenomenon that has happened only once in the available historical records (in 1967).

Effect on Australian Droughts: A 2009 study by Ummenhofer et al. at the University of New South Wales (UNSW) Climate Change Research Centre, has demonstrated a significant correlation between the IOD and drought in the southern half of Australia, in particular the south-east. Every major southern drought since 1889 has coincided with positive/neutral IOD fluctuations including the 1895-1902, 1937-1945 and the current 1995-present droughts.

The research shows that when the IOD is in its negative phase, with cool Indian Ocean water west of Australia and warm Timor Sea water to the north, winds are generated that pick up moisture from the ocean and then sweep down towards southern Australia to deliver higher rainfall. In the IOD positive phase, the pattern of ocean temperatures is reversed, weakening the winds and reducing the amount of moisture picked up and transported across Australia. The consequence is that rainfall in the south-east is well below average during periods of a positive IOD.

The study also shows that the IOD has a much more significant effect on the rainfall patterns in south-east Australia than the El Niño-Southern Oscillation (ENSO) in the Pacific Ocean.

2.4 Continental shelf flow

2.4.1 Overview of continental shelf waters

A continental shelf is an almost flat plain or terrace that borders a continent and slopes gently towards the ocean basin. The offshore boundary is the shelf break, usually at a water depth of $130-200\,\mathrm{m}$. Widths vary from a few kilometres along the Pacific Coast of the Americas, to more than $1000\,\mathrm{km}$ in the Arctic Ocean. Seaward of the break is a steeper continental slope of about 4°, continuing to a depth of about $2-3\,\mathrm{km}$ after which the ocean floor flattens with a slope of 1°, the continental rise, which may extend more than $500\,\mathrm{km}$ to depths up to $4\,\mathrm{km}$.

Continental shelves are influenced by the land and the open ocean. Rivers transport fresh water and dissolved chemical components, including nutrients and mud. These may subsequently be mixed, dispersed by winds, waves, currents, and tides. In general there is a large variety of currents with time scales ranging from seconds (turbulence, wind waves) to months and years (climatic variations). Due to the intensive mixing induced by waves and currents, there is efficient recycling of nutrients from decomposition of organic matter near the ocean floor. This is essential for plant growth and to provide abundant organic matter to support large fish stocks. Also, cold nutrient-

rich oceanic waters intrude onto the shelf, promoting productivity conditions there. Although the waters of the continental shelves compose only 10% of the ocean area, they provide 90% of the world's annual fish catch. It is interesting that Australia's rivers are relatively barren, so that our continental shelves are too. The Australian fish catch is half that of New Zealand.

The continental shelves are also the final destination for various anthropogenic materials and all types of pollutants, including sewage, heavy metals, petroleum compounds, and toxic pesticides. The efficiency of removing these waste products is dependent on the mixing and dispersion due to wave and tidal action.

2.4.2 Western boundary currents

Above we have described the major western boundary currents. The East Australian Current is one of the weakest western boundary currents. Its low volume flux is because part of the South Equatorial Current is directed to the Indian ocean through the Indonesian Outflow. The Current splits between latitudes of 14° and 18°. Near latitude 34° the current separates from the continent and tends to flow towards New Zealand. There are a number of meanders and eddies which remain, generally about three per year being generated. The speed of the current is roughly $1\,\mathrm{m\,s^{-1}}$. An important feature of this current is the Great Barrier Reef, which is a matrix of 2500 individual reefs, with a shallow lagoon adjacent to the coast.

The Agulhas Current off the South African east coast is one of the strongest in the world, with a peak speed of $2.5\,\mathrm{m\,s^{-1}}$. It has some unique features. One is that it runs against the prevailing wind direction in the Southwest Monsoon season, which results in a steepening of wind waves in the region of the current. Between Durban and Port Elizabeth the steepening of these waves produces giant waves with heights of $15 - 18\,\mathrm{m}$. Later, with wave theory, we will show how this is possible. Several ships have been lost due to these waves.

2.4.3 Eastern boundary currents and coastal upwelling

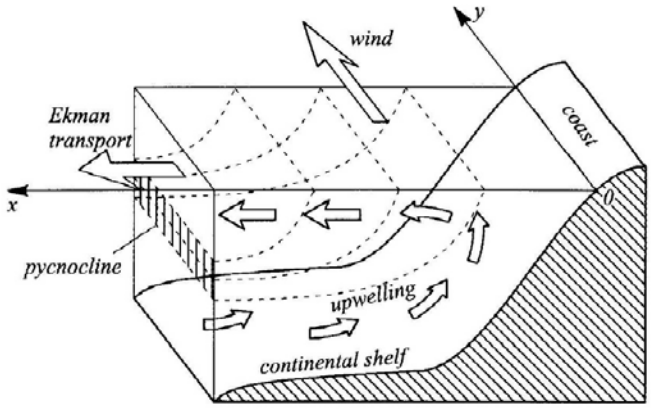

Figure 2-8. Coastal upwelling along coast in the Southern Hemisphere (after Massel, 1999)

The easterly Trade Winds of the subtropics lose their moisture by rain over land so that along eastern ocean coastlines the air is hot and dry in summer. The resulting pressure difference between land and ocean induces equatorial winds along east coasts. In an interesting theory, which we have not considered, this results in an Ekman transport directed offshore, with a lower sea surface near the coast. This is replaced by water which upwells from the deeper layers. These deeper waters are usually colder than the surface waters, richer in nutrients such as nitrates and leading to an abundance of fish. The most famous example is the coast of Peru (when not in an El Niño), with an abundant anchovy harvest. One of the most obvious manifestations of the El Niño is when the upwelling stops and the anchovy harvest fails.

3. Tides

3.1 Introduction

Tides have been observed for thousands of years. From the earliest times it has been realised that there is some connection between tides and the motion of the Moon and the Sun. However, it was only in the seventeenth and eighteenth centuries, with Newton and Laplace that theoretical explanation of the nature of tides and tidal prediction became possible.

The most important constituent in understanding tides is the gravitational attraction between the Earth, Moon, and Sun. The simplest explanation possible is the hypothetical example when the continents on the Earth are neglected and the Earth is assumed to be a perfectly smooth sphere completely covered by water. That water is acted upon by the same forces that act on the solid Earth. The prediction model from this theory is the equilibrium model of tides, as the tides from this model result from the equilibrium of gravitational forces. However, the equilibrium model cannot explain many aspects of tides, especially the varying amplitudes in many locations on the Earth. A substantial improvement in tidal prediction is achieved by considering tides in a dynamic way, as waves. In fact, tides are the longest oceanic waves with periods of the order of 12 hours. This wave approach, revised many times since Laplace's first formulation, is the dynamic model of tides.

Complexity of land boundaries on the Earth and complicated bathymetry cause great difficulties in the prediction of tides at some points on the Earth. However they can be predicted using harmonic (Fourier) analysis of a sufficiently long record of water level fluctuation.

3.2 Tide generating forces and equilibrium theory

3.2.1 The earth-moon system

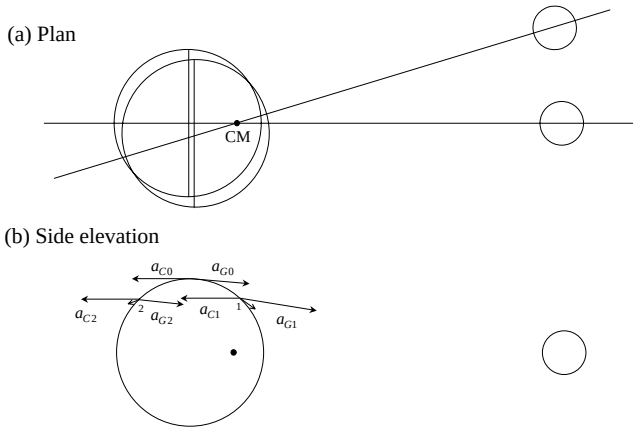

Figure 3-1. The earth-moon system, showing (a) plan, with earth revolving about CM, (b) side elevation showing accelerations on a fluid particle

The tides are a consequence of the simultaneous action of the moon's, sun's and earth's gravitational forces and the revolution of one about each other. We can ignore the earth's rotation on its own axis – even though this contributes forces, they are quite symmetric and do nothing to explain the tidal bulge with semi-diurnal tides, as we are about to do. Consider the earth-moon system in plan, as shown in (a) of Figure 3-1. It can be shown that the common centre of mass CM is actually inside the earth. Now, as the earth-moon system revolves around CM, the orientation of our non-rotating earth does not change, as suggested by the meridional line not turning. (As a guide, hold your hand out on the desk, and make the tip of your thumb perform a horizontal circle – all parts of your hand perform a circle of the same radius; now scrunch your fingertips together to make a ball and repeat the revolution, the principle is the same.) The radius of the circle in which all points move is equal to the distance from the earth's centre to CM. For all points on the earth to move in a circle of this size there is a centripetal acceleration of the same magnitude everywhere and directed parallel to the earth-moon axis toward the moon. This is provided by the moon's gravitational attraction on the centre of the earth. However this attraction is not quite uniform over the earth's surface, varying like $1/r^2$, where r is the distance from any point to the centre of the moon. It is larger

on the near side to the moon and smaller on the side away from the moon.

Now we compare the accelerations (forces per unit mass) at different locations. For a fluid particle in the supposed hemispherical shell surrounding the earth, facing the moon there is a slightly larger gravitational pull by the moon towards the moon compared with the apparent centrifugal force due to the earth's revolution about CM. At such a point 1, as in Figure 3-1(b), there is a centrifugal force a_{C1} and the slightly larger gravitational force due to the moon a_{G1} is as shown, with a resultant force with a component perpendicular to the surface of the earth and a tractive component parallel to the earth's surface. In fact the earth's gravity itself, also perpendicular to the surface, hugely dominates the perpendicular component of the resultant, and it is the tractive force which is the tide-producing force. At the point nearest the moon this tractive force is zero, as it is also at point 0 at the top of the earth in this diagram, in the vicinity of the north pole (actually $23\frac{1}{2}^\circ$ away - but for our present argument, all mention of the poles and rotation are unimportant). Between the nearest point and point 0 the tractive components force water generally equatorward. At point 0, above the centre of the earth, the centrifugal acceleration and the horizontal component of the gravitational acceleration very closely cancel, so that there is no effect there.At point 2, on the other side of the earth from point 1, we might expect there to be even less effect and for the water to be drawn from this side. However, there the centrifugal force is the same, $a_{C1} = a_{C0} = a_{C2}$, but the gravitational pull is now less ($a_{G2} < a_{G1}$) and is less than the centrifugal force. The apparent resultant force is actually away from the moon! In this case, as shown by the resultant, the tractive force is also directed away from the top, point 0. As this is slightly further from CM the effect is slightly less.

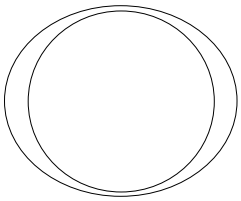

Figure 3-2. Tidal bulges

Movement of water due to these tractive forces on both sides of the earth will continue until the pressure gradient associated with the sloping water surface offsets and balances the tide-producing force. For the earth covered with water an equilibrium state would be reached in the form of an ellipsoid with its two bulges directed towards and away from the moon, as shown in Figure 3-2. These two bulges are responsible for the fact that at many points on the earth's surface, the tides are semi-diurnal, such that their period is about half a day.

The period of the earth's rotation with respect to the moon is $24\,\mathrm{h}50.47'$. This period is called a lunar day, and is the time for successive passages of the moon across a given meridian. The high tides at many locations are almost an hour later each day. However, an equilibrium tide cannot occur at low latitudes on earth. Under the equilibrium concept, two tide bulges can only maintain the same position relative to the moon when they travel around the earth at the same rate as the earth rotates with respect to the moon. Using $40\,000\,\mathrm{km}$ for the earth's circumference at the equator, the bulges' speed should be

$$C = \frac{40\,000}{24.841} = 1610\ \mathrm{km\,h^{-1}} = 447\,\mathrm{m\,s^{-1}}.$$

As the movement of the tide bulges can be considered to be the movement of a very long wave, which we will show to be given by $C = \sqrt{gh}$, where h is the water depth. Using the above value, gives the required depth to be $20.4\,\mathrm{km}$. This water depth does not occur on the earth, and the tidal bulges are unable to follow the earth's rotation. Only around Antarctica, at 60°S, where circumference is shorter and water sufficiently deep, can the semi-diurnal tides be considered as free shallow water waves. Actual tides behave differently and a more complex approach is required. However, the important conclusion follows from the equilibrium theory that the fundamental period of the tides due to the moon is $12\,\mathrm{h}25\,\mathrm{min}$.

3.2.2 The earth-sun system

The sun's mass is about 27 million times larger than the moon, but it is 387 times more distant from the earth. The net effect is that the tractive force due to the sun is about 46% of the moon. The solar-induced components of the tides are influenced by the sun's declination, varying 23.5° either side of the equatorial plane. Tide producing forces due to the sun and moon are additive. When the sun and moon are in alignment (or anti-alignment) the high

tides are higher and the low, lower. Such tides are known as spring tides (nothing to do with the season). When the sun and moon are separated by about $90°$, the tidal range is smaller than average, and the tides are neap tides. Constant changes in the declinations of the sun and the moon and cyclic variations in the position of both with respect to the earth produces tides with elementary components with largely varying periods. As many as 390 tidal components have been identified. The more important ones are shown in Table 3-1.

Species and name	Symbol	Period (hrs)	Relative size %
Semi-diurnal			
Principal lunar	M_2	12.42	100
Principal solar	S_2	12.00	47
Larger lunar elliptic	N_2	12.66	19
Luni-solar semi-diurnal	K_2	11.97	13
Diurnal			
Luni-solar diurnal	K_1	23.93	58
Principal lunar diurnal	O_1	25.82	42
Principal solar diurnal	P_1	24.07	19
Larger lunar elliptic	Q_1	26.87	8
Long period			
Lunar fortnightly	M_f	327.9	17
Lunar monthly	M_m	661.3	9
Solar semi-annual	S_{sa}	4383	8

Table 3-1. Characteristics of some of the principal tide-producing force constituents

3.3 Dynamic model of tides

A comparison of observed tides with the equilibrium tide theory developed by Newton immediately shows various discrepancies. High tide often occurs at the wrong time, with the range of the tide not properly predicted by equilibrium theory. According to equilibrium theory, semi-diurnal tidal ranges would reach their maximum value of about $10.5\,\mathrm{m}$ at equatorial latitudes, whereas observed tides have mean ranges of $0 - 1\,\mathrm{m}$.

When tides propagate into the relatively shallow waters of the continental shelf, their heights increase. At locations within bays the tidal range becomes much higher. For example, in shelf areas of the Bay of Fundy, the Bristol Channel, and the Kimberley Coast, spring tidal ranges exceed $10\,\mathrm{m}$.

The most important reasons for discrepancies between observation and prediction are:

1. The average depth of the oceans is much smaller than the depth of $20\,\mathrm{km}$ which is required to allow the tidal bulges to travel as free long waves at the equator.
2. The earth is not uniformly covered with water – the presence of continents prevents the tidal bulges from propagating around the earth, and complex ocean bathymetry complicates the nature of propagation.
3. Ocean basins have their own natural modes of oscillation, with many resonant frequencies. These interact with tidal oscillations to give a very complicated set of resonances and local amplifications. The Bay of Fundy in eastern Canada has a resonant period of about 12 hours, so it is not surprising that very large ($15\,\mathrm{m}$) semi-diurnal tidal oscillations are set up.
4. Equilibrium theory suggests that water responds immediately to the gravitational and attractive forces. Water has inertia, and satisfies a differential equation – we cannot say that force and amplitude occur simultaneously.
5. Water movement on the earth is affected by the earth's rotation, in the form of Coriolis force.

Pierre-Simon Laplace, in the late 18th century, developed the dynamic theory of tides overcoming some of these problems of the equilibrium theory, but he still postulated a spherical shell of homogeneous ocean. Gradually other people improved the theory, developing various aspects. One of the most interesting was that of Lord Kelvin, who solved the problem of tidal propagation in a rectangular bay. In this case it can be shown that the amplitude of the tidal wave decreases exponentially with increasing distance from the shore, such that surface elevation η varies like

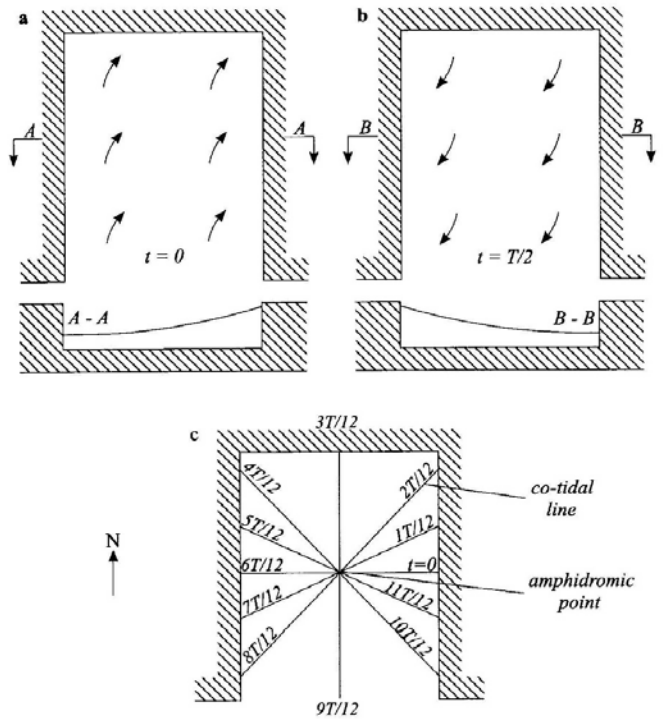

Figure 3-3. Kelvin waves in a rectangular bay in the Northern Hemisphere (from Massel, 1999). (a) Flood tide phase, (b) Ebb tide phase, (c) Total amphidromic system; arrows indicate direction of deflection due to the Coriolis effect.

$\exp(-my)$, where y is distance from the shore, and the attenuation coefficient $m = f/\sqrt{gh}$, where $f = 2\Omega_E \sin\lambda$ and h is the depth. The solution for a rectangular bay in the northern hemisphere is shown in Figure 3-3. What can be observed is the amphidromic point, which is a point at which there is no tidal motion. Around this the tidal wave circulates once per tidal period. Co-tidal lines radiate outwards from the amphidromic points, joining all points where the tide is at the same phase of the cycle. Lines which join locations of the equal tidal range are co-range lines, and they tend to form almost concentric paths about the amphidromic points. Tidal waves within amphidromic systems rotate clockwise in the Southern Hemisphere and anticlockwise in the Northern Hemisphere.

(a) In the North Sea

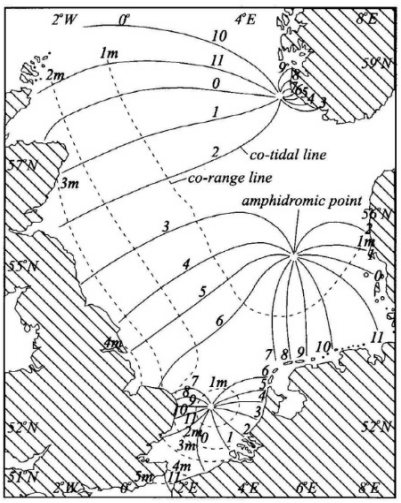

(b) In the Timor Sea

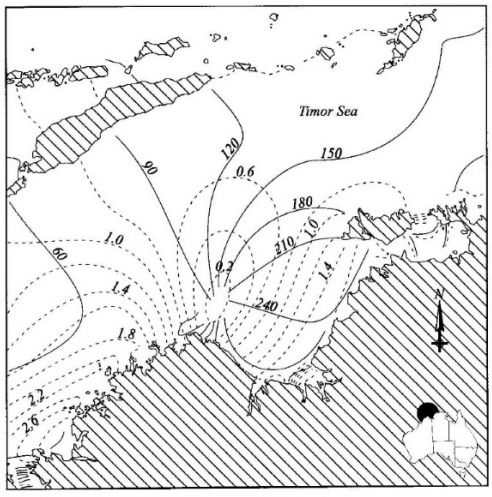

Figure 3-4. Two amphidromic systems (after Massel, 1999)

In a real situation on the rotating earth, the amphidromic systems are much more complicated. Possibly the best-known tides are those in the North Sea (Figure 3-3a), which is a rather shallow sea where frictional effects are

significant. As a result the amphidromic points move away from the source of the tidal energy, which approaches from the Atlantic Ocean from the north and moves anti-clockwise around the basin. The east coast of Britain has high tides because the amphidromic points are shifted to the east, and so the eastern parts of the North Sea experience smaller tides.

Figure 3-3b shows an amphidromic system in the Timor Sea. Further south, in the vicinity of Broome, some very large tides are experienced.

3.4 Harmonic analysis and prediction of tides

Form number: A practical classification of the nature of the tide at a particular point can be characterised by the form number F which is the ratio of the sum of the amplitudes of the major constituents, expressing how relatively important the diurnal contributions are:

$$F = \frac{O_1 + K_1}{M_2 + S_2},$$

where O_1 is the principal lunar diurnal constituent, K_1 is the lunar-solar constituent, M_2 is the principal lunar semi-diurnal constituent, and S_2 is the principal solar semi-diurnal constituent. Tides can be divided roughly as:

$$\begin{aligned} F &= 0 - 0.25 \quad \text{semi-diurnal} \\ F &= 0.25 - 1.5 \quad \text{mixed, predominantly semi-diurnal} \\ F &= 1.50 - 3 \quad \text{mixed, predominantly diurnal} \\ F &> 3 \quad \text{diurnal} \end{aligned}$$

For tides around Mackay, the amplitudes are: $K_1 = 0.390\,\mathrm{m}$, $O_1 = 0.196\,\mathrm{m}$, $M_2 = 1.668\,\mathrm{m}$, and $S_2 = 0.612\,\mathrm{m}$, giving $F = 0.26$, thus just about semi-diurnal. Other types of tides are shown in Figure 3-5.

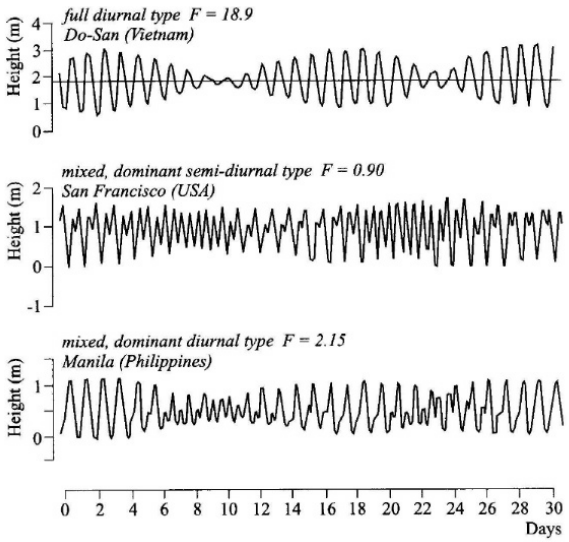

Figure 3-5. Example of various types of tides with different values of form number F (after Massel, 1999)

Prediction of tides: Sophisticated numerical models have been developed to predict tides around the earth, based on the Laplace tidal equations, augmented by the energy dissipation due to bottom friction, especially over shelf areas. These have a root-mean-square error of $3\,\mathrm{cm}$ in the deep ocean, and $10.5\,\mathrm{cm}$ in coastal waters. This is not really good enough for practical use. Still, much use is made of observations of tides at the desired locations for very long periods of time. The tide can be predicted at later times by harmonic analysis, taking the data, extracting out the Fourier components of the main constituents, some of which we saw in Table 3-1. This means that the tide

can be represented by a finite trigonometric series:

$$\eta(t) = \sum_{n=1}^{N} c_n \cos(\omega_n t + \phi_n), \tag{3.1}$$

where the c_n are the Fourier coefficients, ω_n are the radian frequencies, $\omega_n = 2\pi/T_n$, where T_n is the period of the nth contribution, and ϕ_n is a phase shift.

The word harmonic in this context usually means constituent frequencies which are actually fractions of the main. In fact, the way in which components are calculated is by using discrete Fourier transforms of a time series. We will show below how this can be done.

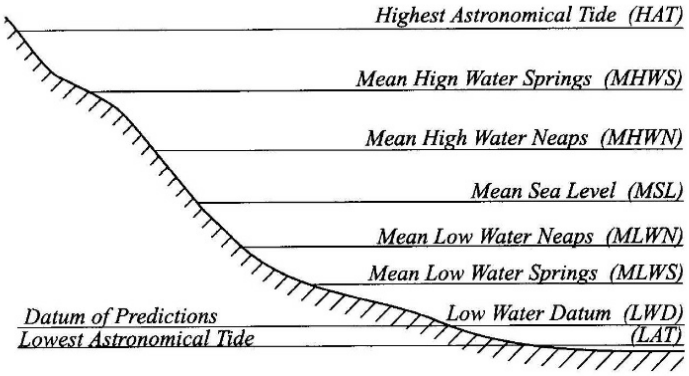

Figure 3-6. Definitions of characteristic tide levels (after Massel, 1999)

Tidal tables:A variety of tide tables, in books or in electronic form, are available for many locations. Often the highest and lowest values for each day are shown. Also, for some locations the most important characteristic water levels are given, such as those shown in Figure 3-6.

Predicted water levels sometimes differ from the observed levels, caused by strong or prolonged winds or by unusually high or low barometric pressure. Coastal currents may also interact with topography and produce local gradients on the sea surface.

In the coastal zone, in estuaries, salt marshes, and mangrove swamps, the development of ecosystems is strongly influenced by the changes of tidal levels and the rhythms they impose in terms of submersion and exposure to the air, resulting temperature and salinity changes, sediment movements, and nutrient fluxes.

4. Surface gravity waves

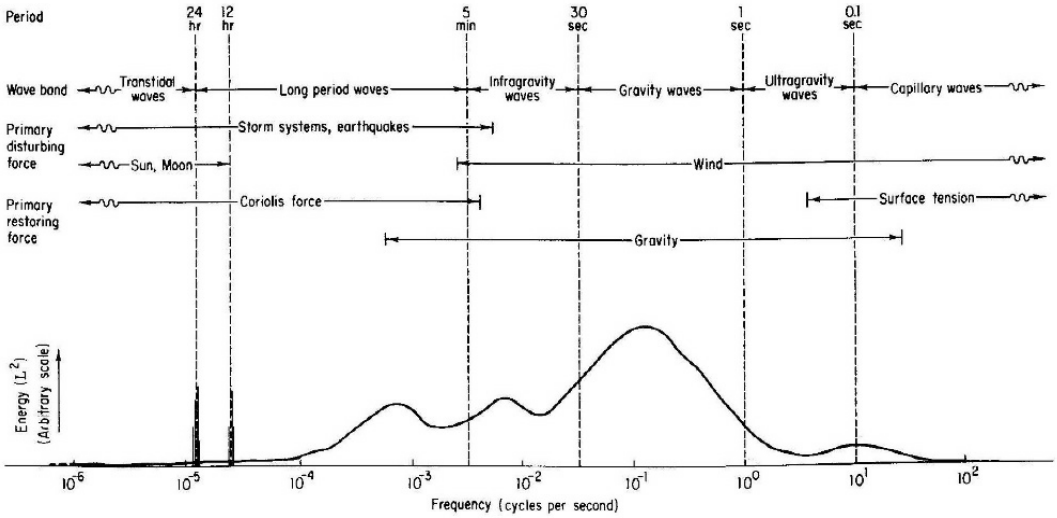

Figure 4-1. Schematic (and fanciful) representation of the energy contained in the surface waves of the ocean – *i.e.* a guess at the power spectrum (after Kinsman, 1984)

Coastal and ocean engineering are primarily concerned with the effects of surface gravity waves, usually generated by wind, where the restoring force is that of the earth's gravity. These waves are of relatively short period, are energetic, and are responsible for most effects of the sea on the coastline and on engineering structures in or beside it. Figure 4-1 shows a representation of the spectrum of gravity waves in the sea. It can be seen that the spectral peak is in the vicinity of waves with a 10 s period, typical waves generated by wind after it has blown over a long fetch. Table 4-1 shows the names of various gravity wave motions, their cause, and a range of typical periods.

Phenomenon	Cause	Period
Wind wave (sea state)	Wind shear	< 15 s
Swell wave (swell state)	Wind wave	< 30 s
Surf beat	Wave group	$1 - 5$ min
Seiche	Wind variation	$2 - 40$ min
Harbour resonance	Surf beat, tsunami	$2 - 40$ min
Tsunami	Earthquake	$5 - 60$ min
Tide	Gravitational attraction	≈ 12 or 24 h
Storm surge	Wind stress and atmospheric pressure variation	$1 - 30$ d

Table 4-1. Gravity waves, their causes and periods

In the wind-generated gravity wave range, two types of wave are generally distinguished:

Wind waves: when the waves are being worked on by the wind that raised them. They are relatively short and steep with short crest lengths. One would expect to have a relationship between the wind speed and the wave height and length.

Swell waves: when the waves have escaped the influence of the generating wind, and wind waves have interacted and coalesced to form higher but longer waves with long crests.

4.1 The equations of fluid mechanics

Now we will consider the mechanics of surface gravity waves in detail. Unlike other areas in hydraulics, where we can often consider the pipe or stream to be essentially one-dimensional, here we have to consider the full unsteady three-dimensional equations of fluid mechanics. The major approximation will be that viscosity can be ignored, which is a very good one for most wave studies. We will find that we can obtain a rather simple formulation –

that was the basis for fluid mechanics in the nineteenth century, until Reynolds and Prandtl opened the way for the treatment of viscosity and turbulence.

4.1.1 Acceleration of a fluid particle and Material derivatives

Consider an elemental parcel of fluid with velocity vector $\mathbf{u}$. At a fixed point in space the acceleration is $\partial\mathbf{u}/\partial t$. However, even in a steady flow field fluid, particles experience acceleration by moving to a position where $\mathbf{u}$ has a different value, as we now show.

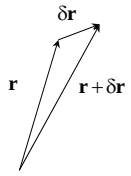

If a fluid element at $\mathbf{r}$ at time t moves to $\mathbf{r}+\delta\mathbf{r}$ at time $t+\delta t$, we can write the Taylor expansion for the velocity at the new point:

$$\mathbf{u}(\mathbf{r}+\delta\mathbf{r},t+\delta t)=\mathbf{u}(\mathbf{r},t)+\delta t\frac{\partial\mathbf{u}}{\partial t}+\delta x\frac{\partial\mathbf{u}}{\partial x}+\delta y\frac{\partial\mathbf{u}}{\partial y}++\delta z\frac{\partial\mathbf{u}}{\partial z}+\text{higher order terms},$$

which we can write as the

$$\mathbf{u}(\mathbf{r}+\delta\mathbf{r},t+\delta t)=\mathbf{u}(\mathbf{r},t)+\delta t\frac{\partial\mathbf{u}}{\partial t}+(\delta\mathbf{r}\cdot\nabla)\,\mathbf{u}(\mathbf{r},t)+\text{higher order terms}, \tag{4.1}$$

where ∇ is the vector gradient operator, which is a vector with direction and magnitude that of the greatest rate of change.

Revision: Vector gradient

The gradient of a scalar function ϕ is the vector which has as components its partial derivatives:

$$\nabla\phi=\frac{\partial\phi}{\partial x}\,\mathbf{i}+\frac{\partial\phi}{\partial y}\,\mathbf{j}+\frac{\partial\phi}{\partial z}\,\mathbf{k}.$$

Written as above, ∇ can be interpreted as a vector differential operator:

$$\nabla=\mathbf{i}\frac{\partial}{\partial x}+\mathbf{j}\,\frac{\partial}{\partial y}+\mathbf{k}\,\frac{\partial}{\partial z}.$$

It has some important properties:

- The gradient vector gives both the magnitude and direction of the maximum rate of change of the scalar at a point.

- The gradient vector is perpendicular to the level surface passing through that point.

- The directional derivative of ϕ with respect to a co-ordinate s in a direction given by a unit vector $\hat{\mathbf{s}}$ is

$$\frac{d\phi}{ds}=\nabla\phi\cdot\hat{\mathbf{s}}.$$

From (4.1), our expression for the acceleration $\mathbf{a}$ of the fluid particle:

$$\begin{aligned}\mathbf{a} &= \lim_{\delta t\to 0}\frac{\mathbf{u}(\mathbf{r}+\delta\mathbf{r},t+\delta t)-\mathbf{u}(\mathbf{r},t)}{\delta t}\\ &= \frac{\partial\mathbf{u}}{\partial t}+\lim_{\delta t\to 0}\left(\frac{\delta\mathbf{r}}{\delta t}\cdot\nabla\right)\mathbf{u}\\ &= \frac{\partial\mathbf{u}}{\partial t}+(\mathbf{u}\cdot\nabla)\,\mathbf{u}.\end{aligned}$$

Usually the brackets in the last term are omitted, and this derivative written D/Dt:

$$\frac{D\mathbf{u}}{Dt} = \frac{\partial \mathbf{u}}{\partial t} + \mathbf{u} \cdot \nabla \mathbf{u}, \tag{4.2}$$

the material or total derivative with respect to time, the rate of change experienced by a fluid particle. The first term is the temporal acceleration, which is zero in steady flow, while the second is the advective acceleration, which exists because the particle moves to a point where the velocity is different. We can obtain similar expressions for the material derivative of any other dynamical or physical point quantity.

Example: consider the difference in temperature gradient experienced by a car sitting in a car park ($\partial T/\partial t$) and one experienced while driving to a nearby mountain range, where one is also travelling at a finite velocity ($\mathbf{u}$) through a medium where the temperature might be changing with position ($\partial T/\partial x$) – the net result is an apparent extra rate of change at the car of $u\,\partial T/\partial x$. Also, of course, there is the vertical rate of rise of the car (w) through the (rather larger) vertical gradient ($\partial T/\partial z$), and possibly a North-South component $v\,\partial T/\partial y$. The total apparent rate of change at the car is

$$\frac{DT}{Dt} = \frac{\partial T}{\partial t} + u\frac{\partial T}{\partial x} + v\frac{\partial T}{\partial y} + w\frac{\partial T}{\partial z}.$$

The best way of writing this conveniently is to show it as

$$\frac{DT}{Dt} = \frac{\partial T}{\partial t} + (u,v,w) \cdot \left(\frac{\partial T}{\partial x}, \frac{\partial T}{\partial y}, \frac{\partial T}{\partial z}\right) = \frac{\partial T}{\partial t} + \mathbf{u} \cdot \nabla T.$$

In a smilar way, replacing T by the velocity vector $\mathbf{u}$, we obtain equation (4.2).

4.1.2 Forces acting on a fluid

Two types of forces act on a fluid particle:

Body forces: The force penetrates the interior of the fluid, such as gravity or apparent forces such as Coriolis or centrifugal forces. Usually they are proportional to the mass of the fluid element, and the force on a small volume element δV is $\mathbf{G}\rho\delta V$, where $\mathbf{G}$ is the force per unit mass.

Gravity force: In a gravity field, where we will adopt the convention in this course that z is the vertical co-ordinate, upwards positive, we obtain $\mathbf{G} = (0, 0, -9.8)$.

Coriolis force: On large scales such as those governing the motion of ocean currents and tides, the effects of the rotation of the earth must be considered, however here we will neglect such terms.

Short-range forces: These often have a molecular origin, due to momentum transfer by molecules across an interface. They are usually proportional to surface area. There are two kinds, pressure forces and shear forces, and they have the same molecular background, but it is convenient to treat them separately, as they have very different magnitudes.

Pressure forces: The force per unit area normal to the surface of a fluid element.

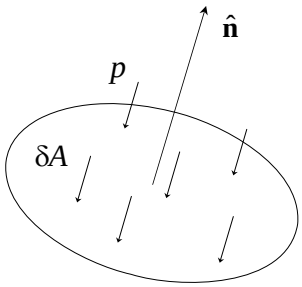

Let $\hat{\mathbf{n}}$ be a unit vector normal to the surface as shown, directed out of the fluid, then the force on the fluid element is

$$\delta\mathbf{F} = -p\,\delta A\,\hat{\mathbf{n}},$$

where p is the pressure. This is a surface force only. Note that it is a force of magnitude $p\delta A$ with direction

given by a unit vector with direction $-\hat{\mathbf{n}}$, that is from the rest of the fluid onto the surface of the element being considered.

Shear forces: The relative motion of real fluids is accompanied by tangential stresses over a surface due to molecular interchange. We cannot observe the molecular motion, but the capability of the fluid to sustain a shearing stress is measurable. This phenomenon is viscosity. We can show that this is small for geophysical applications. In fact it is proportional to $1/R$, where R is the Reynolds number of the flow:

$$\text{Relative importance of viscosity} = \frac{1}{R} = \frac{\nu}{\text{Length scale} \times \text{Velocity scale}},$$

and so for a typical coastal engineering flow situation, say with a velocity scale of $1\,\mathrm{m\,s^{-1}}$ and a length scale of $2\,\mathrm{m}$ we find this ratio to be about 0.5×10^{-6}, and so we can ignore the effects of viscosity.

4.1.3 The momentum equation for an inviscid fluid

Now we consider the motion of a small element of fluid of volume δV. Equating force and the mass of the element times its acceleration, we have

$$\rho \frac{D\mathbf{u}}{Dt}\,\delta V = \rho\,\delta V\,\mathbf{G} - \int_A p\,\hat{\mathbf{n}}\,dA, \tag{4.3}$$

where we have integrated the pressure contributions over A, the entire surface area of the element, even though it is considered elemental. To evaluate this latter term, we make use of a generalised form of Gauss' divergence theorem.

Revision: Gauss' divergence theorem: This fundamental relation was first discovered by Archimedes, relating the surface integral of pressure to a volume integral! It can be stated, for a vector F:

$$\int_V \nabla \cdot\ \mathbf{F}\,dV = \int_A \mathbf{F}\cdot\hat{\mathbf{n}}\,dA,$$

which is Gauss' Divergence Theorem. It is possible to generalise this result, to give, for F or a scalar ϕ:

$$\int_V \nabla \begin{bmatrix} \cdot\mathbf{F} \\ \phi \\ \times\mathbf{G} \end{bmatrix} dV = \int_A \hat{\mathbf{n}} \begin{bmatrix} \cdot\mathbf{F} \\ \phi \\ \times\mathbf{G} \end{bmatrix} dA.$$

Thus we have three connections between volume and surface integrals, for different ∇ operations.

It makes evaluating our integral in equation (4.3) much easier, for instead of having to integrate the complicated surface area integral we can simply replace it by the volume integral of the pressure gradient! We obtain

$$\rho \frac{D\mathbf{u}}{Dt}\,\delta V = \rho\,\delta V\,\mathbf{G} - \int_{\delta V} \nabla p\,dV,$$

and as we are considering an elemental volume we can consider ∇p to be constant throughout, and so we obtain, after dividing through by $\rho\delta V$,

$$\frac{D\mathbf{u}}{Dt} = \mathbf{G} - \frac{1}{\rho}\nabla p, \tag{4.4}$$

which is Euler's equation for the motion of a fluid. It is essentially a conservation of momentum equation. It states that the acceleration of a fluid particle is equal to the body force per unit mass (gravity, Coriolis) plus a contribution from the pressure gradient. If we write out the term for the acceleration in terms of temporal and space derivatives from equation (4.2) we obtain

$$\frac{D\mathbf{u}}{Dt} = \frac{\partial\mathbf{u}}{\partial t} + \mathbf{u}\cdot\nabla\mathbf{u} = \mathbf{G} - \frac{1}{\rho}\nabla p.$$

This is a vector equation which is actually three separate scalar equations in the four dependent variables u, v, w and p. Consider, for example,the x-component:

$$\frac{\partial u}{\partial t} + u\frac{\partial u}{\partial x} + v\frac{\partial u}{\partial y} + w\frac{\partial u}{\partial z} = G_x - \frac{1}{\rho}\frac{\partial p}{\partial x},$$

where G_x is the x component of the body force. In this expanded form the equations start to look complicated.

Their underlying nature is simple.

Hydrostatic pressure distribution: Consider the case where the fluid is at rest, $Du/Dt = 0$. Equation (4.4) becomes

$$\nabla p = \rho \mathbf{G},$$

and as Coriolis force is zero ($u = 0$ here), and consider only gravity, $G = (0, 0, -g)$, where g is gravitational acceleration, the components are

$$\frac{\partial p}{\partial x} = 0, \quad \frac{\partial p}{\partial y} = 0, \quad \frac{\partial p}{\partial z} = -\rho g,$$

with solutions

$$p + \rho g z = C,$$

the hydrostatic pressure distribution, where C is a constant, and which shows that pressure is independent of x and y (constant on a plane of constant elevation) and its variation in the vertical is as shown.

4.1.4 Mass conservation equation

We have already seen that with the momentum conservation equation we have three equations in four unknowns. We need another, and we use the mass conservation equation. If we consider a finite stationary control volume in space, through which fluid flows, then the rate of change of mass inside the volume must be equal to the net rate of change of mass crossing the control surface, as no mass is being created in the volume.

$$\begin{aligned} \text{Rate of change of mass inside the control volume} &= \frac{d}{dt}\int_V \rho \, dV \\ &= \int_V \frac{\partial \rho}{\partial t} \, dV, \end{aligned}$$

as the volume is not changing with time. Now we calculate the mass crossing the control surface S enclosing V. If we consider a small plane element of the surface dA, through which the fluid has a velocity u, then the component of velocity tangential to the element carries no mass in or out. The only contribution is from the velocity normal to the surface, which is $u \cdot \hat{n}$, where $\hat{n}$ is a unit normal directed outwards from ("leaving") the control surface. So (in the spirit of $Q = UA$), the volume flow rate entering via the element is $-u \cdot \hat{n} \, dA$. Multiplying by the fluid density there gives the mass rate entering, and integrating over the whole surface gives

$$\text{Rate at which mass is entering the control volume} = -\int_A \rho \mathbf{u} \cdot \hat{\mathbf{n}} \, dA.$$

Equating the two contributions, we have

$$\begin{aligned} \int_V \frac{\partial \rho}{\partial t} \, dV &= -\int_A \rho \mathbf{u} \cdot \hat{\mathbf{n}} \, dA \\ &= -\int_V \nabla \cdot (\rho \mathbf{u}) \, dV, \quad \text{from Gauss' divergence theorem.} \end{aligned}$$

Bringing both terms to the left and writing as a single integral,

$$\int_V \left(\frac{\partial \rho}{\partial t} + \nabla \cdot (\rho \mathbf{u}) \right) dV = 0,$$

and as this holds for any control volume, the only way that this can be satisfied is if the integrand everywhere is zero, that is,

$$\frac{\partial \rho}{\partial t} + \nabla \cdot (\rho \mathbf{u}) = 0.$$

This is the mass-conservation equation. It can be written in another form by expanding the divergence operator

and re-grouping (Ex. Do this) to give:

$$\frac{D\rho}{Dt} + \rho\nabla\cdot\mathbf{u} = 0.$$

Either form is useful. Each is a partial differential equation in 4 dependent variables, u and ρ. Each immediately demonstrates the result that if the fluid is incompressible, such that ρ is constant, the governing equation is

$$\nabla\cdot\mathbf{u} = \frac{\partial u}{\partial x} + \frac{\partial v}{\partial y} + \frac{\partial w}{\partial z} = 0. \qquad \text{(Mass conservation equation)}$$

It can be shown, by considering a finite material element of volume V that in the limit $V \to 0$ we obtain:

$$\begin{aligned}\nabla\cdot\mathbf{u} &= \lim_{V\to 0}\frac{1}{V}\frac{dV}{dt} = \text{the fractional rate of change of volume of a material element,}\\ &= 0 \quad \text{if the fluid is incompressible.}\end{aligned}$$

That is, the rate of change of volume of an elemental material volume is zero for incompressible flow, as we would expect.

Now, the incompressible mass conservation equation is a partial differential equation in three variables (u, v, w) while Euler's equation (4.4) is three equations in the same variables plus pressure p, so that we now have 4 partial differential equations in 4 unknowns, and provided we have boundary and initial conditions we could solve them numerically, probably stepping forwards in time. However, (4.4) is a nonlinear equation, which makes theoretical solutions difficult. We will find later that there is an astonishing step by which we can obtain theoretical solutions, which is the basis of much coastal and ocean engineering. (Note that if the fluid is compressible we have another variable ρ and it is necessary to introduce an equation of state giving ρ as a function of pressure p.)

4.1.5 The moment of momentum equation and vorticity

Revision: Curl of a vector

The vector or cross product gives the combined vectorial effect of two vectors a and b, written $a\times b$ and is a vector normal to the plane containing a and b, of magnitude equal to the area of the parallelogram defined by a and b. It can be evaluated using the 3×3 determinant

$$\mathbf{a}\times\mathbf{b} = (\mathbf{i}\,a_1 + \mathbf{j}\,a_2 + \mathbf{k}\,a_3)\times(\mathbf{i}\,b_1 + \mathbf{j}\,b_2 + \mathbf{k}\,b_3) = \begin{vmatrix} \mathbf{i} & \mathbf{j} & \mathbf{k} \\ a_1 & a_2 & a_3 \\ b_1 & b_2 & b_3 \end{vmatrix}.$$

The curl of a vector is when the first vector is the gradient operator; if the second is velocity $\mathbf{u}$*, the result is the vorticity, which is a vector which is equal to twice the angular velocity:*

$$\boldsymbol{\omega} = \nabla\times\mathbf{u} = \left(\mathbf{i}\frac{\partial}{\partial x} + \mathbf{j}\frac{\partial}{\partial y} + \mathbf{k}\frac{\partial}{\partial z}\right)\times(\mathbf{i}\,u + \mathbf{j}\,v + \mathbf{k}\,w) = \begin{vmatrix} \mathbf{i} & \mathbf{j} & \mathbf{k} \\ \partial/\partial x & \partial/\partial y & \partial/\partial z \\ u & v & w \end{vmatrix}.$$

In studying the motion of gravity waves and the forces exerted by them we have to solve the entire field of flow, so that we can extract velocities and pressures at all points in the water at all times. We have previously obtained the equation of motion (4.4) for any fluid particle:

$$\frac{D\mathbf{u}}{Dt} = \frac{\partial\mathbf{u}}{\partial t} + \mathbf{u}\cdot\nabla\mathbf{u} = \mathbf{G} - \frac{1}{\rho}\nabla p,$$

which is Euler's equation. We use the identity

$$\mathbf{u}\cdot\nabla\mathbf{u} = \frac{1}{2}\nabla(\mathbf{u}\cdot\mathbf{u}) - \mathbf{u}\times\boldsymbol{\omega},$$

where $\boldsymbol{\omega} = \nabla\times\mathbf{u}$ is the vorticity (twice the angular velocity). Hence Euler's equation becomes

$$\frac{\partial\mathbf{u}}{\partial t} - \mathbf{u}\times\boldsymbol{\omega} = \mathbf{G} - \nabla\left(\frac{p}{\rho} + \frac{1}{2}|\mathbf{u}|^2\right). \qquad (4.5)$$

Now we take the curl ($\nabla\times\ldots$) of the equation. If G is a conservative field (such as gravity, when $G = (0, 0, -g)$), then $\nabla\times G$ is zero. Also, the curl of the gradient operator involving the pressure and "kinetic" term disappears

($\nabla \times \nabla\phi = 0$ for any ϕ), leaving

$$\frac{\partial \boldsymbol{\omega}}{\partial t} - \nabla \times (\mathbf{u} \times \boldsymbol{\omega}) = 0.$$

By manipulation of the vector quantities and using the fact that as $\nabla \cdot \mathbf{u} = 0$ so $\nabla \cdot \boldsymbol{\omega} = 0$:

$$\frac{D\boldsymbol{\omega}}{Dt} = \boldsymbol{\omega} \cdot \nabla \mathbf{u}. \tag{4.6}$$

This is the vorticity equation for an incompressible inviscid fluid in the presence of conservative body forces. The pressure has been eliminated, giving one less unknown, but increasing the order of differentiation involved. It shows how conservation of angular momentum is a very useful concept in fluid mechanics. Note that pressure does not act to change the angular velocity. Viscosity would have, if we had retained it.

4.1.6 Irrotational flow

Now we consider a fluid flow in which initially the vorticity is zero, $\boldsymbol{\omega} = \mathbf{0}$, (the flow is said to be irrotational) such as would be encountered in the sea if it were initially relatively quiescent. This means that the angular momentum (velocity) of every particle is initially zero. Substituting into the right side of equation (4.6) our equation of motion then becomes

$$\frac{D\boldsymbol{\omega}}{Dt} = \mathbf{0},$$

which says that the rate of change of angular velocity/momentum of the fluid particle is zero, and so it is at all times thereafter! Hence we have

$$\boldsymbol{\omega} = \mathbf{0}, \quad \text{or,} \quad \nabla \times \mathbf{u} = \mathbf{0}, \tag{4.7}$$

and we have reduced the equation of motion to a simple linear equation (actually with three components)!

There is a vector identity which states that the curl of the gradient of any scalar quantity is zero: $\nabla \times \nabla\phi = 0$ for any ϕ, and so the equation of motion is satisfied if there is a velocity potential ϕ such that the velocity vector at any point is given by the gradient of ϕ, $\mathbf{u} = \nabla\phi$:

> *If an inviscid incompressible fluid flow is initially irrotational, then the dynamical equation of motion is satisfied if there is a velocity potential ϕ such that $\mathbf{u} = \nabla\phi$, or, $u = \partial\phi/\partial x$, $v = \partial\phi/\partial y$, $w = \partial\phi/\partial z$.*

We have reduced the complicated nonlinear unsteady partial differential equation to merely the existence of a scalar potential function!

4.1.7 Mass conservation equation

We have already seen that if a fluid is incompressible, the equation of mass conservation is $\nabla \cdot \mathbf{u} = 0$.

4.1.8 The field equation

Substituting $\mathbf{u} = \nabla\phi$ into $\nabla \cdot \mathbf{u} = 0$ we obtain the field equation satisfying both momentum and mass conservation:

$$\nabla \cdot \nabla\phi = \nabla^2\phi = \frac{\partial^2\phi}{\partial x^2} + \frac{\partial^2\phi}{\partial y^2} + \frac{\partial^2\phi}{\partial z^2} = 0 \quad \text{throughout the fluid.} \qquad (\text{Laplace's equation})$$

This is Laplace's equation, which is an elliptic partial differential equation. It is at the heart of almost all gravity wave theory. It is the same sort of equation which governs the equilibrium temperature distribution in a heat-conducting solid, or the charge distribution in an electrically conducting medium. It has to be solved subject to boundary conditions, which we will include.

4.1.9 The pressure equation or unsteady Bernoulli equation

It is helpful to go back to the linear momentum equation and obtain an expression for fluid pressure at any point. Consider equation (4.5), written for an irrotational fluid $\omega = 0$:

$$\frac{\partial \mathbf{u}}{\partial t} = \mathbf{G} - \nabla\left(\frac{p}{\rho} + \frac{1}{2}|\mathbf{u}|^2\right).$$

Now as $\mathbf{u} = \nabla\phi$, and in the case of a gravitational field $G = (0, 0, -g)$ we can write $G = \nabla(-gz)$, where the gravitational potential is $-gz$. Re-arranging the terms, and interchanging the order of differentiation between ∇ and $\partial/\partial t$, we obtain the equation

$$\nabla\left(\frac{\partial\phi}{\partial t} + \frac{p}{\rho} + \frac{1}{2}|\mathbf{u}|^2 + gz\right) = 0.$$

This states that throughout the fluid the space derivatives of the quantity inside the brackets are all zero, i.e. it is not a function of space at all. Hence we can write

$$\frac{\partial\phi}{\partial t} + \frac{p}{\rho} + \frac{1}{2}|\nabla\phi|^2 + gz = C(t) \quad \text{throughout the fluid,} \qquad (\text{Pressure equation})$$

where $C(t)$ is a function only of time. This is the pressure equation, or the unsteady Bernoulli equation, and we can use this to determine the pressure at any point in the fluid once we have solved to give $\phi(x, y, z, t)$. Note that $C(t)$ is arbitrary and we often set it to zero, as we can redefine ϕ by adding a function of time to it such that $C = 0$.

4.2 Boundary conditions

4.2.1 Solid boundaries

Moving boundaries: As we have assumed that the flow is inviscid and irrotational we can make no limitation on the flow past a solid boundary, but we can require that there be no component of fluid velocity normal to a solid surface. That is, if u is the fluid velocity, and U is the velocity of any part of a solid boundary, then we have

$$\mathbf{u}\cdot\hat{\mathbf{n}} = \mathbf{U}\cdot\hat{\mathbf{n}}. \qquad (4.8)$$

Calculating the velocity of a moving boundary (a ship, an oscillating structure, the ocean bottom in an earthquake, etc.) can be difficult. It is often easier to express it in terms of material derivatives. Let the boundary be defined by $F(r, t) = 0$. That is, as F is identically zero, such that $DF/Dt = 0$ where this time this means the apparent rate of change of F at a point on the boundary:

$$\frac{\partial F}{\partial t} + \mathbf{U}\cdot\nabla F = 0, \quad \text{on the boundary.}$$

As the boundary is a level surface of F, then ∇F is perpendicular to it, i.e. ∇F is in the direction of $\hat{n}$, and we could re-write equation (4.8) as

$$\mathbf{u}\cdot\nabla F = \mathbf{U}\cdot\nabla F,$$

and hence we have the general solid boundary condition

$$\frac{\partial F}{\partial t} + \mathbf{u}\cdot\nabla F = 0, \quad \text{or,} \quad \frac{\partial F}{\partial t} + \nabla\phi\cdot\nabla F = 0, \qquad \text{on } F = 0. \qquad (4.9)$$

Stationary boundaries: The most common solid boundary condition, which will be the one we use in this course, is where the boundary is not moving, $U = 0$. Substituting into equation (4.8) we obtain

$$\mathbf{u}\cdot\hat{\mathbf{n}} = \nabla\phi\cdot\hat{\mathbf{n}} = \frac{\partial\phi}{\partial n} = 0, \qquad (4.10)$$

from the properties of the gradient operator, where n is a local co-ordinate direction normal to the surface. That is: the derivative of ϕ normal to a stationary impermeable boundary is zero.

4.2.2 The free surface

Where a fluid has a boundary with another fluid (such as oil) or where the other fluid can be ignored (as is often done for the water-air interface), the position of the free surface becomes another unknown dependent variable, $z = \eta(x, y, t)$ for example, where η, like the velocity components u, v and w is still to be found. As a result of this extra unknown, we will require two boundary conditions at the free surface, the kinematic and dynamic free surface boundary conditions:

Kinematic free surface boundary condition: We can follow the procedure for solid boundaries, because

fluid particles remain on the surface. We will introduce the symbol η for the free surface such that $z = \eta(x, y, t)$. Now all we do is to introduce a general function $F(x, y, z, t)$ throughout all space and time which is constant on the free surface. We write

$$F(x, y, z, t) = z - \eta(x, y, t) = 0 \quad \text{on the free surface.}$$

We can obtain our boundary condition there: that particles which start on the free surface remain on the free surface, namely at each particle, F remains constant, thus $DF/Dt = 0$, that is,

$$\begin{aligned} \frac{DF}{Dt} = \frac{\partial F}{\partial t} + u\frac{\partial F}{\partial x} + v\frac{\partial F}{\partial y} + w\frac{\partial F}{\partial z} &= 0, \quad \text{which from our definition of } F \text{ gives} \\ -\frac{\partial \eta}{\partial t} - u\frac{\partial \eta}{\partial x} - v\frac{\partial \eta}{\partial y} + w &= 0, \end{aligned}$$

which we usually write:

$$\frac{\partial \eta}{\partial t} + u\frac{\partial \eta}{\partial x} + v\frac{\partial \eta}{\partial y} - w = 0, \quad \text{or in terms of } \phi, \quad \frac{\partial \eta}{\partial t} + \frac{\partial \phi}{\partial x}\frac{\partial \eta}{\partial x} + \frac{\partial \phi}{\partial y}\frac{\partial \eta}{\partial y} - \frac{\partial \phi}{\partial z} = 0 \quad \text{on } z = \eta,$$

(Kinematic free surface boundary condition KFSBC)

This is the well-known kinematic boundary condition for fluid boundaries. It immediately renders any problem nonlinear, for products of dependent variables appear in it.

Dynamic free surface boundary condition: Usually we can simply assume that the pressure at the surface is a constant, atmospheric pressure, which we can assume to be zero such that the pressure equation becomes

$$\frac{\partial \phi}{\partial t} + \frac{1}{2}|\nabla\phi|^2 + g\eta = C(t), \text{ or, } \frac{\partial \phi}{\partial t} + \frac{1}{2}\left(\left(\frac{\partial \phi}{\partial x}\right)^2 + \left(\frac{\partial \phi}{\partial y}\right)^2 + \left(\frac{\partial \phi}{\partial z}\right)^2\right) + g\eta = C(t) \text{ on } z = \eta.$$

(Dynamic free surface boundary condition DFSBC)

This is also nonlinear, because of the $|\nabla\phi|^2$ term.

4.3 The general problem of wave motion

The problem which we have to solve, in all studies of waves on irrotational and incompressible flows, whether studies of propagating waves or standing waves or considering aspects of propagation, diffraction, reflection or refraction is then: solve Laplace's equation

$$\nabla^2\phi = \frac{\partial^2 \phi}{\partial x^2} + \frac{\partial^2 \phi}{\partial y^2} + \frac{\partial^2 \phi}{\partial z^2} = 0$$

in the layer of water between the bed $z = Z(x, y)$ and the unknown surface $z = \eta(x, y, t)$ subject to the boundary conditions

$$\frac{\partial \phi}{\partial n} = 0 \quad \text{on the bed} \quad z = Z(x, y) \quad \text{(no fluid passes through the bed),}$$

and the nonlinear boundary conditions on the free surface

$$\frac{\partial \eta}{\partial t} + \frac{\partial \phi}{\partial x}\frac{\partial \eta}{\partial x} + \frac{\partial \phi}{\partial y}\frac{\partial \eta}{\partial y} - \frac{\partial \phi}{\partial z} = 0 \quad \text{on } z = \eta, \qquad \text{(KFSBC)}$$

$$\frac{\partial \phi}{\partial t} + \frac{1}{2}|\nabla\phi|^2 + g\eta = 0 \quad \text{on } z = \eta, \qquad \text{(DFSBC)}$$

where we have set $C(t) = 0$. Often we will have lateral boundary conditions, such as on walls or the sides of a harbour where we will also have the no-flow condition $\partial\phi/\partial n = 0$. Occasionally we may have open boundary conditions, such as specifying the lateral boundary conditions in terms of an incident wave field.

This problem is, in general, very difficult to solve. Laplace's equation is linear, and a number of rather wonderful methods exist for that, however there are two main complications: the boundary geometry is irregular, and the surface boundary conditions are nonlinear. Initially we will proceed to linearise the free surface boundary conditions so that the upper boundary is not the wavy irregular surface of the sea, but a horizontal plane at the mean level of the water surface. Still this doesn't simplify the problem sufficiently, and we then restrict ourselves in

this course to problems where the bottom is level, and then generally to problems where the lateral boundaries are either non-existent (waves propagating freely) or are simple geometries such as a cylindrical harbour.

4.4 Linear wave theory

Initially we will consider small motions relative to a mean state of no movement at all. We will place the co-ordinate origin somewhere in the plane of the mean surface level. Let the velocity potential ϕ and the surface elevation η be given by power series in ε, which we can think of as being proportional to the size of disturbance, namely the wave height:

$$\begin{aligned}\phi &= \varepsilon\phi_1 + \varepsilon^2\phi_2 + \ldots \\ \eta &= \varepsilon\eta_1 + \varepsilon^2\eta_2 + \ldots .\end{aligned}$$

Before substituting into the full kinematic and dynamic boundary conditions there is an additional subtlety that the boundary conditions are on $z = \eta$ but we want to express everything at the mean water level $z = 0$. To do this we use Taylor expansions about the latter point. Then, for example, $\partial\phi/\partial x$ at the surface can be expressed as

$$\begin{aligned}\left.\frac{\partial\phi}{\partial x}\right|_{z=\eta} &= \left.\frac{\partial\phi}{\partial x}\right|_{z=0} + \eta\left.\frac{\partial^2\phi}{\partial x\partial z}\right|_{z=0} + \ldots \\ &= \varepsilon\left.\frac{\partial\phi_1}{\partial x}\right|_{z=0} + \varepsilon^2\left.\frac{\partial\phi_2}{\partial x}\right|_{z=0} + \ldots + \left(\varepsilon\eta_1 + \varepsilon^2\eta_2 + \ldots\right)\left(\varepsilon\left.\frac{\partial^2\phi_1}{\partial x\partial z}\right|_{z=0} + \ldots\right) \\ &= \varepsilon\left.\frac{\partial\phi_1}{\partial x}\right|_{z=0} + O\left(\varepsilon^2\right).\end{aligned}$$

This is the result that we might have written down instinctively, but we can see that to perform such operations to higher orders considerable care must be taken. Substituting such expressions into the nonlinear free surface boundary conditions we obtain the almost-obvious result that we would have obtained simply by neglecting products of quantities in the boundary conditions:

$$\begin{aligned}&\varepsilon\left(\frac{\partial\eta_1}{\partial t} - \frac{\partial\phi_1}{\partial z}\right) = 0 \quad \text{on } z = 0, \text{ the mean surface level,} \\ &\varepsilon\left(\frac{\partial\phi_1}{\partial t} + g\eta_1\right) = 0 \quad \text{on } z = 0.\end{aligned}$$

However, as we are not going to consider second-order terms it is notationally simpler just to replace $\varepsilon\phi_1$ by ϕ etc., and so we obtain the linear boundary conditions in relatively simple form for small displacements about a state of no motion:

$$\frac{\partial\eta}{\partial t} - \frac{\partial\phi}{\partial z} = 0 \quad \text{on } z = 0, \text{ the mean surface level,} \tag{KLBC}$$

$$\frac{\partial\phi}{\partial t} + g\eta = 0 \quad \text{on } z = 0, \text{ the mean surface level.} \tag{DLBC}$$

Now it is convenient to eliminate η as a variable, and so we differentiate the second equation with respect to t and subtract the two equations to give the single linear free surface boundary condition

$$\frac{\partial^2\phi}{\partial t^2} + g\frac{\partial\phi}{\partial z} = 0 \quad \text{on } z = 0. \tag{4.11}$$

Our general problem now is to solve Laplace's equation throughout the region where we need a solution, with this as the boundary condition on the horizontal flat-top boundary $z = 0$.

4.4.1 Linear wave motion over a flat bed

The remaining boundary condition is the linear no-flow boundary condition $\partial\phi/\partial n = 0$ on all solid boundaries, including the sea bed. In general, however, such problems are not soluble, and here we will restrict ourselves to problems where the sea bed is horizontal, $Z = -d$, where d is the mean depth. Our geometrical domain is now the region between the two planes $z = -d$ and $z = 0$.

4.4.2 Steady two-dimensional waves

This is the most important problem in coastal and ocean engineering, where we consider the propagation of a train of periodic waves. Consider the two-dimensional problem of the propagation of waves in one (x) direction over the horizontal bottom:

$$\begin{aligned}
\frac{\partial^2\phi}{\partial x^2}+\frac{\partial^2\phi}{\partial z^2} &= 0 \quad \text{in the water layer } -d\leqslant z\leqslant 0,\\
\frac{\partial\phi}{\partial z} &= 0 \quad \text{on the sea bed } \quad z=-d, \text{ and}\\
\frac{\partial^2\phi}{\partial t^2}+g\frac{\partial\phi}{\partial z} &= 0 \quad \text{on the mean surface level } \quad z=0.
\end{aligned}$$

Experience suggests that we assume a solution of the form corresponding to travelling waves

$$\phi = A\cosh k(z+d)\sin k(x-ct), \tag{4.12}$$

where A is a constant and $k=2\pi/\lambda$ is the wave number, which is more convenient to use than the wavelength λ itself. The quantity c is a velocity of propagation. It can be shown that any function of $x-ct$ corresponds to a disturbance travelling steadily without change, in this case a sinusoidal wave. (If we have, in general, $f(x-ct)$, then at x at time $t+\Delta t$, the solution is $f(x-c(t+\Delta t))=f((x-c\Delta)-ct)$, the solution which was upstream at $x-c\Delta$ at time t.)

Firstly we verify that the assumed solution (4.12) satisfies the 2-D Laplace's equation throughout the water layer $-d\leqslant z\leqslant 0$:

$$\begin{aligned}
\frac{\partial\phi}{\partial x} &= kA\cosh k(z+d)\cos k(x-ct) \quad (=u, \text{ horizontal fluid velocity}),\\
\frac{\partial\phi}{\partial z} &= kA\sinh k(z+d)\sin k(x-ct) \quad (=v, \text{ vertical fluid velocity}),\\
\frac{\partial^2\phi}{\partial x^2} &= -k^2A\cosh k(z+d)\sin k(x-ct),\\
\frac{\partial^2\phi}{\partial z^2} &= k^2A\cosh k(z+d)\sin k(x-ct),
\end{aligned}$$

and summing the last two it is clear that the two-dimensional Laplace's equation is satisfied.

Now we verify that (4.12) satisfies the bottom boundary condition on the sea bed $z=-d$. Substituting that into the expression for $\partial\phi/\partial z$ we obtain a term $\sinh 0=0$, and the condition is satisfied.

Linear dispersion relation: This leaves us to satisfy the linear boundary condition on $z=0$. We obtain

$$\frac{\partial^2\phi}{\partial t^2} = -k^2c^2A\cosh k(z+d)\sin k(x-ct),$$

and substituting $z=0$ we obtain

$$\left.\frac{\partial^2\phi}{\partial t^2}\right|_{z=0}+\left.g\frac{\partial\phi}{\partial z}\right|_{z=0}=0=-k^2c^2A\cosh kd\,\sin k(x-ct)+gkA\sinh kd\,\sin k(x-ct),$$

and taking out common factors which are in general not zero, the only way that this can be satisfied is if the relation

$$\frac{c^2}{gd}=\frac{\tanh kd}{kd}=\frac{\tanh 2\pi d/\lambda}{2\pi d/\lambda} \tag{4.13}$$

is satisfied. This, the linear dispersion relation, is the most important expression in coastal and ocean engineering, showing us how the dimensionless wave speed $c/\sqrt{gd}$ depends on the relative wavelength λ/d. It is plotted in Figure 4-2. There are a number of points which can be made about this relationship:

- Wave speed depends on wavelength – the term dispersion implies the characteristic of an arbitrary disturbance to disperse into its different wavelength components
- Longer waves travel faster than shorter ones

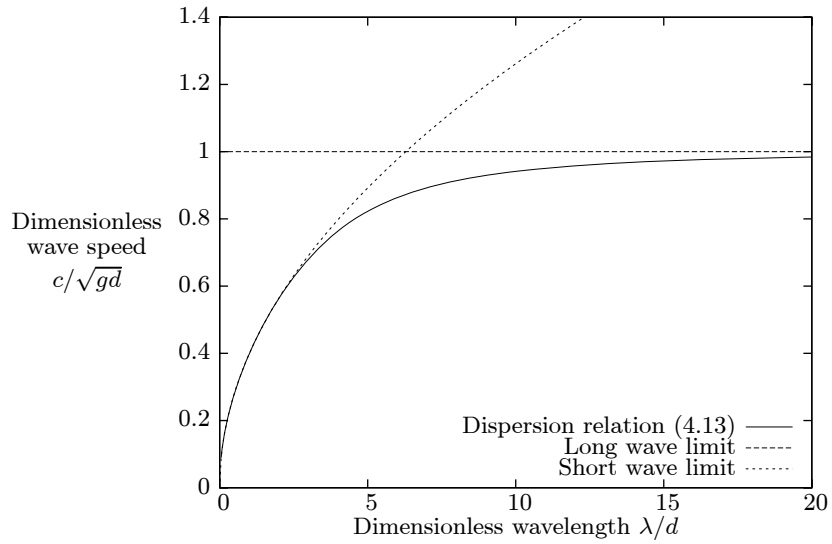

Figure 4-2. Linear dispersion relation, showing long and short wave limits

- In the long wave / shallow water limit $\lambda/d \to \infty$, $\tanh 2\pi d/\lambda \to 2\pi d/\lambda$, and

$$c = \sqrt{gd},$$

  the classical result for the speed of long waves on still water which we can get from hydraulic theory. When waves are sufficiently long, speed is independent of length.

- Waves longer than about 15 times the water depth can be considered long waves
- In the short wave / deep water limit $\lambda/d \to 0$, $\tanh 2\pi d/\lambda \to 1$, and

$$c = \sqrt{\frac{g\lambda}{2\pi}}$$

  such that when water is sufficiently deep, speed is independent of depth

- Waves shorter than twice the water depth can be considered short waves, which might be considered a surprising result

Solution in terms of wave height: Now let us consider the solution. Because our system of equations was homogeneous (ϕ occurred in all terms), we have not been able to determine the constant A. In fact, in most problems, it is the crest-trough wave height H which is specified. We can connect the two from the dynamic linear boundary condition:

$$\begin{aligned} \eta &= -\frac{1}{g}\left.\frac{\partial \phi}{\partial t}\right|_{z=0} \\ &= \frac{Akc}{g}\cosh kd\,\cos k\left(x-ct\right), \end{aligned} \tag{4.14}$$

which shows that the free surface varies sinusoidally, like many waves that we see on water. Now, the wave height is the difference between the crest, when $x - ct = 0$ and $\cos k\left(x - ct\right) = 1$, and the trough when $k\left(x - ct\right) = \pi$ and $\cos k\left(x - ct\right) = -1$, thus

$$H = 2\frac{Akc}{g}\cosh kd\,,$$

giving

$$A = \frac{H}{2}\frac{g}{kc\cosh kd}$$

and the solution for both ϕ and η is

$$\phi = \frac{H}{2}\frac{g}{kc}\frac{\cosh k(z+d)}{\cosh kd}\sin k(x-ct), \tag{4.15}$$

$$\eta = \frac{H}{2}\cos k(x-ct). \tag{4.16}$$

Of course, we could write c in terms of kd from the dispersion relation, but it seems simpler to keep it like this. Note that horizontal variation is sinusoidal, as we expect. Vertical variation of ϕ, expressing approximately the variation of velocities and the departure of pressure from hydrostatic as we will see, is like

$$\frac{\cosh k(z+d)}{\cosh kd},$$

which is equal to 1 on the surface $z = 0$, and which becomes smaller as we go deeper into the water, i.e. as z becomes larger negative.

In the case of deep water, $kd \to \infty$, both numerator and denominator become large, and it can be shown that

$$\frac{\cosh k(z+d)}{\cosh kd} \sim \frac{e^{k(z+d)}}{e^{kd}} = e^{kz},$$

and we see that the variation of ϕ with z is exponentially decaying, as z becomes increasingly negative. In this deep water case the bottom boundary is satisfied without requiring the cosh function as this goes exponentially to zero. It is interesting to see the value of this quantity when we are half a wavelength down into the water, that is, when $kz = k \times -\lambda/2 = -2\pi/\lambda \times \lambda/2 = -\pi$, and we get $e^{-\pi} = 0.0432$. That is, only half a wavelength down into the water the amount of disturbance due to the waves is only about 4% of that at the surface. This was suggested by the results on Figure 4-2. It also shows how, in the case of a storm, a submarine does not have to go far down into the water to ride it out with ease!

Fluid velocities: It is the derivatives of ϕ which are rather more physically of use. Differentiating we obtain

$$u = \frac{\partial\phi}{\partial x} = \frac{H}{2}\frac{g}{c}\frac{\cosh k(z+d)}{\cosh kd}\cos k(x-ct),$$

$$w = \frac{\partial\phi}{\partial z} = \frac{H}{2}\frac{g}{c}\frac{\sinh k(z+d)}{\cosh kd}\sin k(x-ct).$$

These too are periodic in $x - ct$, with a maximum positive horizontal velocity under the crests and a maximum negative value of the same magnitude under the troughs.

Pressure under waves: Now we take the pressure equation anywhere in the fluid and linearise it, here by simply neglecting the term which is the square of the velocity:

$$\frac{\partial\phi}{\partial t} + \frac{p}{\rho} + gz = 0 \quad \text{throughout the fluid,} \tag{4.17}$$

hence we have, substituting (4.15) for ϕ and differentiating, giving an expression for pressure anywhere in the fluid:

$$\frac{p}{\rho g} = -z + \frac{H}{2}\frac{\cosh k\,(z+d)}{\cosh kd}\cos k\,(x-ct)\,.$$

We can verify this for all points on the free surface by substituting $z = \eta$, except that in the $\cosh k\,(\eta+d)$ term we neglect η as this term is already multiplied by H and in our derivation we have ignored all terms of magnitude H^2 and higher. Then substituting equation (4.16) for η we obtain $p = 0$ on $z = \eta$, as we should.

Flow fields under waves: Figure 4-3 shows the velocity and pressure fields under sinusoidal waves. In each, the pressure under the crest has been plotted, as has the distributions of horizontal velocity under the crests and troughs of the waves. Figure (a) is for a wave of length $\lambda/d = 1$, the wavelength equal to the depth. In this case, $kd = 2\pi$, and the velocity field and the disturbance pressure field (relative to hydrostatic) die off exponentially the deeper we go into the water. At a depth equal to half the wavelength almost all activity has ceased. Figure (b) shows a wave of length $\lambda/d = 5$, and it can be seen that now the effects of the wave are felt on the bottom, even though there is some diminution relative to the surface. Figure (c) for a wave of length $\lambda/d = 10$, on the boundary of long waves, shows that the velocity decays very little with depth and the pressure is closely hydrostatic.

(a) Wave of length $\lambda/d = 1$, showing exponential decay

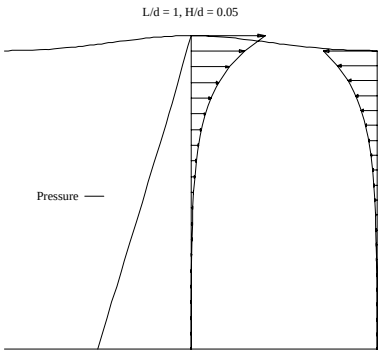

(b) Wave of length $\lambda/d = 5$, now showing less diminution with depth

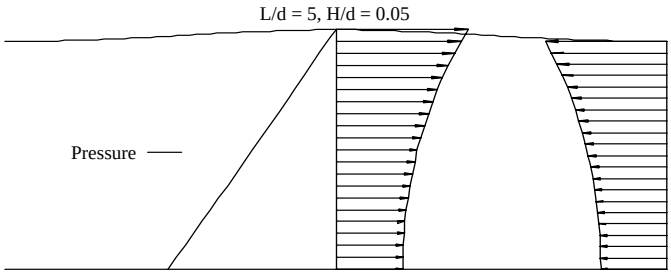

(c) Long wave of length $\lambda/d = 10$, with pressure distribution under crest now closely hydrostatic and horizontal velocity profiles under trough and crest showing little diminution with depth

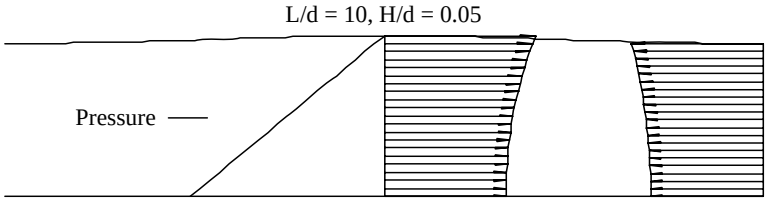

Figure 4-3. Flow fields, with pressure distributions under crest and horizontal velocity profiles under trough and crest.

The direction of wave propagation in these pictures is from left to right. It is clear that under the crests the fluid velocity is also in that direction. Under the troughs, however, the velocity is in the other direction, as given by the trigonometric functions in the solution for ϕ. In our theory we have assumed that there is no current on which the waves are riding. If there is a current, then this can affect the horizontal velocities quite markedly, and if we want to calculate forces on structures then we must include the effects of current. We will do this later, and will also examine some more accurate nonlinear theories. Meanwhile we will now examine solutions for standing waves and harbour oscillations.

A common first step – solving for wavelength when period is known: We have the linear dispersion relation, equation (4.13):

$$\frac{c^2}{gd} = \frac{\tanh kd}{kd}.$$

If aerial or remote sensing methods were used in an engineering investigation, the wavelength could be obtained directly by measurement. In most investigations, however, we measure waves at a point using a gauge or buoy and so we know the wave period τ rather than the wavelength λ (and hence k). In either case, we will need to know the other quantity as well. If we substitute the definition of wave speed $c = \lambda/\tau = 2\pi/k\tau$ into the dispersion relation (4.13) – for the case of no underlying current – we obtain an expression for the wave period which we can write as

well in terms of σ, the radian frequency of the waves:

$$\sigma = \frac{2\pi}{\tau} = \sqrt{gk\,\tanh kd}. \tag{4.18}$$

It is usual to express this also in dimensionless terms, so that we write, first in terms of wavenumber and frequency and then in terms of the more immediate physical quantities of period and wavelength:

$$\sigma\sqrt{\tfrac{d}{g}} = \sqrt{kd\,\tanh kd}, \quad \text{or} \quad \frac{2\pi}{\tau\sqrt{g/d}} = \sqrt{\frac{2\pi d}{\lambda}\,\tanh\frac{2\pi d}{\lambda}} \tag{4.19}$$

If period τ is measured, this is a nonlinear transcendental equation for wavelength λ, which can be solved by standard numerical means such as trial and error, bisection, or Newton's method. These are presented in Fenton & McKee (1990). Also in that paper a convenient empirical explicit approximation is presented, with little theoretical justification:

$$k = \frac{\sigma^2}{g}\left(\coth((\sigma\sqrt{d/g})^{3/2})\right)^{2/3}. \tag{4.20}$$

It is accurate to within 1.5% over all wavelengths, which is probably accurate enough for practical purposes, as in this theory we have linearised the equations (neglected terms proportional to the square of the wave height) and have neglected all effects of current. It is exact in both long wave (shallow water) and short wave (deep water) limits respectively. This could be used as an initial approximation if greater refinement were required.

A more recent formula by Guo (2002) is an even more accurate approximation to the linear dispersion relation:

$$kd = \frac{\sigma^2 d}{g}\left(1 - e^{-\left(\sigma\sqrt{d/g}\right)^{5/2}}\right)^{-2/5} \tag{4.21}$$

Long wave / shallow water limit: as $\lambda/d \to \infty$, $\tanh\frac{2\pi d}{\lambda} \sim \frac{2\pi d}{\lambda}$, and the right side of the "exact" equation (4.19) becomes $2\pi d/\lambda$, giving

$$\lambda \sim \tau\sqrt{gd}.$$

The approximation (4.20) in this limit, when the wave period becomes large such that the frequency σ becomes small, gives

$$k = \frac{\sigma^2}{g}\left(\coth((\sigma\sqrt{d/g})^{3/2})\right)^{2/3} \sim \frac{\sigma^2}{g} \times \left((\sigma\sqrt{d/g})^{-3/2}\right)^{2/3} = \frac{\sigma}{\sqrt{gd}},$$

also giving the correct limiting behaviour $\lambda \sim \tau\sqrt{gd}$

Short wave / deep water limit: as $\lambda/d \to 0$, $\tanh\frac{2\pi d}{\lambda} \sim 1$, and the right side of the "exact" equation (4.19) becomes $\sqrt{2\pi d/\lambda}$, giving

$$\lambda \sim \frac{g\tau^2}{2\pi}.$$

The approximation (4.20) in this limit, when the wave period becomes small such that the frequency σ becomes large, gives

$$k = \frac{\sigma^2}{g}\left(\coth((\sigma\sqrt{d/g})^{3/2})\right)^{2/3} \sim \frac{\sigma^2}{g},$$

also giving the correct limiting behaviour $\lambda \sim g\tau^2/2\pi$.

4.4.3 Standing waves

We will return to steady two-dimensional waves later, as it is often necessary to obtain more accurate solutions than we have presented here. Another important case of linear motion over a flat bed is that of standing waves, which can often be seen in the vicinity of a sea wall or other vertical barrier, when the incoming waves are reflected such that the resultant wave field is one of standing waves, where the waves seem to bob up and down at a point, rather than progressing. Most of the governing equations are the same as for steady waves, it is just that the lateral boundary conditions are different. As our equations are linear we can superimpose the motion of two travelling wave trains progressing in opposite directions. Hence from equation (4.12) we write the solution as

$$\phi = A\cosh k(z+d)\sin k(x-ct) + A\cosh k(z+d)\sin k(x+ct),$$

where the second term contains $x + ct$, showing wave propagation in the negative x direction. Combining these terms we have

$$\begin{aligned}\phi &= A\cosh k(z+d)\ (\sin k(x-ct) + \sin k(x+ct)) \\ &= A\cosh k(z+d) \times 2\ \sin kx\ \cos kct \\ &= 2A\cosh k(z+d)\ \sin kx\ \cos \sigma t, \end{aligned} \tag{4.22}$$

where we have substituted σ for kc (coming from $c = \lambda/\tau$). Now the velocity of propagation is meaningless, but the waves do have a definite frequency (and period). If we substitute this into the linear surface boundary condition (4.11):

$$\frac{\partial^2\phi}{\partial t^2} + g\frac{\partial\phi}{\partial z} = 0 \quad \text{on} \quad z = 0,$$

we obtain equation (4.18):

$$\sigma = \frac{2\pi}{\tau} = \sqrt{gk\ \tanh kd}.$$

Now we want to obtain an expression for the wave height, so we use the dynamic linear boundary condition in the form of equation (4.14):

$$\begin{aligned}\eta &= -\frac{1}{g}\left.\frac{\partial\phi}{\partial t}\right|_{z=0} \\ &= \frac{2A\sigma}{g}\cosh kd \sin kx \sin\sigma t.\end{aligned}$$

Now, when $kx = 0, \pi, 2\pi, \ldots$ ($x = 0, \lambda/2, \lambda, \ldots$) this gives zero, showing that the surface does not move there, and they are nodes, just as in vibrating strings or organ pipes. At $kx = \pi/2, 3\pi/2, \ldots$ ($x = 0, \lambda/4, 3\lambda/4, \ldots$) the surface will show periodic maxima and minima as it bobs up and down. When $t = \tau/4$, $\sigma t = \pi/2$, and the surface has a maximum $\eta = H/2$. Half a period later, at $t = 3\tau/4$ it has a minimum at $\eta = -H/2$. This gives us enough information to solve for A:

$$A = \frac{H}{4}\frac{g}{\sigma\cosh kd},$$

a similar expression to that obtained previously for propagating waves. The solution is now

$$\phi = \frac{H}{2}\frac{g}{\sigma}\frac{\cosh k\,(z+d)}{\cosh kd}\sin kx\cos\sigma t \tag{4.23}$$

$$\eta = \frac{H}{2}\sin kx\sin\sigma t. \tag{4.24}$$

We obtained the above solution by simply considering the combination of two travelling waves. It shows that at $x = 0$ there is a node ($\eta \equiv 0$). It is probably more convenient to have an anti-node at $x = 0$, corresponding to an impermeable wall being located there. We substitute the shifted co-ordinate $x' = x - \lambda/4$ into equations (4.23) and (4.24), in which case the term

$$\sin kx = \sin k(x' + \lambda/4) = \sin(kx' + 2\pi/\lambda \times \lambda/4) = \sin(kx' + \pi/2) = \cos kx'$$

and then simply replace x' by x to show that we can simply replace $\sin kx$ by $\cos kx$ in equations (4.23) and (4.24):

$$\phi = \frac{H}{2}\frac{g}{\sigma}\frac{\cosh k\,(z+d)}{\cosh kd}\cos kx\cos\sigma t \tag{4.25}$$

$$\eta = \frac{H}{2}\cos kx\sin\sigma t. \tag{4.26}$$

We can immediately verify that this problem, of an infinite train of standing waves, also corresponds to a standing wave between two vertical walls. We differentiate the expression for ϕ to give the horizontal velocity:

$$u = \frac{\partial\phi}{\partial x} = \frac{H}{2}\frac{gk}{\sigma}\frac{\cosh k\,(z+d)}{\cosh kd}\sin kx\cos\sigma t,$$

and hence when $kx = 0, \pi, 2\pi, \ldots = j\pi$, for $j = 1, 2, \ldots$, the horizontal velocity is zero, corresponding to the same boundary condition provided by a vertical wall. If two vertical walls are a distance L apart, this means we can have $kL = j\pi$. As $k = 2\pi/\lambda$ this gives $2L/\lambda = j$, hence $\lambda/L = 2/j = 2, 1, 2/3, 1/2, 2/5, \ldots$ such that any one of an infinite number of wavelengths between them are possible, starting with twice the distance between

them. The longer waves are more easily excited and hence are more likely. They have longer periods too, as might have been expected. Figure 4-4 shows a situation where two walls are a distance of four water depths apart, and where the first mode, $\lambda/L = 2$ has been excited. The figure shows the water surface at the two extremes, as well as the streamlines of the flow. It can be seen that the flow is of a seiching nature, where the whole body of water seems to oscillate back and forth. The surface is, possibly surprisingly, not a straight line, but is a cosine function.

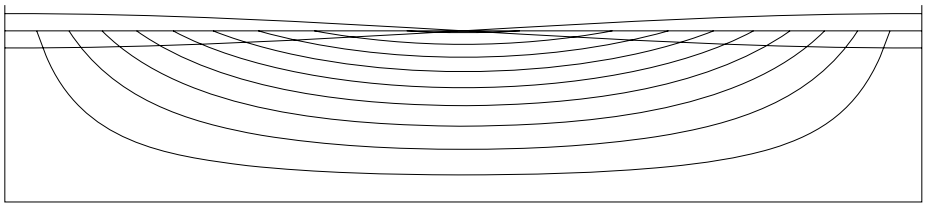

Figure 4-4. Standing wave, showing maximum and minimum water levels at the surface and streamlines in the water

Pressure under the waves and force on the wall: Now we can use linear theory to calculate the pressure at any point in the water and from this to compute the force on the walls. We have equation (4.17) obtained by linearising the unsteady Bernoulli equation

$$\frac{\partial \phi}{\partial t} + \frac{p}{\rho} + gz = 0 \quad \text{throughout the fluid.}$$

Hence, substituting equation (4.25):

$$\frac{p}{\rho g} = -z + \frac{H}{2}\frac{\cosh k\,(z+d)}{\cosh kd}\cos kx \sin \sigma t. \tag{4.27}$$

Note that when we substitute $z = \eta$, the elevation of the free surface given by equation (4.26), and ignoring terms of order H^2, we obtain $p = 0$, as we should. It can be seen that the variation of pressure in the vertical is the same as that for propagating waves, and we can show that for deep water the variation (relative to the hydrostatic term) is like $\exp kz$, showing exponential decay as z becomes negative. Of some interest is the total horizontal force per unit length P on one of the walls, at $x = 0$:

$$P = \int_{-d}^{\eta} p(0,z)\,dz,$$

where we have treated this in a scalar sense. Substituting the expression for pressure at $x = 0$:

$$\begin{aligned}
\frac{P}{\rho g} &= -\frac{z^2}{2} + \frac{H}{2k}\sin\sigma t \frac{\sinh k\,(z+d)}{\cosh kd}\bigg|_{-d}^{\eta} \\
&= \frac{1}{2}\left(d^2 - \eta^2\right) + \frac{H}{2k}\frac{\sinh k\,(\eta+d)}{\cosh kd}\sin\sigma t \\
&= \frac{1}{2}d^2 + \frac{H}{2k}\tanh kd\,\sin\sigma t,
\end{aligned}$$

where we have, in keeping with the accuracy of the theory, neglected all terms of order H^2. Clearly the first part of the solution, $d^2/2$ is the hydrostatic component. In situations where walls are backed by landfill, the actual force on the wall is not an important design consideration, however for walls constructed on the sides of piers or on rows of piles, the force is important for design, and in this situation, typically there is still water on the other side of the wall, so that the net force P_* is that due to the wave motion only. Hence,

$$\frac{P_*}{\rho g d^2} = \frac{1}{2}\frac{H}{d}\frac{\tanh kd}{kd}\,\sin\sigma t$$

This gives an expression for the pulsating force – and we can see that it is sinusoidal in nature, having a positive maximum when the surface is highest at the wall, $\sin\sigma t = 1$, and negative when the surface is lowest, $\sin\sigma t = -1$. This negative value might be unexpected - but it means that fixing devices holding planks in place have to be designed too.

The expression for P_* depends on the dimensionless wavelength in the ratio $\tanh kd\,/\,kd$. For long waves, when kd is small, and the pressure does not decay down into the water, the ratio is equal to 1 and could have been obtained just by considering the fluid to have constant wave-induced pressure against the wall. For shorter waves (larger kd) the ratio becomes smaller. Long waves create the largest forces because the pressure does not decay with depth.

4.4.4 Short-crested waves

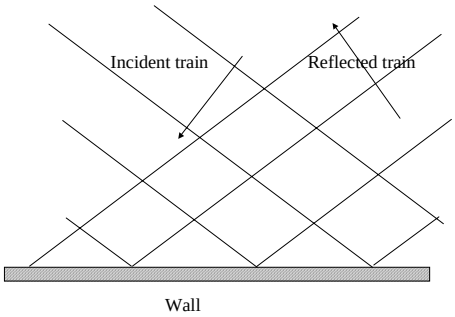

Figure 4-5. Plan view of periodic wave train obliquely incident on a vertical wall, showing reflected wave train and resultant diamond-shaped pattern

A type of wave motion which combines some features of both steady waves and standing waves is that of short-crested waves, when two wave trains intersect at an angle, such as when a wave train is obliquely incident on a vertical wall and is perfectly reflected. The resulting wave train is diamond-shaped when viewed in plan, and at any point the wave motion is still periodic in time (as well as being periodic in x and periodic in y).This can also

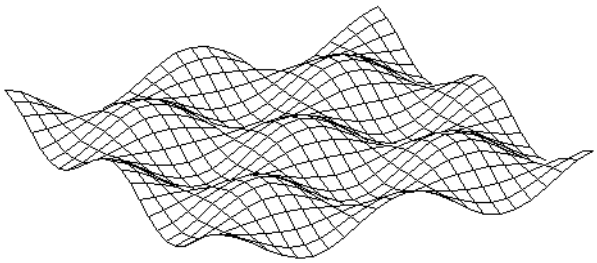

Figure 4-6. Water surface of a short-crested wave system

be studied using linear theory, and the forces on the wall calculated.We will examine this later when we touch on nonlinear theories.

4.4.5 Harbour oscillations

The potential for oscillation of harbours of idealised shapes can be studied using the method of separation of variables, as above, assuming that Laplace's equation holds throughout the water, satisfying the linear free surface boundary condition, and satisfying no-flow boundary conditions on the flat bed $z = -d$, and on vertical walls defining the harbour, a close-enough approximation for practical purposes. In all cases the variation with z can be represented by $\cosh\kappa(z+d)/\cosh\kappa d$ as before, where κ expresses the rapidity of variation with z but ceases to have the direct significance of the wavenumber k in these more general geometries. The linear free surface boundary condition leads to the same relation between frequency of oscillation σ and the quantity κ:

$$\sigma = \frac{2\pi}{\tau} = \sqrt{g\kappa\,\tanh\kappa d}. \tag{4.28}$$

The values of κ are determined by the rest of the problem, which depends on its geometry. If we let

$$\phi = \Phi(x,y)\,\frac{\cosh\kappa(z+d)}{\cosh\kappa d},$$

then substituting into Laplace's equation gives

$$\nabla_2^2\Phi + \kappa^2\Phi = 0, \tag{4.29}$$

where ∇_2^2 is the two-dimensional Laplace operator.

Rectangular harbours: Here it is convenient to use cartesian co-ordinates, and we will consider a harbour of dimensions L_x and L_y. We let

$$\Phi = A\cos\frac{m\pi x}{L_x}\cos\frac{n\pi y}{L_y}, \tag{4.30}$$

where m and n are integers, equal to 0 or greater.We can verify that u, the x component of velocity in the fluid, is proportional to $\partial\Phi/\partial x$ which is proportional to $\sin m\pi x/L_x$, which is 0 at $x=0$ and $x=L_x$, satisfying the boundary conditions on two opposite sides of the harbour If $m=1$ it has no other intermediate zeroes, and we have the fundamental mode of oscillation. Similar results hold for y and the other two sides of the harbour. The only other equation to satisfy is equation (4.29), and substituting gives the condition

$$\left(\frac{m\pi}{L_x}\right)^2 + \left(\frac{n\pi}{L_y}\right)^2 = \kappa^2. \tag{4.31}$$

Now, for any integer values of m and n a value of κ can be calculated, and from equation (4.28) the corresponding period of oscillation found. This can be done and compared with likely input from external gravity waves and infra-gravity waves to test the possibility of resonance, and hence unreasonable oscillations.

Circular harbours: It can be shown that in cylindrical co-ordinates the Laplace equation condition, equation (4.29), becomes

$$\frac{\partial^2\Phi}{\partial r^2} + \frac{1}{r}\frac{\partial\Phi}{\partial r} + \frac{1}{r^2}\frac{\partial^2\Phi}{\partial\theta^2} + \kappa^2\Phi = 0.$$

A solution is

$$\Phi = AJ_n(\kappa r)\cos n\theta,$$

where J_n is a Bessel function of order n. The integer n expresses the frequency of variation around the harbour. If $n=0$ then there is no variation with θ and all motion is axisymmetric; if $n=1$ then there is a single period of variation around the harbour and so on.

The possible values of κ are determined by the boundary condition on the perimeter, which we suppose to be at a radius of R. The condition that there be no fluid flow across the circumference can easily be shown to give the condition

$$J_n'(\kappa R) = 0, \tag{4.32}$$

where $J_n'(\kappa R) = dJ_n(x)/dx|_{x=\kappa R}$. For a given radius of harbour, the knowledge of the roots of this equation then give us the possible values of κ.

Figure 4-7 shows the first two Bessel functions plotted. The condition given by equation (4.32) is that the edge of the harbour can occur where the graph is horizontal. For the J_0 function we can show that these are at $x=3.83$ and $x=7.02$, while for the J_1 function the first values are $x=1.84,\ 5.33$, and 8.54. The oscillations are shown more graphically in Figures 4-8 and 4-9. In the former it is clear where possible bounding cylinders (the harbour perimeters) might exist, and how the motion is an axisymmetric one. In the case of the $n=1$ oscillation, we have seen on Figure 4-7 how a smaller value of κR satisfies the equation $J_1'(\kappa R)=0$, and so for a given physical radius, an $n=1$ oscillation with a smaller value of κ is possible. This is the fundamental seiching mechanism, where the motion is the circular equivalent of that shown in Figure 4-4, with an apparent motion of water from one side of the harbour to the other. In a problem of determining the natural periods of oscillation, the procedure is, given the first few roots of the lower order Bessel functions, and the radius R of the harbour, then determine κ, the parameter which determines the variation in the z direction, and then to determine the frequency (and hence

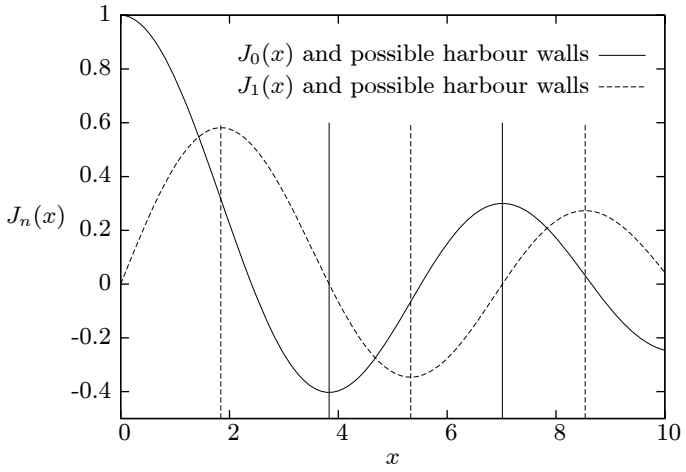

Figure 4-7. Bessel functions $J_0(x)$ and $J_1(x)$ and possible positions of walls

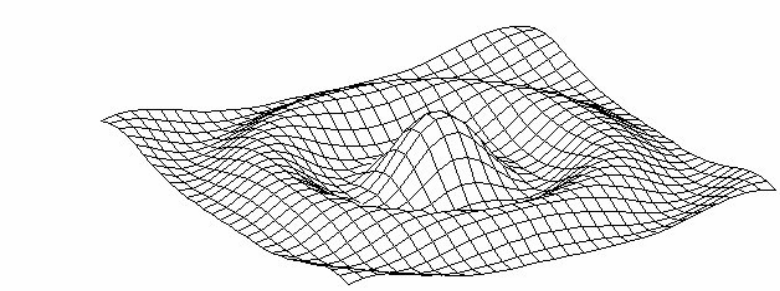

Figure 4-8. Circular harbour oscillations in the $n = 0$ (axisymmetric) mode; possible perimeters are cylinders with radii where the surface is horizontal.

period) from the linear dispersion relation:

$$\sigma = \frac{2\pi}{\tau} = \sqrt{g\kappa \tanh \kappa d}.$$

4.4.6 Wave energy

The energy content in a wave is made up of both potential and kinetic energy.

Potential energy: We will calculate the energy per unit width in one wave by considering an element of width 1 and length dx and with elevation η. The potential energy due to the deformation of the free surface dV is

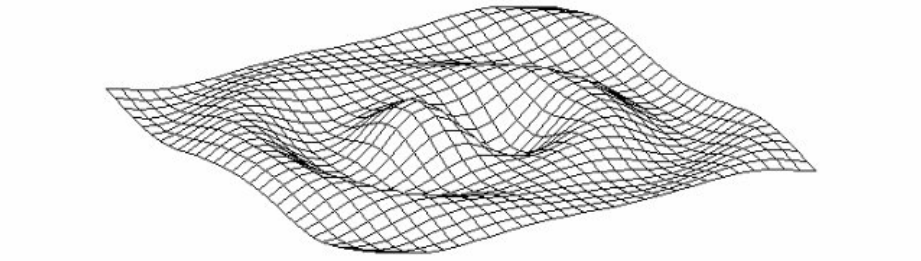

Figure 4-9. Circular harbour oscillations in the $n = 1$ mode; possible perimeters are cylinders with radii where the the radial derivative is zero, not so obvious here.

given by the mass times g times the elevation of the centre of mass,

$$dV = \rho g \times 1 \times \eta \times dx \times \frac{\eta}{2},$$

hence the potential energy per unit width in one wave V:

$$\begin{aligned} V &= \frac{\rho g}{2}\int_0^\lambda \eta^2\,dx \\ &= \frac{\rho g}{2}\times\left(\frac{H}{2}\right)^2\times\int_0^\lambda \cos^2 k(x-ct)\,dx \\ &= \frac{\rho g}{2}\times\left(\frac{H}{2}\right)^2\times\int_0^\lambda \frac{1}{2}\left(1+\underbrace{\cos 2k(x-ct)}_{\text{Periodic, integral}=0}\right)dx \\ &= \frac{1}{16}\rho g H^2\lambda. \end{aligned}$$

Kinetic energy: This is due to particle motion, and is denoted by T.

$$T = \frac{\rho}{2}\int_0^\lambda\int_{-d}^{\eta}\left(u^2+w^2\right)\,dz\,dx \approx \frac{\rho}{2}\int_0^\lambda\int_{-d}^{0}\left(u^2+w^2\right)\,dz\,dx,$$

where, to within our accuracy for linear wave theory we have replaced the upper limit in the integral over z by 0, the mean surface level. We have

$$\begin{aligned} u &= \frac{H}{2}\frac{g}{c}\frac{\cosh k(z+d)}{\cosh kd}\cos k(x-ct), \\ w &= \frac{H}{2}\frac{g}{c}\frac{\sinh k(z+d)}{\cosh kd}\sin k(x-ct), \end{aligned}$$

hence

$$\begin{aligned} u^2+w^2 &= \left(\frac{H}{2}\frac{g}{c}\frac{1}{\cosh kd}\right)^2\left(\cosh^2 k(z+d)\,\cos^2 k(x-ct)+\sinh^2 k(z+d)\,\sin^2 k(x-ct)\right) \\ &= \left(\frac{H}{2}\frac{g}{c}\frac{1}{\cosh kd}\right)^2\left(\cosh^2 k\,(z+d)-\sin^2 k\,(x-ct)\right), \\ &= \left(\frac{H}{2}\frac{g}{c}\frac{1}{\cosh kd}\right)^2\left(\tfrac{1}{2}\cosh 2k(z+d)+\tfrac{1}{2}\cos 2k(x-ct)\right), \end{aligned}$$

giving

$$\begin{aligned} \int_{-h}^{0}\left(u^2+w^2\right)\,dz &= \left(\frac{H}{2}\frac{g}{c}\frac{1}{\cosh kd}\right)^2\times\int_{-d}^{0}\left(\tfrac{1}{2}\cosh 2k(z+d)+\tfrac{1}{2}\cos 2k(x-ct)\right)\,dz \\ &= \left(\frac{H}{2}\frac{g}{c}\frac{1}{\cosh kd}\right)^2\left(\frac{\sinh 2kd}{4k}+d\cos 2k\,(x-ct)\right) \end{aligned}$$

and integrating with respect to x from 0 to λ and multiplying by $\rho/2$ gives

$$\begin{aligned} T &= \frac{\rho\lambda}{2}\left(\frac{H}{2}\frac{g}{c}\frac{1}{\cosh kd}\right)^2\times\frac{\sinh 2kd}{4k} \\ &= \frac{1}{16}\rho\lambda H^2\frac{g^2\tanh kd}{c^2k}, \end{aligned}$$

and as $c^2 = g/k \times \tanh kd$, we obtain

$$T = \frac{1}{16}\rho g H^2 \lambda,$$

and surprisingly, this is the same as the expression for potential energy. What is also interesting is that both expressions show that the mean potential and kinetic energy per unit area, T/λ and V/λ are both independent of the wave period or length.

Energy transport: The next step is to investigate the transmission of energy of a train of sinusoidal waves. Let P be the wave power per unit crest width. The value of P is a combination of the advection (transport) of potential and kinetic energy plus the work done by the pressures per unit width. We can show, that if $E = T+V = \rho g H^2/8$, the total energy per unit of area, then

$$P = Ec_g,$$

where c_g is the group velocity,which is the mean speed at which energy is transmitted, and it can also be shown to be the speed at which a group of waves travels. In fact, we can express this in terms of the wave speed:

$$\frac{c_g}{c} = \frac{1}{2}\left(1 + \frac{2kd}{\sinh 2kd}\right). \tag{4.33}$$

In the limit of deep water (short waves) as $kd \to \infty$, this becomes $c_g/c = 1/2$, showing that in deep water the energy travels at half the speed of the waves themselves. In shallow water, as $kd \to 0$, $c_g/c = 1$, and the energy is transmitted at the speed of the waves. The behaviour is shown in figure 4-10.

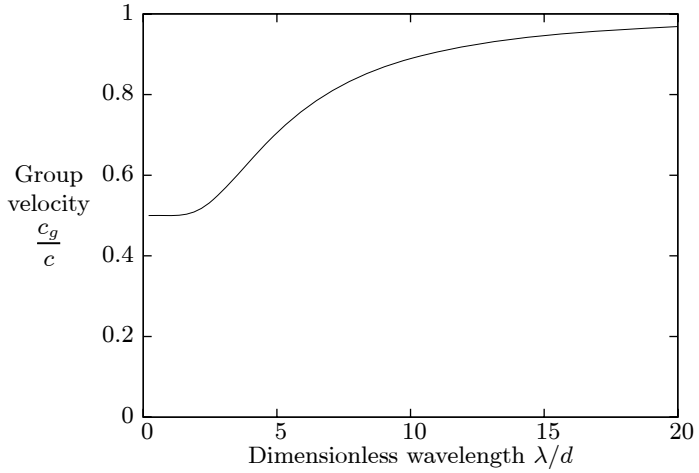

Figure 4-10. Relative group velocity and its variation with wavelength

4.4.7 Superposition of waves of different frequencies, beats

In some applications it is more convenient to use the wavenumber and wave frequency, rather than the wave speed. We note that as wave speed $c = \lambda/\tau$, substituting $\lambda = 2\pi/k$ and $\tau = 2\pi/\sigma$, we obtain the relations

$$c = \frac{\sigma}{k}, \quad \text{or} \quad \sigma = kc,$$

hence we write for the fundamental solution

$$\eta = \frac{H}{2}\cos k(x - ct) = \frac{H}{2}\cos\left(kx - kct\right) = \frac{H}{2}\cos\left(kx - \sigma t\right).$$

Now we consider two wave trains. As the equations we have developed are linear , we can superpose solutions, and here we will consider the interference of two wave trains travelling in the same direction with different wavenumbers k_1 and k_2 and different frequencies σ_1 and σ_2. For simplicity, the amplitude is taken to be the same in both

waves. Hence we write.

$$\begin{aligned}\eta_1 &= \frac{H}{2}\cos(k_1 x - \sigma_1 t)\\ \eta_2 &= \frac{H}{2}\cos(k_2 x - \sigma_2 t).\end{aligned}$$

Adding gives

$$\eta_1 + \eta_2 = \frac{H}{2}\left(\cos(k_1 x - \sigma_1 t) + \cos(k_2 x - \sigma_2 t)\right).$$

We consider the two frequencies and wavenumbers to be slightly different from the "carrier" values by writing

$$\begin{aligned}\sigma_1 &= \sigma - \frac{\Delta\sigma}{2} \text{ and } k_1 = k - \frac{\Delta k}{2}\\ \sigma_2 &= \sigma + \frac{\Delta\sigma}{2} \text{ and } k_2 = k + \frac{\Delta k}{2}.\end{aligned}$$

By suitable trigonometric manipulations it is possible to write the combined solution as

$$\eta_1 + \eta_2 = H\,\cos(kx - \sigma t)\,\cos\left(\tfrac{1}{2}\left(\Delta k\, x - \Delta\sigma t\right)\right),$$

and this consists of the basic carrier wave but modulated by the envelope function

$$\cos\left(\tfrac{1}{2}\left(\Delta k\, x - \Delta\sigma t\right)\right) = \cos\left(\tfrac{1}{2}\Delta k\left(x - \frac{\Delta\sigma}{\Delta k}t\right)\right),$$

so that the apparent velocity of the envelope wave is $\Delta\sigma/\Delta k$. In the limit of vanishing small Δk, (hence a wave group of infinite length) this becomes $d\sigma/dk$, and this is c_g, the group velocity. We recall that the wave energy is proportional to the square of the wave height, and so no energy can propagate past a node, as the wave height is zero there. Therefore the energy must travel with the speed of the group of waves.

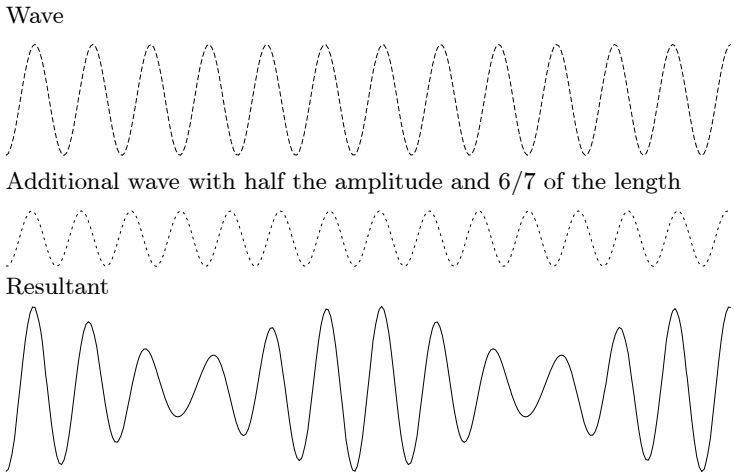

Figure 4-11. Two wave trains combined, showing the beat phenomenon

Figure 4-11 shows the phenomenon for two wave trains, the second having a length 1/7 less than the first, and an amplitude of 50%. Remember the old surfer's rule: every seventh wave is large ...

Now consider the linear dispersion relationship

$$\sigma^2 = gk\tanh kd.$$

Differentiating,

$$2\sigma\frac{d\sigma}{dk} = g\tanh kd + gkd\,\mathrm{sech}^2\, kd,$$

hence

$$\begin{aligned}\frac{d\sigma}{dk} &= c_g = \frac{\sigma\left(g\tanh kd + gkd\,\mathrm{sech}^2\,kd\right)}{2gk\tanh kd}\\ &= c\times\frac{\tanh kd + kd\,\mathrm{sech}^2\,kd}{2\tanh kd}\\ &= c\times\frac{\sinh kd/\cosh kd + kd/\cosh^2 kd}{2\sinh kd\,/\cosh kd}\\ &= c\times\frac{1}{2}\left(1+\frac{2kd}{\sinh 2kd}\right), \quad \text{as } \sinh 2kd = 2\sinh kd\cosh kd.\end{aligned}$$

which agrees with equation (4.33).

4.5 Shoaling, refraction and breaking

4.5.1 Shoaling

We can use our energy theory to apply to waves shoaling – moving into gradually decreasing water depths. Initially we consider the situation where a regular wave train moves so that the wave crests are parallel to the depth contours. This implies that here the energy contained within a certain width in deep water remains within the same width in shallow water. Although the previous theory is not strictly applicable to this case since the bottom is not horizontal, the restriction of small bottom slope permits the assumption that locally the wave behaves as if it were in locally constant depth. Hence, the power crossing any section at one point is the same as anywhere else, and so

$$P = E\,c_g = E_0\,c_{g0},$$

where the 0 subscripts denote the deep water values. Thus we have

$$\frac{1}{8}\rho g H^2 c_g = \frac{1}{8}\rho g H_0^2 c_{g0},$$

or,

$$\frac{H}{H_0} = \sqrt{\frac{c_{g0}}{c_g}} = K_s,$$

the Shoaling Coefficient, showing that as the local group velocity c_g decreases with water depth, the wave height increases. We can substitute our expressions to give

$$K_s = \sqrt{\frac{c_0}{c}\times\frac{1}{1+\frac{2kd}{\sinh 2kd}}}, \tag{4.34}$$

where c_0 is the wave speed in deep water and c that at depth d. We can relate these two by writing $c_0 = \sigma/k_0$ and $c = \sigma/k$, where σ is the frequency of the waves, which is the same whether they are in deep or shallow water, giving

$$\frac{c_0}{c} = \frac{k}{k_0}$$

and in fact we can use the linear dispersion relation for the frequency at both points:

$$\sigma = \sqrt{gk\tanh kd} = \sqrt{gk_0}, \tag{4.35}$$

as in deep water, when $d\to\infty$, $\tanh kd\to 1$. This gives

$$\frac{k}{k_0} = \frac{1}{\tanh kd},$$

and substituting into (4.34) gives

$$\begin{aligned}K_s &= \left(\tanh kd\left(1+\frac{2kd}{\sinh 2kd}\right)\right)^{-1/2} &(4.36)\\ &= \left(\tanh kd + kd\left(1-\tanh^2 kd\right)\right)^{-1/2}. &(4.37)\end{aligned}$$

The significance of this is that it enables us to calculate the wave height at any depth, important for design purposes. Multiplying the linear dispersion relationship (4.35) by $\sqrt{d/g}$ gives

$$\sigma\sqrt{d/g} = \sqrt{kd\,\tanh kd}. \tag{4.38}$$

The two equations, (4.38) and (4.37) (the latter has been developed for these lecture notes – (4.36) is the usual form) enable a shoaling calculation to be done. For a given wave frequency σ and water depth d, (4.38) is a transcendental equation which can be solved for k, and this can then be substituted into (4.37) to give the ratio of the wave height at that point to that in infinite depth.

The practical procedure is then

1. For a given wave period, calculate the frequency $\sigma = 2\pi/\tau$.
2. The problem is then, for a given depth d, to solve the transcendental equation $\sigma = \sqrt{gk\tanh kd}$ for k at that depth. Four methods can be mentioned:
   a. Calculate a table or graph of $\sigma\sqrt{d/g}$ for various values of kd and then interpolate in the table or read off the graph the appropriate value of k for the given value of σ.
   b. Use the tables and graph provided in many textbooks, notably Protection Manual (1975, Appendix C, Volume 3).
   c. Use a numerical method to solve the equation, such as bisection, trial-and-error etc.
   d. The simplest is to use the approximate expression of Fenton & McKee (1990):

$$kd = \frac{\sigma^2 d}{g}\left(\coth((\sigma\sqrt{d/g})^{3/2})\right)^{2/3}. \tag{4.39}$$

3. Use equation (4.36) or (4.37) to calculate K_s. The latter equation seems a bit simpler.

In practice, rather than specifying a value of frequency σ, usually the deep-water wavelength λ_0 (usually "L_0") is presented. In deep water we have $\sigma = \sqrt{gk_0}$, giving

$$\lambda_0 = \frac{g\tau^2}{2\pi},$$

and the ratio of d/λ_0 has more obvious physical significance than $\sigma\sqrt{d/g}$.

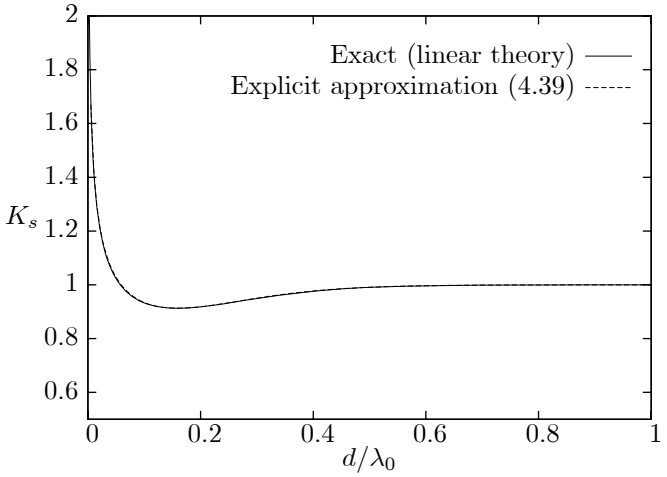

Figure 4-12. Variation of relative wave height (shoaling coefficient K_s) with dimensionless depth d/λ_0

Now we present a graph showing the variation of $K_s = H/H_0$ with dimensionless depth d/λ_0 obtained as suggested above, in one case solving the transcendental equation at each depth, and in the other using the approximate explicit expression of (4.39). It can be seen that the two sets of results almost coincide. It may come as a surprise that, such is the dependence of the group velocity on kd, that as the wave shoals the amplitude actually starts to decrease initially (only after $d \approx 0.5$, in agreement with our earlier experience that waves do not feel the bottom until this depth). Then, at about $d/\lambda_0 \approx 0.16$ the function has a minimum, and after that the wave height grows

quickly as the shore is approached.

4.5.2 Refraction of waves

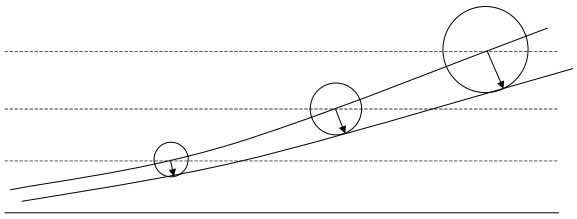

Figure 4-13. Geometric construction after Huygens, showing waves approaching shore and the closest inshore having a smaller speed, leading to bending of the wave crest.

Many surface wave characteristics can be shown to have analogous behaviour with other wave phenomena. In the case of the refraction of gravity waves a good analogy is found in geometric optics, where Snell's law of refraction plays an important role. During the above discussion on wave shoaling attention was drawn to the fact that as waves entered shallower water from deep water, the phase velocity, wavelength and wave height all changed, but the wave period did not. There it was assumed that wave crests were always parallel to the gradually-varying straight depth contours. Now we consider a more general case, as depicted in Figure 4-13. When the long-crested waves approach the shoreline obliquely, that part of a wave which is closest to the shore is in water of smaller depth, and as the wave speed increases with depth, this part of the wave has a smaller velocity. We construct circles of radius $c\Delta t$, where Δt is an interval of time, showing where a point on a wave crest can be at a time Δt later. By drawing an envelope to all such circles we have an approximation to the wave crest at the later time, and it is clear that it has apparently turned towards shallower water. The wave is subject to a continuous refraction which tends to align the wave front to the depth contours. Figure 4-14 shows more details of a wave field. The orthogonals or wave rays on the diagram represent the directions that the wave fronts are taking.

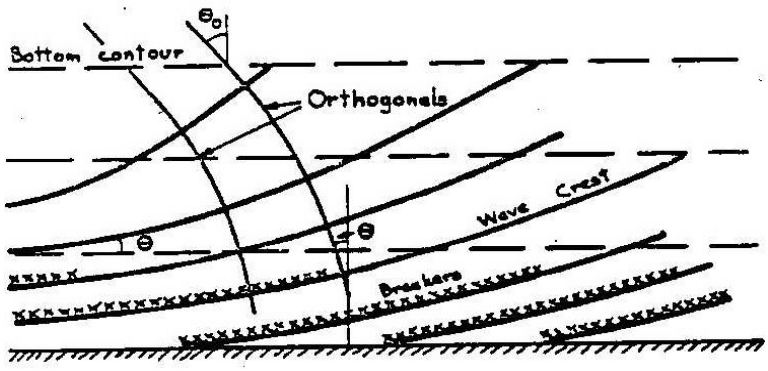

Figure 4-14. More detailed drawing (after Graze) showing refraction of the wave field and the position of breaking waves

Now we consider more general topographies, as shown in Figure 4-15, showing how waves are refracted towards shallower water, which means that they refract towards ridges and to headlands, and away from valleys or bays. This has important implications for sand movement on coastlines and for surfers, as now the wave power is not distributed uniformly along the coast at the coast, but will be concentrated at headlands. We can do the same kinds of calculations as we did for straight shoaling, but here we will have to take into account that in different parts the wave orthogonals may have converged (diverged) with an apparent increase (decrease) in power per unit span.

4.5.3 Wave refraction theory

Here we describe the theory briefly (see Dean and Dalrymple, 1984, p104 for a longer discussion, which is quite interesting). The way in which most solutions of shoaling are performed is to calculate the positions of a system of orthogonals to the wave fronts (crests), and then to calculate the wave shoaling using the above methods by allowing for the convergence or divergence of the wave orthogonals.

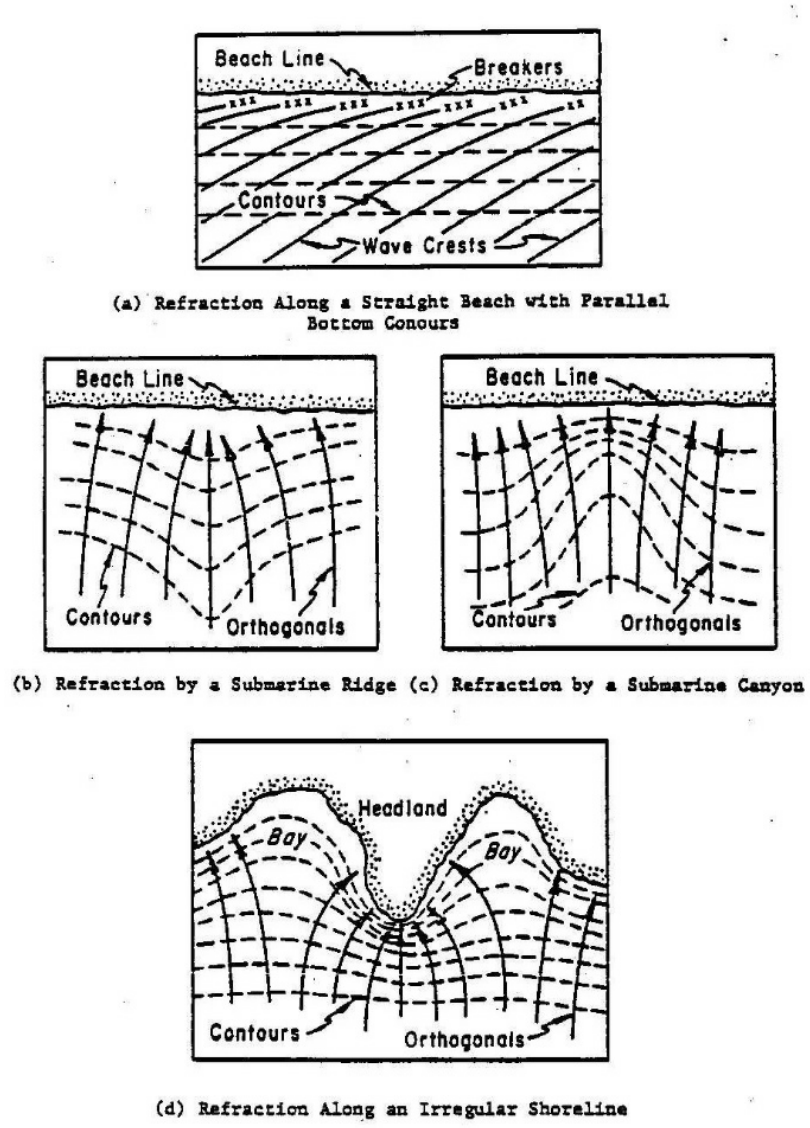

Figure 4-15. The shoaling of wave trains over some common topographies (after Graze)

Consider Figure 4-16. It can be shown that, if θ is the angle that a wave orthogonal makes with the x axis, then the governing equation is

$$\frac{\partial\left(k\sin\theta\right)}{\partial x}-\frac{\partial\left(k\cos\theta\right)}{\partial y}=0, \tag{4.40}$$

where x is normal to the beach and y is along the beach. For a situation where the contours are parallel there is no longshore variation in the y direction and the equation reduces to

$$\frac{d\left(k\sin\theta\right)}{dx}=0, \quad \text{or} \quad k\sin\theta=\text{Constant}.$$

This means that the long-shore projection of the wavenumber is constant. We can divide by frequency σ to give

$$\frac{\sin\theta}{c}=\text{Constant}=\frac{\sin\theta_0}{c_0},$$

where the 0 subscripts denote the deep water values. This is Snell's law, originally found in geometric optics, relating the change in direction of a wave to the change in wave speed. As the wave speed is smaller in shallower water, then so is the angle the waves make to the normal to the beach. Thus θ decreases as the wave shoals.

In general, offshore contours are irregular, and in an engineering investigation it is necessary to solve the more general problem. Historically, ray-tracing techniques were developed to solve this. Using some calculus, it can

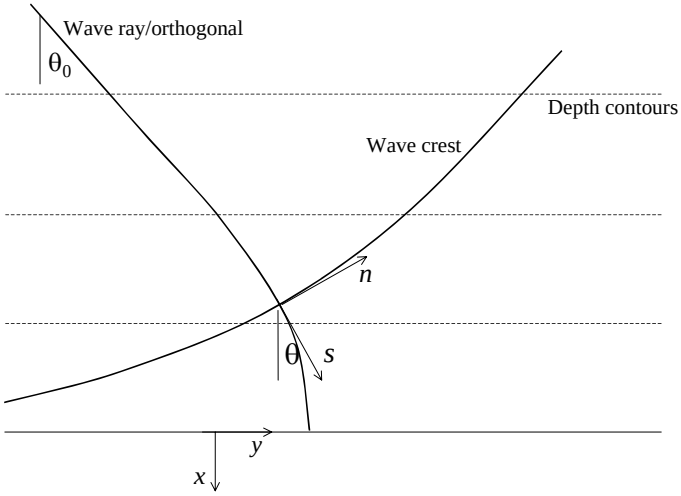

Figure 4-16. Wave crest and ray/orthogonal and general and local co-ordinates

be shown that the equation governing the wave angle can be written in (s, n) cordinates, s in the direction of propagation and n perpendicular, giving

$$\frac{\partial \theta}{\partial s} = \frac{1}{k}\frac{\partial k}{\partial n}.$$

To evaluate this we use the dispersion relation $\sigma = \sqrt{gk \tanh kd}$, so that at a given point where we know the depth, we can solve this to give k, and also to give $\partial k/\partial n$. Use of the approximation (4.39) for k as a function of σ and d would make this procedure rather simpler. Having evaluated the right side, this gives us $\partial\theta/\partial s$, which is the curvature of the ray, and so the ray can be projected forward, and the procedure repeated. Computer programs which do this are known to have a number of problems, such as when, due to numerical errors or irregular topography, the rays come too close, giving locally infinite energy and a breaking down of the theory probably before the waves themselves break! Nevertheless they are widely used by the engineering profession to calculate the wave field at a site of interest.

Having calculated the paths of various rays, as there is no energy flux across the wave rays, the total energy flux between two adjacent rays at one point is the same as at another point. Our previous theory for the change of height with distance was essentially two-dimensional, where we considered waves shoaling normal to the beach. Now we simply modify the theory by multiplying by b, the distance between two rays at a general point and in deep water, to give $P = E\,c_g\,b = E_0\,c_{g0}\,b_0$,where the 0 subscripts denote the deep water values. Thus, as above, we obtain

$$\frac{H}{H_0} = \sqrt{\frac{c_{g0}}{c_g}}\sqrt{\frac{b_0}{b}} = K_s K_r,$$

where, in addition to the Shoaling Coefficient introduced above, we have the Refraction Coefficient $K_r = \sqrt{b_0/b}$.

4.5.4 A model of refraction on a plane beach

Here we use the approximation for wavenumber to get an explicit differential equation. We have Snell's law for the case where the contours are parallel:

$$k(x)\sin\theta = C = k_0 \sin\theta_0.$$

However, in terms of cartesian co-ordinates,

$$\tan\theta = \frac{dy}{dx},$$

and so the differential equation becomes

$$\frac{dy}{dx} = \tan\theta = \tan\left(\sin^{-1}\left(\frac{C}{k(x)}\right)\right) = \frac{1}{\sqrt{\frac{k(x)^2}{C^2} - 1}}$$

Now we use the approximation of (4.39):

$$k(x) = \frac{\sigma^2}{g}\left(\coth((\sigma\sqrt{d(x)/g})^{3/2})\right)^{2/3},$$

which gives the differential equation

$$\frac{dy}{dx} = \left(\left(\frac{\left(\coth((\sigma\sqrt{d(x)/g})^{3/2})\right)^{2/3}}{\sin\theta_0}\right)^2 - 1\right)^{-1/2}.$$

Now we can assume a particular form of depth variation. The simplest is that of a uniform slope α: $d(x) = D - \alpha x$. We solve the differential equation numerically for three different wave periods for a slope of $\alpha = 0.01$, $\theta_0 = 45°$, starting $50\,\mathrm{km}$ out to sea. Results are shown in figure 4-17. It is clear how the long waves feel the bottom much further out at sea and are more affected by the process of refraction. Short waves remain relatively unaffected until close inshore.

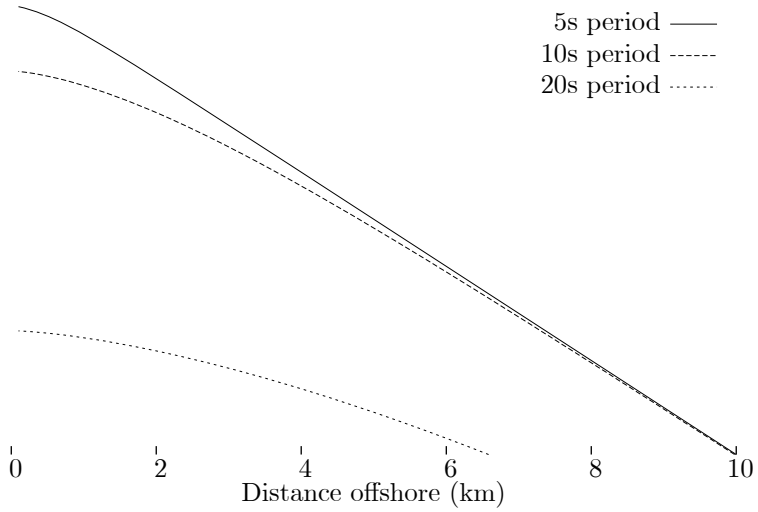

Figure 4-17. Plan view showing trajectories of waves on a beach of slope 0.01 for different periods

4.5.5 Waves breaking in shallow water

The shoaling coefficient indicates that the wave height will approach infinity in very shallow water, which is not realistic. At some depth, a wave of given characteristics will become unstable and break, dissipating energy in the form of turbulence. When designing a structure which at times may be inside the surf zone it becomes necessary to be able to predict the location of the breaker line.

The means by which waves break depends on the nature of the bottom and the characteristics of the wave, as shown in Figure 4-18. There are three main types:

Spilling breakers: For very mildly sloping beaches, typically the waves are spilling breakers, and is characterised by breaking gradually over a long distance such that many waves occur within the surf zone (defined as that region where the waves are breaking, extending from the beach to the seaward limit of the breaking). The rate of energy loss is small, permitting a nearly complete reforming of the waves should they once again progress into deep water, such as when they cross a sand bar. The wave remains almost symmetrical, with foam gently spilling down the front face of the breaking wave. By the time the wave reaches the top of the beach, the energy of the wave has been almost completely absorbed, with little or no reflection.

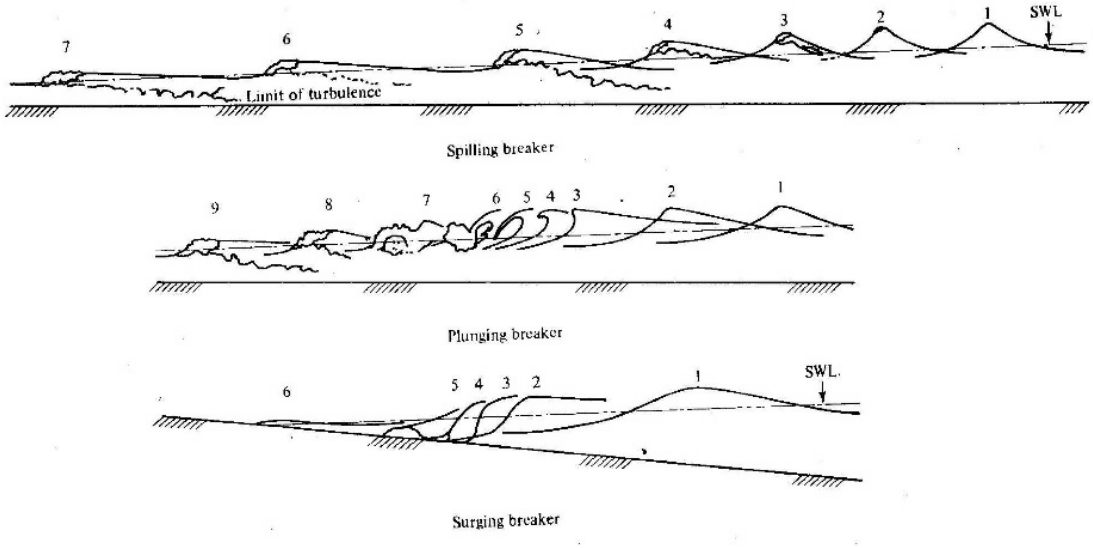

Figure 4-18. Three types of wave breaking on beaches (after Svendsen). The small figures denote different stages of the breaking process.

Plunging breakers: These occur on steeper beaches and are characterised by the crest of the wave curling over forward and impinging onto part of the wave trough, sometimes trapping air, and plunging with a loud report. Considerable energy is dissipated in this manner by turbulence, and considerable fun is had by surfers before that moment of plunging. There are few measurements of the breaking criteria for such waves.

Surging breakers: These waves occur on very steep beaches and are characterised by narrow or non-existent surf zones, and high reflection. Sometimes a fourth type is added – collapsing, which is a combination of plunging and surging.

Laboratory experiments have shown that breaker types can be classified depending on the so-called surf similarity parameter

$$\xi = \frac{\beta}{\sqrt{H_b/\lambda_0}},$$

where β is the beach slope, H_b is the wave height at breaking point, and λ_0 is, as previously, the deep-water wavelength. The classification is

Type	ξ
Spilling	< 0.4
Plunging	$0.4 - 2$
Surging	> 2

4.6 Diffraction

Wave diffraction is the process by which waves are scattered by structures in the sea. This might be the simple truncation of a wave by a breakwater, or the scattering of incident waves by a large petroleum production platform, one whose physical dimensions are comparable with the wavelength. Examples are shown in Figure 4-19. Diffraction occurs on the sheltered side of the breakwater such that the waves are cut-off by the breakwater, and then as they propagate energy spreads laterally, leading to the diffraction patterns shown. The wave disturbance is transmitted into the ”shadow zone” behind the breakwater, and as the energy is now travelling also parallel to the wave crest, the energy per unit length of wave crest is being reduced. That part of the wave which is reflected by the breakwater will tend to form a standing wave system, with a wave height twice that of the incident wave.

A quantitative understanding of the effects of wave diffraction is relevant to the planning and evaluation of harbour layouts, including the extent and location of wave-absorbing features on the perimeter of the harbour. The solutions can become quite complicated, as they involve solving Laplace’s equation with mixed boundary conditions. Many solutions can be taken from geometric optics. A simple introduction is given in Dean & Dalrymple (1984, #4.9).

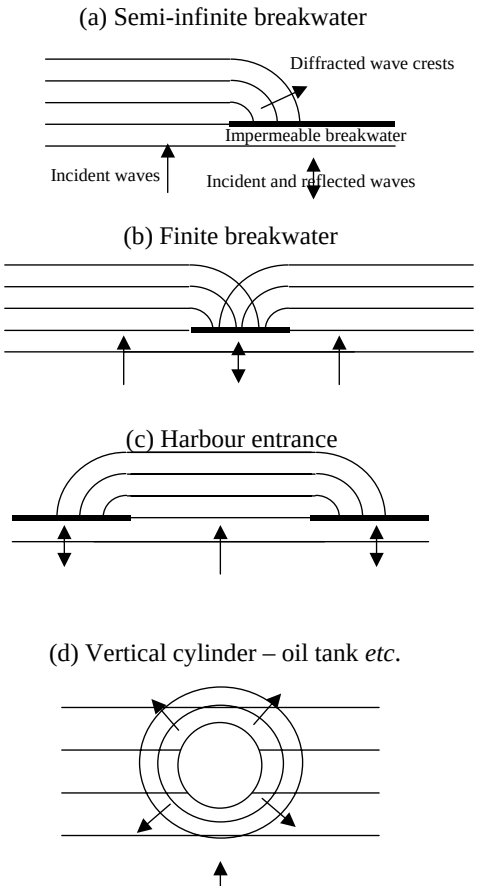

Figure 4-19. Typical wave diffraction patterns

4.7 Nonlinear wave theories

4.7.1 Introduction

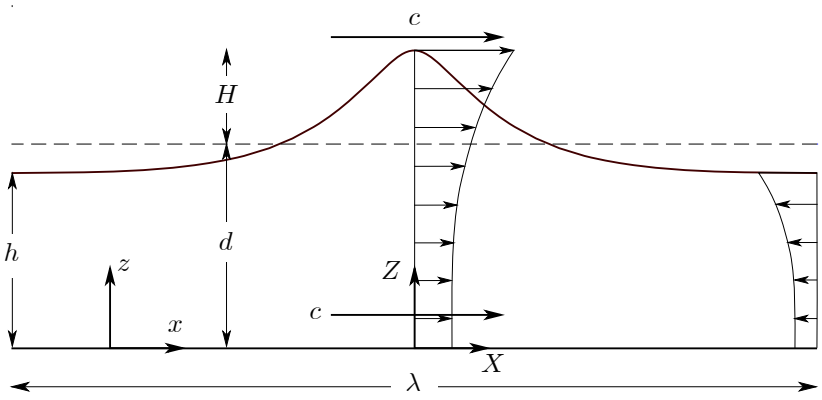

Figure 4-20. One wave of a steady train, showing principal dimensions, co-ordinates and velocities

Earlier we considered the steadily-propagating motion of sinusoidal waves using linear wave theory. That is, in fact, a rather too severely limiting approximation for some applications in coastal and ocean engineering, in particular the latter, where it is necessary to be able to calculate accurately the fluid velocities which act on structures. Figure 4-20 shows the physical situation, where we have now shown the wave rather more accurately – with a sharper crest and longer troughs. The field of steady wave theories has been an important one, even applying these theories in a rather idealised manner.

In practice, the general case of water wave motion is where disturbances propagate in varying directions over water which might be flowing on a shear current, over varying permeable or deformable topography. It is not possible to solve this general problem analytically. Instead, it is convenient to assume that locally at least the bed is impermeable and flat, that disturbances are of infinite length transverse to the direction of propagation such that the flow is two-dimensional, that the fluid is homogeneous and incompressible. It is possible to obtain analytical solutions which correspond to a single periodic wave train which propagates steadily without change of form – the steady wave problem.

There are two main theories for steady waves – Stokes theory, most suitable for waves which are not very long relative to the water depth; and Cnoidal theory, suitable for the other limit where the waves are much longer than the depth. In addition there is one important numerical method – the Fourier approximation method which solves the problem accurately, and is now widely used in ocean and coastal engineering.

4.7.2 Steady waves: the effects of current and the governing equations

- Three physical dimensions uniquely define a wave train: the mean depth d, the wave crest-to-trough height H, and wavelength λ – and by the Buckingham π Theorem, this means that two dimensionless quantities uniquely define a wave train, for example, H/d and λ/d.
- Many presentations of theory have assumed that the wave period can replace the wave length as the third parameter identifying a wave train.
- However, waves generally travel on a finite current which is determined by oceanographic and topographic factors. The wave speed relative to an observer depends on the current, such that waves travel faster with the current than against it. Contrary to the implicit assumptions of most presentations of steady wave theory, no theory can predict the actual wave speed. What the theories do predict, however, is the speed of the waves relative to the current.
- Usually in practical problems, however, it is not the wavelength which is known – rather it is the period, which does not uniquely specify the problem. To do that we also need to know the current on which the wave is riding, if we don't then any solution is an approximate one only.
- Consider the wave as shown in Figure 4-20, with a frame of reference (x, z), x in the direction of propagation of the waves and z vertically upwards with the origin on the flat bed. The waves travel in the x direction at speed c relative to this frame. It is this stationary frame which is the usual one of interest for engineering and geophysical applications. Consider also a frame of reference (X, Z) moving with the waves at velocity c, such that $x = X + ct$, where t is time, and $z = Z$. The fluid velocity in the (x, z) frame is (u, w), and that in the (X, Z) frame is (U, W). The velocities are related by $u = U + c$ and $w = W$.
- In the (X, Z) frame all fluid motion is steady, and consists of a flow in the negative X direction, roughly of the magnitude of the wave speed, underneath the stationary wave profile. The mean horizontal fluid velocity in this frame, for a constant value of Z over one wavelength λ is denoted by $-\bar{U}$. It is negative because the apparent flow is in the $-X$ direction. The velocities in this frame are usually not important, they are used to obtain the solution rather more simply.
- The quantity $\bar{U}$ is obtained in each nonlinear wave theory as a function of the wave dimensions. In papers prior to 1985 it was this which was referred to as the wave speed – it is actually the wave speed relative to the water.
- In the stationary frame of reference the time-mean horizontal fluid velocity at any point is denoted by $\bar{u}_1$, the mean current which a stationary meter would measure. Relating the velocities in the two co-ordinate systems gives

$$\bar{u}_1 = c - \bar{U}. \tag{4.41}$$

  If $\bar{u}_1 = 0$ then $c = \bar{U}$, so that in this special case the wave speed is equal to $\bar{U}$. This is Stokes' first approximation to the wave speed, usually incorrectly referred to as his "first definition of wave speed", and is that relative to a frame in which the current is zero.
- A second type of mean fluid speed is the depth-integrated mean speed of the fluid under the waves in the frame in which motion is steady. If Q is the volume flow rate per unit span underneath the waves in the (X, Z) frame, the depth-averaged mean fluid velocity is $-Q/d$, where d is the mean depth. In the physical (x, z) frame, the depth-averaged mean fluid velocity, the "mass-transport velocity", is $\bar{u}_2$, given by

$$\bar{u}_2 = c - Q/d. \tag{4.42}$$

If there is no mass transport, $\bar{u}_2 = 0$, then Stokes' second approximation to the wave speed is obtained: $c = Q/d$. Most theoretical presentations give Q as a function of wave parameters.

- In general, neither of Stokes' first or second approximations is the actual wave speed, and in fact the waves can travel at any speed. Usually the overall physical problem will impose a certain value of current on the wave field, thus determining the wave speed.

4.7.3 Stokes theory

- All variation in the x direction can be represented by Fourier series and the coefficients in these series can be written as series in terms of wave height / water depth. Substitution of these high order perturbation expansions into the governing nonlinear equations and manipulation of the series yields the solution, via a series of linear problems.
- The standard modern version of Stokes theory, with terms to fifth order in wave height, is that of Fenton (1985).
- If the three dimensions, water depth d, wave height H and wave length λ are known, then all quantities such as fluid velocities etc. can be calculated. However if unsteady fluid velocities are to be calculated it is still necessary to know the wave speed c or the current on which the wave rides.
- Stokes theory provides an equation for $\bar{U}$ as a function of H, d and λ:

$$\bar{U}(k/g)^{1/2} = C_0 + \varepsilon^2 C_2 + \varepsilon^4 C_4 + \dots , \tag{4.43}$$

where the coefficients C_0, C_2 and C_4 depend on kd. Substituting equation (4.43) and the definition of wave speed $c = \lambda/\tau$ into equation (4.41) and re-writing the equation in terms of the wavenumber throughout, we obtain

$$\left(\frac{k}{g}\right)^{1/2} \bar{u}_1 - \frac{2\pi}{\tau(gk)^{1/2}} + C_0(kd) + \left(\frac{kH}{2}\right)^2 C_2(kd) + \left(\frac{kH}{2}\right)^4 C_4(kd) + \ldots = 0, \tag{4.44}$$

which is a nonlinear transcendental equation for the wavenumber k, provided depth d, height H, period τ and mean current $\bar{u}_1$ are all known. An example is $C_0 = \sqrt{\tanh kd}$.

- One very important approximation is that of linear theory, which we have already had – we neglect the terms proportional to $(kH)^2$ and $(kH)^4$,giving

$$\left(\frac{k}{g}\right)^{1/2} \bar{u}_1 - \frac{2\pi}{\tau(gk)^{1/2}} + C_0(kd) = 0,$$

and if we further neglect the current $\bar{u}_1$ we recover our familiar linear dispersion relation. It is no more difficult numerically to solve (4.44) than this equation.

- Nonlinear wave theories such as Stokes show that higher waves travel faster.
- The neglect of current will not give a large error in the calculated wavenumber, as $\bar{u}_1 \ll c$, however, now when one goes to compute the fluid velocities in the geophysical frame, this may be important. Theories give explicit formulae for U, the velocity in the steady frame. When we add c to give $u = c + U$, the velocity in the geophysical frame, it is important to know c and to do this we need to know the current.
- Stokes theory breaks down if the wavelength is greater than 10 times the depth.

4.7.4 Cnoidal theory

- The cnoidal theory for the steady water wave problem follows from a shallow water approximation, in which it is assumed that the waves are much longer than the water is deep.
- A first order solution shows that the surface elevation is proportional to $\mathrm{cn}^2(\alpha X|m)$, where $\mathrm{cn}(.|.)$ is a Jacobian elliptic function of argument αX and modulus m and which gives its name to the theory. This solution shows the long flat troughs and narrow crests characteristic of waves in shallow water.
- Various versions of cnoidal theory have been presented. Fenton (1979) gave a fifth-order theory, which assumed that current was zero. This was corrected in a review article by Fenton (1990), and a more modern version was given in another review article by Fenton (1999*a*).
- The cnoidal theory breaks down in deep water (short waves) in a manner complementary to that in which

Stokes theory breaks down in shallow water (long waves).

4.7.5 Accuracy and areas of validity

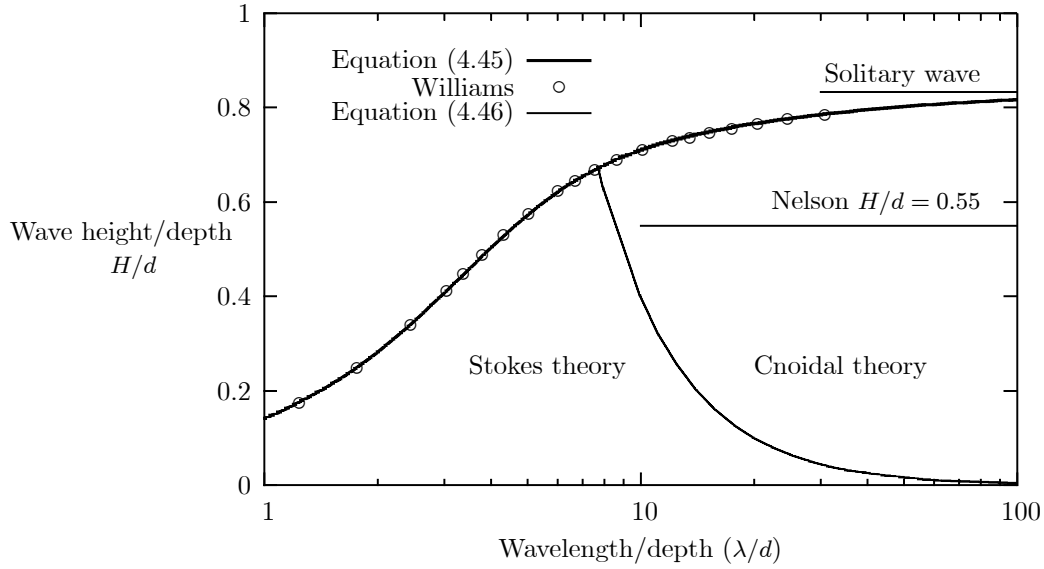

Figure 4-21. Region of possible waves

An empirical expression for the relative height of the highest wave H_m/d as a function of wavelength has been obtained by Fenton (1990):

$$\frac{H_m}{d} = \frac{0.141063\ (\lambda/d) + 0.0095721\ (\lambda/d)^2 + 0.0077829\ (\lambda/d)^3}{1 + 0.078834\ (\lambda/d) + 0.0317567\ (\lambda/d)^2 + 0.0093407\ (\lambda/d)^3}, \tag{4.45}$$

and is shown plotted in Figure 4-21. The equation was obtained from computational results of Williams (1981). It was obtained by solving the full nonlinear problem of a steadily-progressing wave over a horizontal bottom (which we have solved for small waves), and should be considered a guide. Most relevant in the context of spilling breakers is the fact that for long waves, the highest wave has $H_m/d \approx 0.83$. However, also shown plotted are the disturbing results of Nelson (1994, 1997), who in a series of field and laboratory experiments never observed waves higher than 0.55 of the water depth.

Hedges (1995) showed that the boundary between Stokes and cnoidal theories' areas of application is

$$\mathbf{U} = \frac{H\lambda^2}{d^3} = 40, \tag{4.46}$$

where U is the Ursell number

$$\mathbf{U} = \frac{H/d}{(d/\lambda)^2} = \frac{\text{"Nonlinearity" (measure of height)}}{\text{"Shallowness" (measure of depth/length)}},$$

which can be used to characterise waves. Those with a large Ursell number are generally long high waves, and cnoidal theory is best, whereas for small Ursell number (deeper water), Stokes theory is most applicable. This is shown on the figure. The Fourier approximation method works well for all waves up to within about 1% of the highest.

4.7.6 Fourier approximation methods

- A limitation to the use of both Stokes and cnoidal theories has been that they have been widely believed, to be not accurate for all waves. This is not entirely true (see Fenton 1990). Fifth-order theory in the versions as presented above are of acceptable engineering accuracy almost everywhere within the range of validity of each.
- Where it might be necessary to obtain results of high accuracy, where a structure of major importance is to be designed and where design data are accurately known, or where it is necessary to use a method which

is valid in both deep and shallow water, then numerical solution of the full nonlinear equations is a better option, which is what is provided by this method.

- The usual method, suggested by the basic form of the Stokes solution, is to use a Fourier series which is capable of accurately approximating any periodic quantity, provided the coefficients in that series can be found.
- Calculate the coefficients numerically by solving the full nonlinear equations.
- More accurate than either of the perturbation expansion approaches described above, because its only approximations are numerical ones, and not the essential analytical ones of the perturbation methods.
- The Fourier approximation version of Fenton (1988) rather automates the process, and is recommended by the Coastal Engineering Manual, http://140.194.76.129/publications/eng-manuals/em1110-2-1100/PartII/PartII.htm, Page II-1-51. The computer program is available to anybody who wants it:
URL: *http://johndfenton.com/Lectures/Coastal-and-Ocean-Engineering/Fourier.zip*

5. The calculation of forces on ocean structures

There are two limits which can be considered for the calculation of the forces and the design of ocean structures.

5.1 Structural element much smaller than wavelength – drag and inertia forces

In this case the structure is considered not to modify the wave. The force on each part of the structure is due to the fluid velocity and acceleration fields around the part. Very complicated structures, such as piled jackets made up of (very large) tubular steel connections can be analysed by superimposing the force on each component. In this case, the velocity and acceleration fields can be taken from a steady wave theory such as Stokes, cnoidal, or the Fourier approximation method. Once the kinematics of the field have been determined, the calculation of the forces are not, in principal, complicated.

5.1.1 The Morison (MOJS) equation

These notes have been taken from Wikipedia.

In fluid dynamics the "Morison equation" is a semi-empirical equation for the inline force on a body in oscillatory flow. It is sometimes called the "MOJS equation" after all four authors – Morison, O'Brien, Johnson and Schaaf – of the 1950 paper in which the equation was introduced.

The Morison equation is used to estimate the ocean surface wave loads in the design of oil platforms and other offshore structures.

The Morison equation is the sum of two force components: an inertia force in phase with the local flow acceleration and a drag (physics)|drag force proportional to the (signed) square of the instantaneous flow velocity. The inertia force is of the functional form as found in potential flow theory, while the drag force has the form as found for a body placed in a steady flow. In the heuristic approach of Morison, O'Brien, Johnson and Schaaf these two force components, inertia and drag, are simply added to describe the force in an oscillatory flow.

The Morison equation contains two empirical hydrodynamics coefficients – an inertia coefficient and a drag coefficient – which are determined from experimental data. As shown by dimensional analysis and in experiments by Sarpkaya, these coefficients depend in general on the Keulegan-Carpenter number, Reynolds number and surface roughness. The descriptions given below of the Morison equation are for uni-directional on-flow conditions as well as body motion.

Fixed body in an oscillatory flow: In an oscillatory flow with flow velocity $u(t)$, the Morison equation gives the inline force parallel to the flow direction:

$$F = \underbrace{\rho C_m V \dot{u}}_{F_I} + \underbrace{\frac{1}{2}\rho C_d\, A u|u|}_{F_D},$$

where $F(t)$ is the total inline force on the object, the inertia force $F_I = \rho C_m V\,\dot{u}$, is the sum of the Froude-Krylov force $\rho V\dot{u}$ and the hydrodynamic mass force $\rho\, C_a V\,\dot{u}$, the drag force $F_D = \frac{1}{2}\,\rho C_d A u\,|u|$, $C_m = 1 + C_a$ is the inertia coefficient, and C_a the added-mass coefficient, A is the cross-sectional area of the body perpendicular to the flow direction, V is volume of the body.

For instance for a circular cylinder of diameter D in oscillatory flow, the reference area per unit cylinder length is $A = D$ and the cylinder volume per unit cylinder length is $V = \frac{1}{4}\pi D^2$. As a result, $F(t)$ is the total force per unit cylinder length:

$$F = C_m \rho \frac{\pi}{4} D^2 \dot{u} + C_d \frac{1}{2} \rho D u\,|u|.$$

Besides the inline force, there are also oscillatory lift forces perpendicular to the flow direction, due to vortex shedding. These are not covered by the Morison equation, which is only for the inline forces.

Moving body in an oscillatory flow: In case the body moves as well, with velocity $v(t)$, the Morison equation becomes:

$$F = \underbrace{\rho V \dot{u}}_{a} + \underbrace{\rho C_a V\,(\dot{u} - \dot{v})}_{b} + \underbrace{\frac{1}{2}\rho C_d A\,(u - v)\,|u - v|}_{c}.$$

where the total force contributions are: a: Froude-Krylov force, b: hydrodynamic mass force, c: drag force.

Limitations

- The Morison equation is a heuristic formulation of the force fluctuations in an oscillatory flow. The first assumption is that the flow acceleration is more-or-less uniform at the location of the body. For instance, for a vertical cylinder in ocean surface gravity waves this requires that the diameter of the cylinder is much smaller than the wavelength. If the diameter of the body is not small compared to the wavelength, diffraction effects have to be taken into account.
- It is assumed that the asymptotic forms: the inertia and drag force contributions, valid for very small and very large Keulegan-Carpenter numbers respectively, can just be added to describe the force fluctuations at intermediate Keulegan-Carpenter numbers. However, from experiments it is found that in this intermediate regime – where both drag and inertia are giving significant contributions – the Morison equation is not capable to describe the force history very well. Although the inertia and drag coefficients can be tuned to give the correct extreme values of the force.
- When extended to orbital flow which is a case of non uni-directional flow, for instance encountered by a horizontal cylinder under waves, the Morison equation does not give a good representation of the forces as a function of time.

5.1.2 The Keulegan—Carpenter number

$$K_C = \frac{VT}{L},$$

where: V is the amplitude of the flow velocity oscillation (or the amplitude of the object's velocity, in case of an oscillating object), T is the period of the oscillation, and L is a characteristic length scale of the object, for instance the diameter for a cylinder under wave loading.

A closely related parameter, also often used for sediment transport under water waves, is the "displacement parameter" $\delta = A/L$, with A the excursion amplitude of fluid particles in oscillatory flow. For sinusoidal motion of the fluid, $A = VT/2\pi$ and $K_C = 2\pi\delta$.

The Keulegan—Carpenter number can be directly related to the Navier—Stokes equations, by looking at characteristic scales for the acceleration terms:

- convective acceleration: $(\mathbf{u}\cdot\nabla)\mathbf{u} \sim V^2/L$,
- local acceleration $\partial\mathbf{u}/\partial t \sim V/T$. Dividing these two acceleration scales gives the Keulegan—Carpenter number.

A somewhat similar parameter is the Strouhal number, in form equal to the reciprocal (mathematics)|reciprocal of the Keulegan-Carpenter number. The Strouhal number gives the vortex shedding frequency resulting from placing an object in a steady flow, so it describes the flow unsteadiness as a result of an instability of the flow downstream of the object. While the Keulegan-Carpenter number is related to the oscillation frequency of an unsteady flow, into which the object is placed.

5.2 Structural element comparable with wavelength – diffraction forces

In the case of a wave being scattered, or diffracted by the structure, it is necessary to solve the quite complicated problem of the incident wave train plus the scattered waves, the two being combined such that at all places on the structure, the fluid velocity normal to the structure is zero. As an example, we can consider the problem of the diffraction by a vertical circular cylinder, first solved by MacCamy & Fuchs (1954).

Consider the input velocity potential due to a train of incident periodic waves:

$$\phi_I = \sqrt{\frac{g}{k^3}} B_1 \frac{\cosh kz}{\cosh kd} \sin k\left(x - ct\right), \tag{5.1}$$

where ϕ_I is the velocity potential, k is the wavenumber, $k = 2\pi/\lambda$, the B_1 can be obtained from equation (4.15), and c is the speed as the waves propagate in a direction parallel to the x axis. In fact, in this case it is possible to write the incident wave can be written in cylindrical coordinates as an infinite series of Bessel functions

$$\phi_I = -i\sqrt{\frac{g}{k^3}} B_1 \frac{\cosh kz}{\cosh kd} e^{-i\omega t} \sum_{m=0}^{\infty} \beta_m J_m(kr) \cos m\theta. \tag{5.2}$$

where $\beta_0 = 1$, $\beta_m = 2i^m$ for $m \geq 1$, wave frequency $\omega = kc$, and $J_m\left(\ldots\right)$ is a Bessel function. Now to add on the scattered wave, we have to ensure that on the walls of the cylinder of radius a the normal velocity is zero. It can be shown that the resulting complete solution $\phi = \phi_I + \phi_R$ including incident and reflected waves can now be written

$$\phi = -i\sqrt{\frac{g}{k^3}} B_1 \frac{\cosh kz}{\cosh kd} e^{-i\omega t} \sum_{m=0}^{\infty} \beta_m \left(J_m(kr) - \frac{J'_m(ka)}{H'_m(ka)} H_m(kr) \right) \cos m\theta. \tag{5.3}$$

We have the linearised pressure equation (Unsteady Bernoulli Equation) for the pressure in a fluid:

$$\frac{\partial \phi}{\partial t} + \frac{p}{\rho} + gz = 0, \tag{5.4}$$

throughout the fluid. Now, we can substitute equation (5.3) into this to obtain the pressure at any point. The force can now be found by integration:

$$\mathbf{F} = -\int_A p\, \hat{\mathbf{n}}\, dA, \tag{5.5}$$

where $\hat{\mathbf{n}}$ is a unit normal vector directed from the solid surface into the fluid, and A is the wetted surface area. In the case of the circular cylinder, $\hat{\mathbf{n}} = \mathbf{i}\cos\theta + \mathbf{j}\sin\theta$ and the element of area is $a\, d\theta\, dz$, so that we obtain

$$\mathbf{F} = -a \int_0^d \int_0^{2\pi} p\, \left(\mathbf{i}\cos\theta + \mathbf{j}\sin\theta\right)\, d\theta\, dz, \tag{5.6}$$

and we can show that there are no transverse forces, and the in-line forces can be calculated.

It has been difficult – and any geometrical complication makes the solution correspondingly much more complicated. There are computer programs that can solve the problem for arbitrary bodies.

6. Wind generation of waves and wave prediction

The most obvious cause of surface waves is wind. Aristotle realised that wind on the sea surface played an important role in the development of waves. Historically, many approaches have been used to describe the basic mechanism for the transfer of wind energy to surface waves. Present understanding of the wave generation mechanism is based on two models proposed by Phillips and Miles. The Phillips model is applicable in the early stage of wave generation, while Miles' model predicts further wave growth. For the detailed mechanisms, reference can be made to books such as Massel (1999, #3.5).

In the last 30 years there has been a lot of work on the generation of waves and the development of operational wave models around the world (see, *e.g.* Khandekar 1989). Use of such wave-prediction models involves an enormous amount of effort, and more data than one is likely to possess. Due to the varying nature of the wind as well as the interaction of different storms, the sea and swell state are generally observed not to have the simple wave train characteristics discussed in the earlier sections. Any examination of waves under the action of wind clearly shows the confused nature of the system. Lord Rayleigh wrote "the basic law of the seaway is the apparent lack of any law". The modern trend in coastal engineering is to attack wave prediction by characterising the sea statistically, by investigating the energy spectrum to be expected for different situations and by using probability theories to forecast the occurrence of specified wave heights and periods. Such a method was developed by Pierson and Neumann, which is necessary when a possible range of harbour frequencies has to be investigated, such as for harbour resonance.

However, many coastal engineering problems are often influenced by the wave height, characterised by a single value. This older method still has a wide degree of acceptance. Empirical formulae have been developed by Sverdrup-Munk-Bretschneider (SMB). This is the most convenient wave prediction system to use when a limited amount of data and time are available. This is set out most conveniently in the Protection Manual (1975, Chapter 3). The formulae are written in terms of the significant wave height H_s, which is the average of the highest one-third of wave heights, which is close to the mean wave height estimated by the human eye, and the associated significant wave period T_s. The generation of wind waves is mainly a function of wind speed U; the distance over which the wind acts, called the fetch length F; the duration of the wind t, and the depth of water d. The fetch will depend on the particular direction chosen, and a number of different possibilities might have to be considered, usually limited by the first land encountered in a given direction. The duration with which the wind might blow can be inferred from meteorological records. The procedures are set out in Protection Manual (1975, Chapter 3). For a particular location and wind strength, the significant wave height is either fetch-limited or duration-limited, depending on which provides the greater restriction on the growth of waves. If a location is fetch-limited, this means that the duration is longer than the time taken for a disturbance travelling at the group speed to traverse the fetch, and it is the fetch which limits the wave characteristics. Otherwise, the wind cannot blow at that strength for a sufficiently long time, and it is this duration which provides the limitation.

6.1 Predicting waves in deep water

The procedure for waves in water of finite depth is similar, but more complicated. It is given in Protection Manual (1975, #3.6), but in these notes we will confine ourselves to the deep water case.

A dimensional analysis of the above parameters shows that the quantities can be arranged in terms of the dimensionless groups

$$\frac{gH_s}{U^2}, \frac{gF}{U^2}, \frac{gT_s}{U} \text{ and } \frac{gt}{U},$$

where the depth of water enters after we have calculated the deep-water values. Bretschneider obtained empirical relationships, of which we present the two simplest:

$$\frac{gH_s}{U^2} = 0.283 \tanh\left(0.0125 \left(\frac{gF}{U^2}\right)^{0.42}\right) \tag{6.1}$$

$$\frac{gT_s}{U} = 7.54 \tanh\left(0.077 \left(\frac{gF}{U^2}\right)^{0.25}\right), \tag{6.2}$$

with a rather longer expression for the dimensionless duration gt/U also as a function of gF/U^2. These are presented as charts in archaic units in the Protection Manual (1975, #3.51). It is rather easier to use the dimensionless chart presented here as Figure 6-1. The figure contains the plots which have been scaled to fit on the same axes, so

that the quantities which are plotted are $gt/U \times 10^{-5}$, the unscaled gH_s/U^2, and then $gT_s/U \times 10^{-1}$.

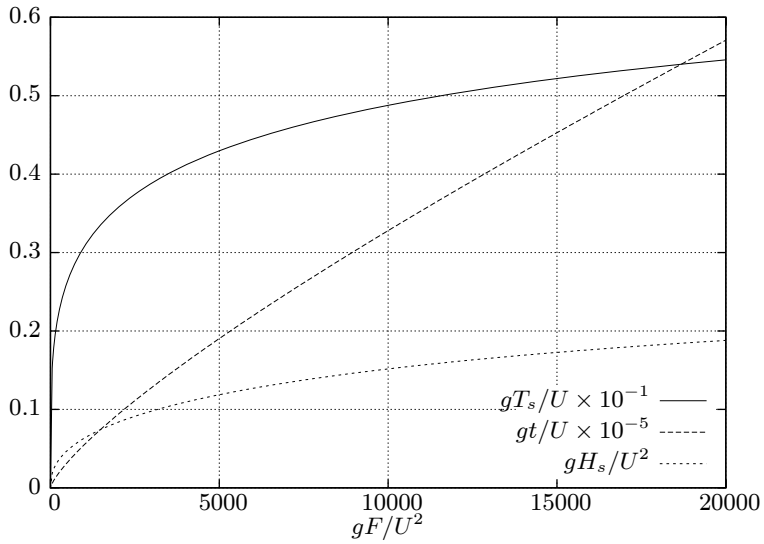

Figure 6-1. Plot of dimensionless equations for duration, wave height and wave period

1. Adopt values of fetch F and duration t expected at a site for a given direction and wind speed U.
2. Calculate the dimensionless fetch gF/U^2.
3. Calculate the dimensionless duration gt/U from equation (3-23) given in the Protection Manual (1975) or from Figure 6-1, and compare the expected duration with that so obtained.
4. If the actual expected duration is less than the calculated duration for that fetch, the field is duration limited From the expected duration, calculate the equivalent fetch by solving equation (3-23) or use Figure 6-1.
5. Otherwise, if the expected duration is greater than that calculated, the wave field is limited by the actual fetch.
6. Use the equivalent or the actual fetch to calculate the significant wave height and period, using equations (6.1) and (6.2).

We will provide an example as to how the equations and/or the diagram can be used.

Example: For a wind speed of $20\,\mathrm{m\,s^{-1}}$, and an expected duration of $10\,\mathrm{h}$, calculate the expected wave height and period for (a) a fetch of $120\,\mathrm{km}$, and (b) a fetch of $400\,\mathrm{km}$. Here we will present results from detailed calculation. Repeat for yourself using Figure 6-1. It is quite appropriate to use $g \approx 10\,\mathrm{m\,s^{-2}}$.

(a) Fetch $120\,\mathrm{km}$: $gF/U^2 = 10 \times 120000/20^2 = 3000$. The solid line gives $gt/U \times 10^{-5} = 0.128$, from which we obtain $t = 7.1\,\mathrm{h}$, which is less than the expected duration, so it is fetch limited, and we can calculate or read off the values, $gH_s/U^2 = 0.098$, $H_s = 3.9\,\mathrm{m}$, and $gT_s/U \times 10^{-1} = 0.39$, $T_s = 7.8\,\mathrm{s}$.

(b) Fetch $400\,\mathrm{km}$: $gF/U^2 = 10 \times 400000/20^2 = 10000$. The solid line gives $gt/U \times 10^{-5} = 0.327$, from which we obtain $t = 18.2\,\mathrm{h}$, which is greater than the expected duration, so it is duration limited. For the expected duration of $t = 10\,\mathrm{h}$, we obtain $gt/U = 18000$. If we were solving this numerically we would have to solve the transcendental equation (3-23), and we get $F = 186\,\mathrm{km}$. By using the graph, taking $gt/U \times 10^{-5} = 0.18$ and reading off the abcissa, we get $gF/U^2 \approx 4700$ and $F \approx 190\,\mathrm{km}$. Then we calculate or read off $gH_s/U^2 = 0.116$, $H_s = 4.6\,\mathrm{m}$, $gT_s/U \times 10^{-1} = 0.422$, $T_s = 8.4\,\mathrm{s}$.

7. Tsunami

7.1 Introduction

Tsunami is a Japanese term that means ”harbour wave”, or indeed ”harbour waves”, as it is the plural form as well[1]. It is used worldwide to describe a large sea wave generated by sea-floor disturbance. We will use it as a singular and plural noun (one tsunami, many tsunami).

7.1.1 Generation

There are three main mechanisms:

Volcanic eruptions leading to spectacular tsunami such as the 1883 Krakatau event. On August 26 and 27, 1883, the Krakatau volcanic island erupted fiercely, after beginning eruptions on May 20 of that year (p28 Simkin & Fiske 1983). Many villages and towns were washed away. The formation of the tsunami, whether by submarine explosions, by the sudden rush of water into the volcanic chamber when the side was blown out, or by caldera collapse, remains uncertain. However, in all cases, as suggested by Figure 7-1, there will be less land under the sea, and the initial disturbance will be negative.

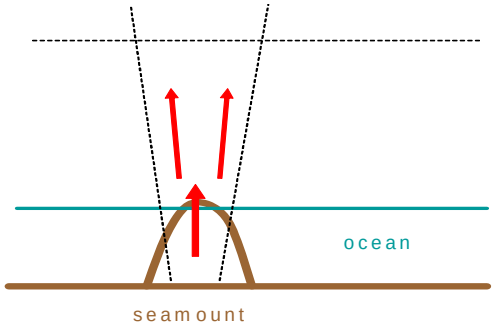

Figure 7-1. Mechanism for generation by a volcanic explosion such as Krakatau, where much earth and rock is blown into the atmosphere, leading to the generation of a negative wave (drawn by Prof. P. G. Baines)

Undersea landslides such as the 1998 Aitape tsunami off the northern coast of Papua-New Guinea. These may be rapid events, but are not instantaneous. Nevertheless, we would expect an initial displacement resembling that shown in Figure 7-2, which will result in a wave of depression propagating onshore, followed by a wave of elevation. There is some evidence (see Figure 7-3) that the 2004 Sumatran tsunami might actually have been caused by this mechanism, although the original cause of the landslides was undersea earthquakes.

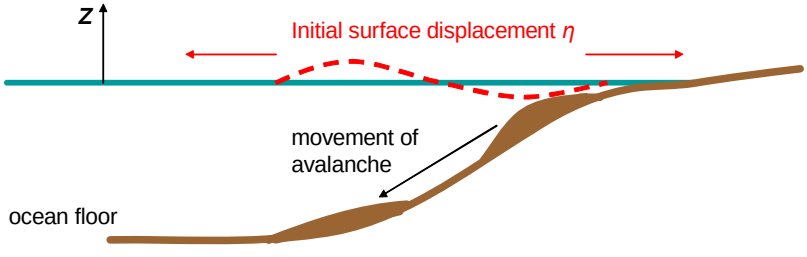

Figure 7-2. Mechanism for generation by an undersea landslide, showing generation of negative wave which is incident on the coast (drawn by Prof. P. G. Baines)

Undersea earthquakes of magnitude greater than 6.5 on the Richter scale and which have focal depths less than $50\,\mathrm{km}$ are the principal cause of tsunami. Not all such events produce tsunami, and the generation mechanism differs from event to event. The majority of them originate under great depths in the sea. Their precise origins are unknown, and tsunami have never been recorded in mid-ocean. Seismic activity occurs along volcanic island arcs, which usually consist of subduction boundaries, where one plate passes underneath another, such as that south of

[1] According to a spokesperson for the Japan Information and Cultural Centre, Melbourne

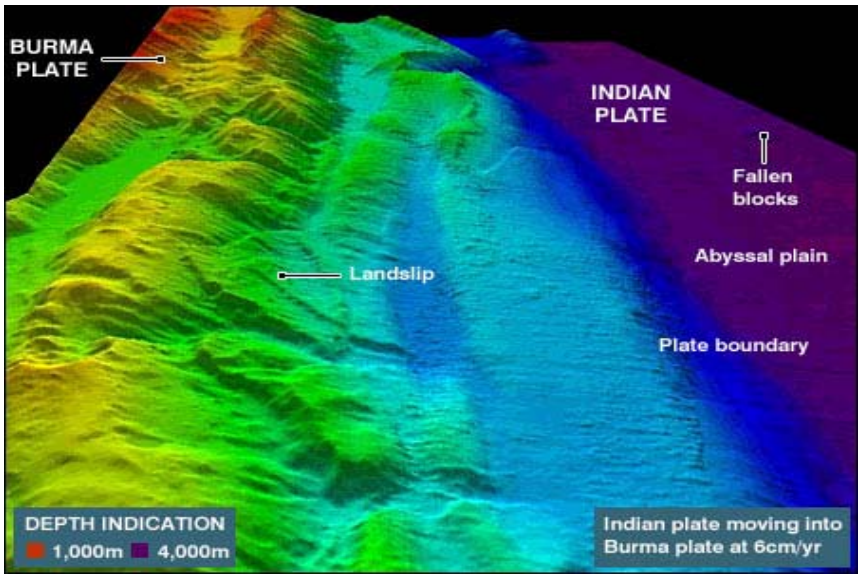

Figure 7-3. Underwater topography along the line of Sunda fault off Sumatra recorded by the Royal Navy after the 2004 event, showing extensive landslips.

Java and Sumatra or the Aleutian Islands off Alaska. Subduction zone earthquakes, are the most common source of destructive tsunami, and the Sumatran tsunami of 26 December 2004 was caused at least indirectly by this mechanism. They might be generated as shown in Figure 7-4, which is taken from Australia (2004), and which shows something of the complexity of tsunami generation.

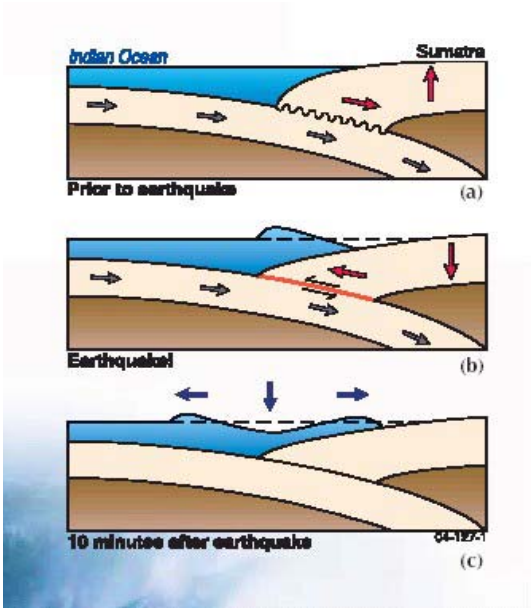

Figure 7-4. A possible mechanism for generation by a subducting plate boundary: (a) the lower subducting plate drags against the upper plate, causing flexure; (b) stress on the plate boundary causes the upper plate to rebound to its initial, unflexed position, displacing the sea surface; (c) the displaced sea surface propagates outwards as a tsunami.

This, however, does not explain why the first wave is often negative. That is easily done, however, by considering the case as shown in Figure 7-5, where the upper plate does not rebound, and the net displacement of the undwerater bottom is all negative.

Figure 7-6 shows the location of tsunami sources in the Paccific Ocean. The worst tsunami have been generated by the very active subduction interfaces off Chile and in the Aleutian Islands. In the Indian Ocean the most active subduction interface is associated with the Sunda fault, just south of Java and Sumatra.

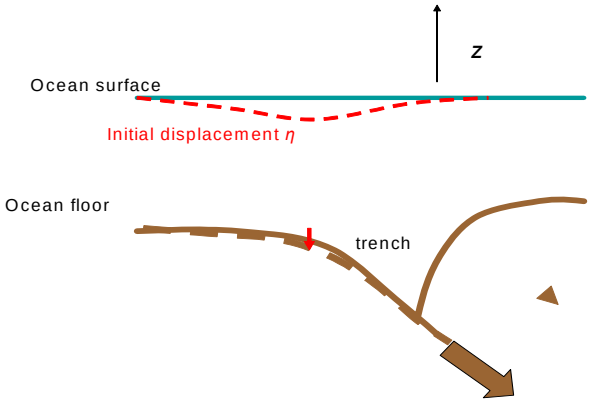

Figure 7-5. Subduction zone generation, where the upper plate does not rebound, while the subducting plate slides downwards, causing a negative displacement on the sea surface (drawn by Prof. P. G. Baines)

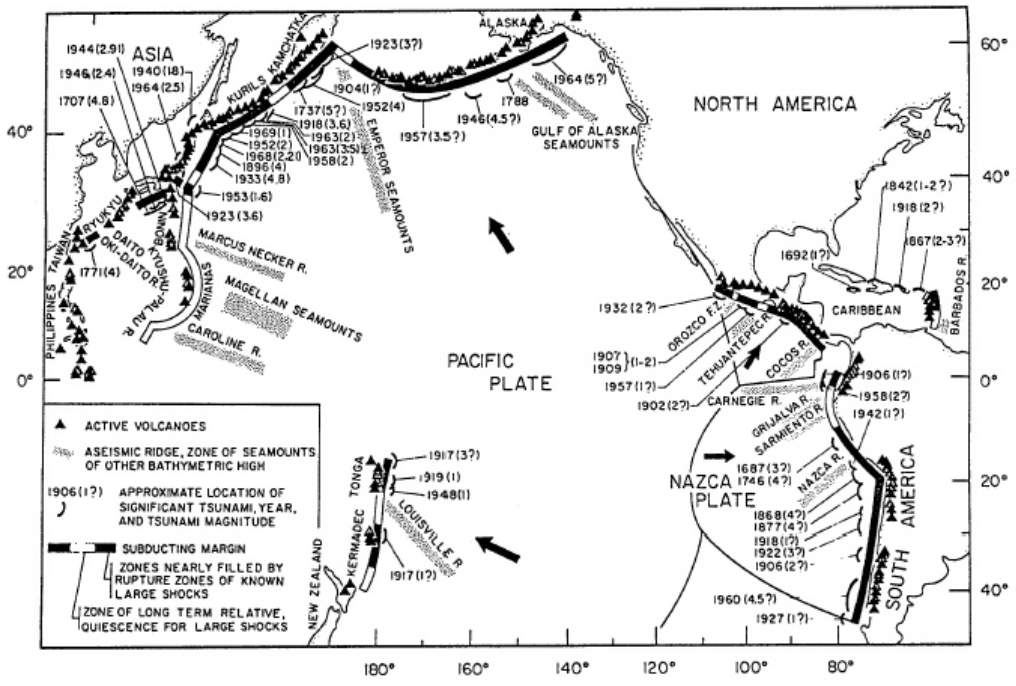

Figure 7-6. Location of tsunami source areas in the Pacific Ocean, after Kelleher

7.1.2 Propagation across the ocean

The height of a tsunami in the open ocean might be of the order of $0.5\,\mathrm{m}$, but its wavelength might be several tens of kilometres: any change of water surface elevation can hardly be recognised. Period of waves: $5\,\mathrm{min}$ to $40\,\mathrm{min}$, corresponding to a length of $70 - 500\,\mathrm{km}$. This long period suggests that tsunamigenesis is a relatively slow process, possibly the process of subduction or undersea landslides taking place over an extended period.

7.1.3 Effects on coasts

Approaching land, the period remains the same, the wave speed decreases ($c \sim d^{1/2}$) so that its length is less, and to conserve energy, the height of waves increase (height $\sim d^{-1/4}$). The situation in the vicinity of the coastline is very complicated, and the time history of the motion is governed by the local topography. As the waves approach shallower water, the individual amplitudes become larger. Ultimately the progress of each wave is arrested at the shoreline, and typically about 40% of the energy is scattered back out to sea. The water on the coastal shelf is set into oscillation characteristic of the region in question. Typically, following a moderate rise or recession of sea level, there are three to five major oscillations, after which there is a reduction in amplitude. Often the second or third wave might be the highest. Almost all of the damage occurs during the short interval of the large oscillations,

which in some areas encroach upon the land to the extent of some tens of metres above sea level. Such areas are relatively few, and around most of the oceanic perimeter local oscillations rarely exceed the normal tide range.

7.2 When the first evidence of a tsunami is recession of the sea

There are many reports that often the first obvious warning of a tsunami is when the sea recedes dramatically, leaving fish flapping on the former seabed, and people go down to investigate and profit, and then the REAL tsunami comes in ...? The evidence for this includes:

- Classical Greek and Roman writings
- the photo of Kalutara beach in Sri Lanka, Figure 7-10 below, on 26 December 2004.
- Numerous other reports of the same tsunami – in some locations.

7.2.1 Possible explanations for negative first wave

Does the wave speed depend on wavelength such that the tsunami waves actually travel as a group and individual waves travel through the group and in 50% of cases the trough arrives first? Conventional thinking (all tsunami waves are long such that their velocity is independent of wavelength and all waves will travel at the same speed) suggests this is not the answer.

Does the subduction mechanism mean that in one direction the first wave generated is one of depression, and in the other one of elevation? The evidence is varied – the first wave of the Sumatran tsunami was a recession at Sri Lanka but a positive first wave at Cocos Island, an isolated place due south of the epicentre. However the former was located on a line perpendicular to the major line of activity, while the latter is roughly in line with it.

Is the initial disturbance of a tsunami actually negative? There are actually some simple physical explanations that this is true – for all three generation mechanisms described above. If we consider a volcanic eruption such as Krakatau.

Can we appeal to mass-conservation and energy arguments?

Large lateral movement at toe ~10m; Typical slope ~1%; Increase in elevation at toe 0.1m; Decrease in elevation behind toe to provide the mass that has moved forward rather than up, and hence a general decrease in the water level?

Energy – rather than being so prescriptive, can we just say that after all the movement of the rock, it is likely, while strain energy might have provided some of that necessary for the motion, that the potential energy of the rock mass will provide some? The potential energy will be less afterwards than before, it will generally have slumped, and hence the water surface too will have dropped.

Now, after a long journey, the harmless depression wave has reached the shore, but at the rear, the elevation part has split into a train of higher waves because of the effects of finite depth, and they are now about to wreak havoc

7.3 Some aspects of tsunami behaviour

7.3.1 Soliton fission on a shelf

Figure 7-7 shows an aspect of the behaviour of a wave as it crosses a shelf, showing how the height of the wave increases, as expected, but not all that much, in accordance with Green's $d^{-1/4}$ law, however it also shows the fission of the wave ("soliton") and the generation of a wave train. The figure is from computations which solve Laplace's equation and all nonlinear boundary conditions without any essential approximations (Fenton 1993). The vertical scale is, of course, grossly distorted.

7.3.2 Final onrush of a positive tsunami

This is described in Kajiura & Shuto (1990): "for tsunami less than $2\,\mathrm{m}$ high, gradual rise and fall of the water level on the beach is usually observed. Tsunami $2\,\mathrm{m}$ to $5\,\mathrm{m}$ high raise the water level by sending one short wave after another, the latter overtaking and lying upon the former. Tsunami higher than $5\,\mathrm{m}$ show an abrupt rise of the water surface near the shoreline, followed by a sudden breaking". Figure 7-8 shows representation of that. In each

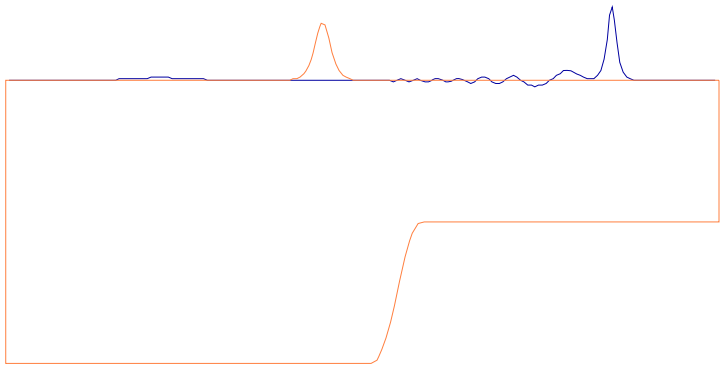

Figure 7-7. Soliton fission and generation of waves as a soliton crosses a shelf

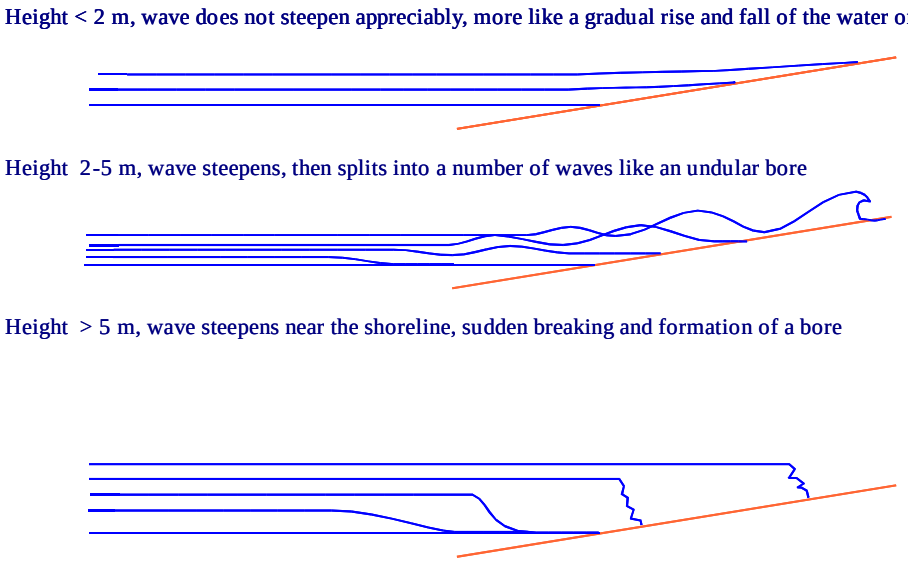

Figure 7-8. Conventional beliefs and interpretations of the behaviour of positive tsunami waves classified according to height.

case, the waves are following conventional behaviour as predicted by different water wave theories.

7.3.3 Propagation behaviour of a negative tsunami

Figure 7-9 shows a computer simulation, where an initial negative tsunami is generated just off a marked shelf break, similar to the Sumatran Tsunami of 26 December 2004. As predicted by linear long wave theory, the tsunami splits into two of half the height. One travels out to sea as shown, slowly varying as it does. The other almost immediately encounters shoaling water, and immediately its amplitude starts to increase and its propagation velocity decreases even more markedly. It can be seen on the right that the negative wave reaches the shore first, but that the water at the back of the negative wave starts to develop a large positive height and seems to continue to grow. This picture seems to describe the observed behaviour in a number of locations. Figure 7-10 shows an aerial photograph of Kalutara Beach, Sri Lanka, on 26 December 2004, showing the first effect of the tsunami, a large withdrawal of water from the beach.

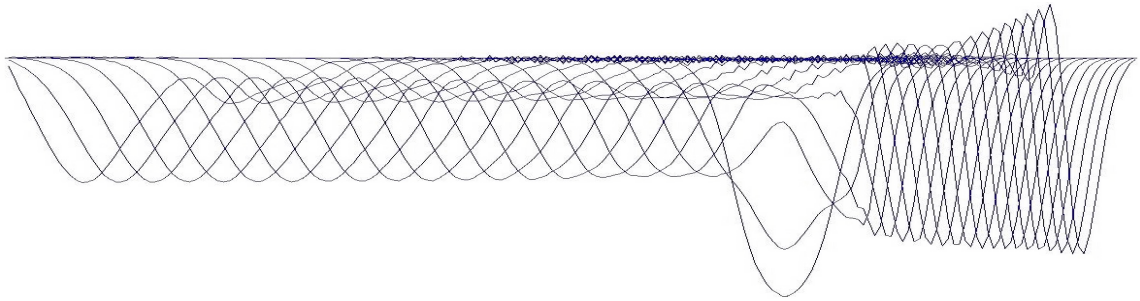

Figure 7-9. Computer simulation of an initially negative tsunami

Figure 7-10. Aerial photograph of Kalutara Beach, Sri Lanka, on 26 December 2004.

7.4 Tsunami generated by the Krakatau eruption of 1883

This was one of the most remarkable occurrences in nature in the modern age. Many books have been written about it. A total of about 14 tsunami waves were recorded at Tanjung Priok (p.378 Simkin & Fiske 1983), with a mean period of $2\,\mathrm{h}02\,\mathrm{min}$, and in the first wave the water rose about $3\,\mathrm{m}$ in a few minutes.

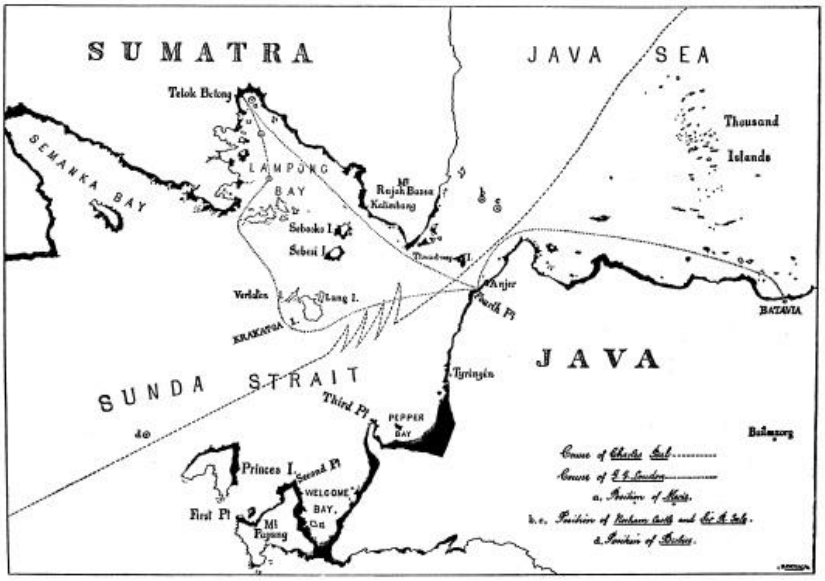

Figure 7-11. Areas submerged by the Krakatau tsunami of 1883 in metres (from Symons 1888), taken from from p299 of Symons (1888)

Figure 7-11 shows the areas inundated by the tsunami.

The damage caused by tsunami is most severe in V-shaped bays struck by a short-period tsunami. A well-known example of this is Lampong Bay north of Krakatau. At the head of this bay is Telukbetung, where in the Krakatau eruption a wave height of $15\,\mathrm{m}$ was observed, the same height as at points much closer to the volcano (see Figure 7-12).

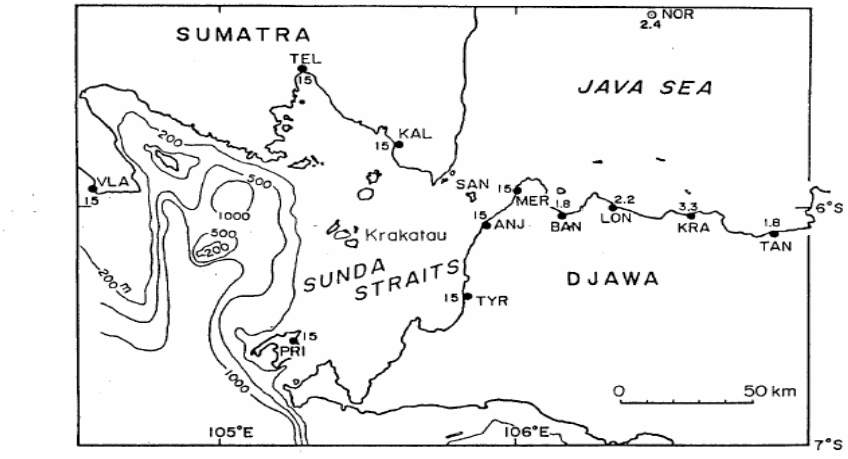

Figure 7-12. Distribution of the observed maximum height of the Krakatau tsunami in metres (from (Yokoyama 1981), adapted from (Wharton 1888)).

7.5 An investigation of tsunami risk on an island near the Sunda Strait

In 1991 the lecturer carried out an investiagation of tsunami risk for a proposed development on the island of Pulau Panjang. The relative lack of problems from an explosion of Krakatau is explained by the refraction diagram shown

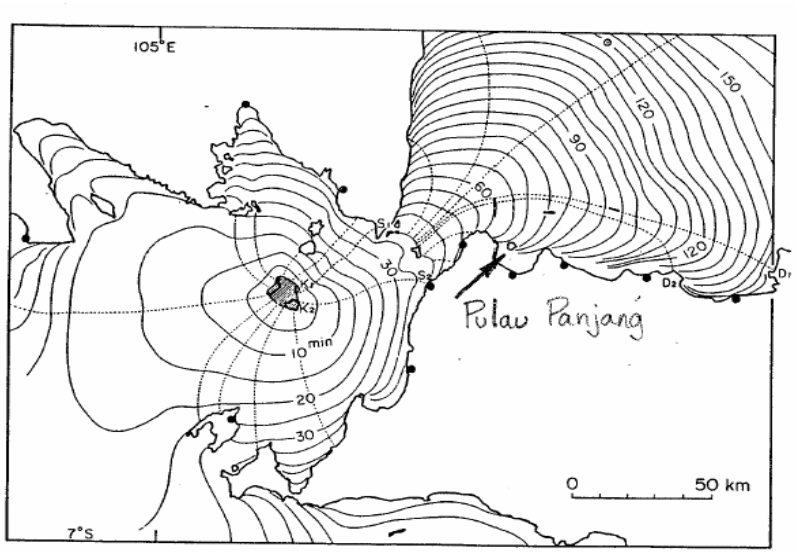

Figure 7-13. Refraction diagram of the tsunami caused by the 1883 Krakatau eruption, Figure 7 of Yokoyama (1981)

on Figure 7-13. This shows the wave crests at various times, and the dashed lines are wave orthogonals drawn at right angles to the crests. When these orthogonals are widely spaced, the wave energy is distributed over a greater width, and the wave height is correspondingly less. Several features shown in the diagram are of importance for the protection of Pulau Panjang. These are:

1. The island Pulau Sangiang in the middle of the Sunda Strait acts very much as its English name, namely "Thwart-way". This was originally given because it blocked navigation, however it is also a massive barrier to waves propagating north-eastwards, leaving a considerably smaller gap through which they can pass.
2. Those waves which do pass through the gap have a marked tendency to be refracted by the shallower topography onto the peninsula in the vicinity of Merak.
3. This leaves a relatively narrow gap through which waves pass which will subsequently wash onto the coast all the way from the top of the peninsula near Pulau Panjang, almost to Jakarta. This means that the relatively small energy contained in that gap is distributed all the way along the coast.
4. All the way along that coastline, refraction acts as to continually spread out and diminish the wave energy.

The resultant important effect is that the waves which were some 30-40m high in the region of Krakatau were only about 2m high at Pulau Panjang.

If a tsunami were to approach the island from the likely north-easterly or northerly direction, it would initially be in the form of a wave, probably of elevation, with a front face which would have a tendency to steepen as it approached shoaling water. Usually, the worst possible case of underwater topography is where the bottom is a long uniform slope until the beach. In this case, the wave can grow in height in accordance with principles of energy conservation. The initial growth would be in accordance with Green's Law, based on assumptions that the wave motion is low relative to the water depth and much longer than that depth, showing that the wave height is proportional to $d^{-1/4}$, where d is the local depth. When the wave height becomes large enough, it steepens in accordance with the full nonlinear equations, untils it forms a turbulent bore, in which all the water is travelling at a velocity comparable with the wave speed. It is this situation which is the most dangerous, and which seems to have been the case in the Merak coast region in 1883, because the magnitude of the tsunami was large relative to the water depth.

In the case of Pulau Panjang, there would be much less tendency for the wave to steepen catastrophically. This is because the size of tsunami would be considerably less than that in the Sunda Strait in 1883. It is calculated that even in the Krakatoa event, that a height of about $2\,\mathrm{m}$ prevailed on Pulau Panjang, and that the expected tsunami height from seismic origins in the Sunda Strait would be about $30\,\mathrm{cm}$. Examination of Admiralty and Indonesian Charts show the water off the island to be quite deep, at least $10\,\mathrm{m}$ until very close to the island, when the bottom shoals quite abruptly. This shows that the wave height relative to water depth is such that nonlinear steepening would not begin until the last couple of hundred metres, and then this region is so short that the cumulative effect

of the steepening would be small. There should be no tendency for a large amplitude breaking wave to occur.

The wavelength of tsunami can be calculated approximately using a small period wave corresponding to a locally-generated tsunami, of about $10\,\mathrm{min}$. With the depth around Pulau Panjang of about $15\,\mathrm{m}$, and using the formula for wave speed $c = \sqrt{gd}$ where g is gravitational acceleration and d is the depth, gives a wavelength of more than $7\,\mathrm{km}$. In the case of the period of 2 hours of the 1883 event, a wavelength of more than $80\,\mathrm{km}$ is obtained. It is more likely that local topography in Banten Bay would play an important local role. If any protection against tsunami were ever to be provided, however, this shows that the observed effect on the island is not that of waves of a short length, but that of a gradual rise in the water level around the island as a whole.

In the unlikely event of a tsunami exceeding $2\,\mathrm{m}$ (in the case of an equivalent Krakatau eruption, the worst scenario), if parts of the island were flooded this would not be with the catastrophic high fluid velocities associated with large tsunami incident on restricted volumes of water. Damage would not be structural, but would be that usually associated with flooding, namely the effects of salinity and water on buildings and structures.

8. Coastal engineering

In the past there was a pre-occupation with hard solutions to coastal engineering problems (consider the catalogue of catastrophic solutions shown as slides). Structures such as breakwaters, groynes and sea walls have been used for beach and harbour protection. The unfortunate truth is that almost everywhere that hard solutions have been adopted, they have failed somewhere. Hard solutions, are, however, good for engineering consultants and construction companies. They are, almost everywhere, bad for the coast.

8.1 An example of a beach investigation – Mission Bay, Auckland

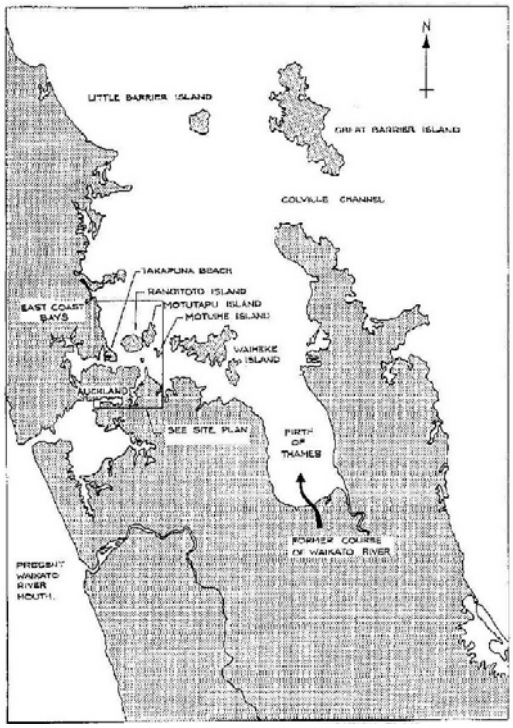

Figure 8-1. Location plan

Mission Bay is one of Auckland's most popular beaches. An investigation in 1987-89 has been described by Hamill, Christian & Fenton (1989). It provides an interesting example of the processes which might be investigated when considering the supposed degradation of conditions on a beach. The original stimulus came from residents who claimed to have observed a gradual loss of sand from the beach, and the study was funded by the Auckland City Council.

Historically the beach had a natural source of sand from material washed out from the mouth of the Waikato

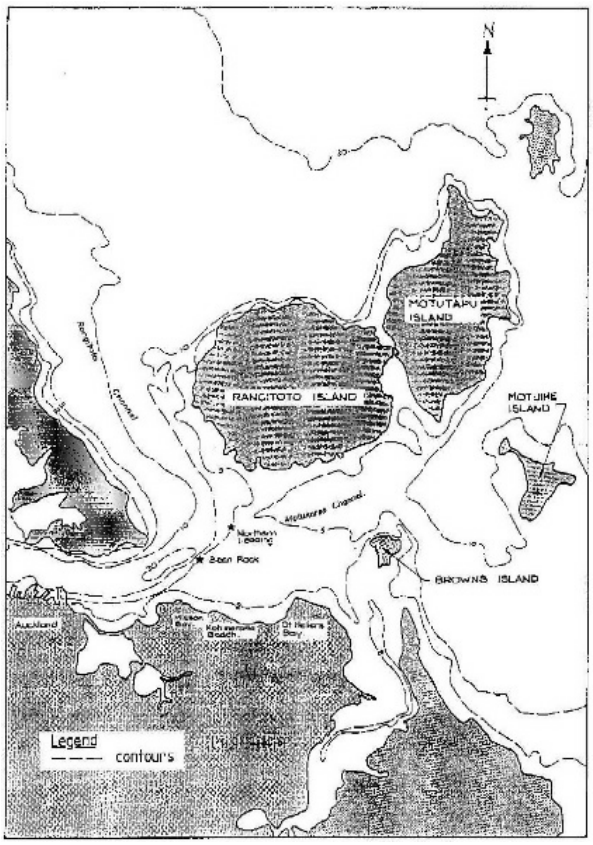

Figure 8-2. Site location

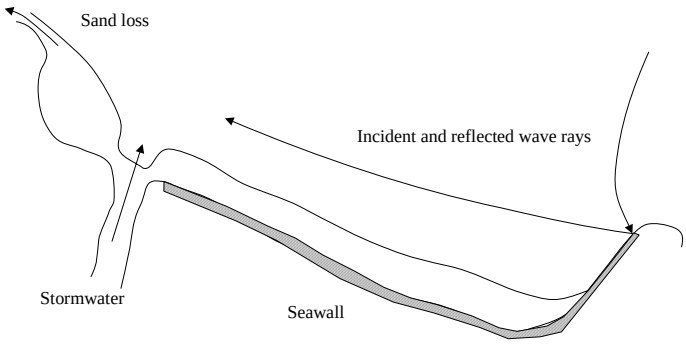

Figure 8-3. Mission Bay, showing important processes

River when it discharged through the Firth of Thames, and from the erodible cliffs around the eastern beaches of Auckland (note that the prevailing sand transport is from east to west). However, since construction of a sea wall all along the eastern suburbs coastline there was a severely reduced source of beach material. Also, prior to Rangitoto's appearance some 800 years ago the dominant fetch was from the north. Rangitoto then sheltered the beach from waves coming from this direction, positioning the critical fetch between Rangitoto and Motuihe Islands.

A bay which has had any sediment supply to it cut off will erode to a particular shape. Once this shape is reached the beach will maintain "static equilibrium", where incoming waves refract into the bay and break simultaneously around the whole periphery. This implies that there is no longshore component of breaking wave energy and hence no littoral drift. In the case of Mission Bay the provision of the sea wall prevented the removal of material from

the beach and exacerbated the problem. The layout of the beach at Mission Bay is shown in Figure 8-3.

In the 1930s roads and houses with hard surfaces were built, so that there was an increase in stormwater runoff passing through a stormwater channel at the western end of the beach. At high tide the stormwater entered the sea as a jet which was diffused in the seawater, but at low tides the stormwater cut a channel through the sand and transported it towards the water's edge, where it could more easily be moved by the waves. The beach, in an attempt to maintain equilibrium, moved sand to replace that which had gone, which slowly reduced the level of the sand along the beach, which in turn exposed the sea wall which then served to aggravate the problem.

- The first part of the investigation was a data collection exercise. Historical records of beach profile and plan shape were studied to try to determine a long-term pattern. At the same time local residents came forward with various explanations for the disappearance of the beach ("removal of the jetty in the 1930s", "the beach cleaner").
- Beach profiles provide a history of sediment movement, and developing a complete physical history would have been useful to provide an understanding, however such profiles were only available from 1977. For the study two new sites were developed and beach profiles regularly taken. The monthly records of the profiles produced no firm trends, but clearly showed the variable and dynamic nature of processes on the beach. The movement of material was found to be highly dependent on the prevailing wind direction. During north-easterly storms the sand was transported from east to west, but during the westerly winds which were milder but more frequent, the sediment returned along the beach. Dynamic equilibrium existed.
- Field measurements were taken to provide data for expected wavelengths, heights, and wave period during a north-easterly storm. A measuring buoy was installed, and the result was that the design conditions were: $H_s = 0.5\,\mathrm{m}$, $T_s = 3.33\,\mathrm{s}$, and $\lambda = 16.5\,\mathrm{m}$. A computer study of wave refraction was undertaken, and typical results are shown in Figure 8-4. It can be seen that some small reefs offshore provide protection for the most dangerous wind direction. At the same time a wind-rose was drawn from a nearby station from data from 1955 to 1962. The strongest wind came from the East-North-East during winter and spring. The largest fetch was from the North-East, between Rangitoto and Brown's Island. This combination of large fetch and strong winds created the most lethal wind direction.

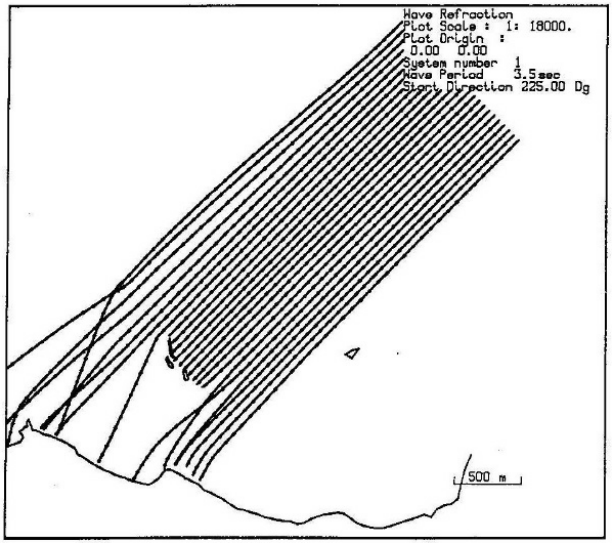

Figure 8-4. Wave refraction diagram, input waves with a heading of 225°, $T_s = 3.5\,\mathrm{s}$.

The waves from this direction reflected obliquely off the wall at high tide and continued to travel, but now towards the West, roughly parallel to the beach, and potentially carrying sand with them. At the western end of the beach the movement of material was slowed down because of the mass of sand which had been transported there, encouraging waves to break on the beach rather than reflect off the wall. However, the stormwater aggravated the condition by encouraging the sand to move around the rocky point, effectively losing the sand forever to Mission Bay.

- To determine the most suitable method for preventing further erosion, a scale mobile bed model of the bay was constructed in the Fluid Mechanics laboratory at Auckland University. The scales were 1:150 horizontal and 1:40 vertical. The granular material used was crushed coal, with a specific gravity of 1.3 and d_{50} of $1.14\,\mathrm{mm}$, so that it transported readily. Approximately 25 different configurations were tested, which could

be classified into four groups:

a. Control experiments – to provide a comparison, with the beach as it was, with and without stormwater.

b. Retentive experiments – structures were constructed, such as groynes, breakwaters, and sea walls at both ends, to retain the sand within the bay.

   Any of the retentive schemes also required some beach nourishment program to recover the sand which had already moved around the point at the western end.

c. Preventive experiments – aimed at preventing waves from reflecting from the wall, by using energy absorbers on the wall, building up the beach, and building artificial reefs off the beach.

d. Stormwater – run at high and low tides. Options tested included: piping the stormwater under the beach; transferring stormwater flow to the eastern end of the beach, and separating the stormwater outflow from the beach with a rough low groyne. The most effective was piping the stormwater under the beach.

It was concluded that the erosion was caused by a combination of beach alignment, the stormwater outfall, and reflection off the sea wall. Any combination of hard structures such as groynes and sea walls only made conditions worse somewhere on the beach, and had the major defect of preventing the gradual return of sand under gentler prevailing winds.

The most effective solutions were the artificial beach nourishment/returning scheme, rip-rap on the previously-smooth sea wall to roughen it and reduce reflection, and the provision of an extra reef out at sea. The latter, however, would have required massive works and would have interfered with navigation. The main solution adopted was the gentle one of beach nourishment, effectively re-circulating sand already lost or about to be lost and building up beaches so that the sea-walls were protected from wave action.

Overall, the conclusion was that erosion was not caused by one major problem, but a combination of minor ones: the mixture of fetch orientation, climate, topography, the sea wall which enhanced littoral drift, and the stormwater channel. It was concluded that the situation was reversible, by nourishing the beach with sand already removed and allowing it to pass along the beach during the predominantly south-westerly winds. It was best to allow natural processes to continue unhindered and to achieve a beach as close to equilibrium as possible. To assist with this, the stormwater was recommended to be piped under the beach. It was suggested that the sand movement be continuously monitored by measuring beach profiles at regular intervals. There was an emphasis on a flexible, unobtrusive and reversible low-key solution: "designs which acknowledge the imbalance of nature's forces and attempt provide for nature's losses give a more lasting solution than one which imposes on nature in an attempt to control it."

Historical note: The proposed gentle and cheap solution did not resonate well with some leading consultants or their hired retired academic consultant. They proposed a solution which consisted of an L-shaped breakwater turning back along the beach, constructed of boulders, rising to $2\,\mathrm{m}$ above the water level and extending along the beach for a distance of $200\,\mathrm{m}$, thereby destroying the nature of the beach and the views up the Rangitoto Channel. This was overcome politically by a friend of the lecturer taking him down to the beach one Sunday morning, using surveying equipment to install scaffolding at various cross sections of the proposed structure, taking photographs from the shore and then colouring in the whole proposed breakwater on the photos and showing this to a perplexed City Council. This might have carried the day, but it is still not clear if it did or not. What did ultimately decide was a financial crisis which allowed no money for the obscene "improvement". In fact, there was no money for anything, and the beach is there still ... Many morals can be drawn, including one that the forces of darkness are omnipresent, that rationality does not always prevail, and that sometimes one can be just lucky.

Further historical note: The above description was used by a coastal activist in New Zealand, David Sissons. He has brought the history more up to date (2003) in an article "We can learn from Auckland's experience" on http://homepages.ihug.co.nz/~sissons/Auckland_experience.html. He wrote:

> *Auckland City are spending millions of dollars on fixing up the beach erosion caused by seawalls and stormwater drains. They wish they could get them back to a natural state like we still have at Tahunanui.*
>
> *Auckland's Mission Bay is now one of its most popular beaches, but only after the Council has spent about $7 million on correcting the problems caused by the sea wall and the stormwater drains.*
>
> *The wall was built in the 1920s to protect a coastal reclamation. Since then, storm waves reflecting off it have combined with the flow of stormwater from six outfalls draining the surrounding suburbs to steadily lower the level of the sand in front of the wall. Eventually the sea undermined the foundation of the wall.*

Rather than just adding a new foundation and waiting for the sea to undermine it again, Auckland City Council repaired the existing foundation, diverted the stormwater drains away from the beach, and brought in a large amount of new sand from Pakiri Beach, over 60 kilometres away.

It has been so successful that the other five communities along Tamaki Drive all want the same done to their beaches. It comes at a continuing cost - $70,000 per year to move the sand back up the beach because the sea wall still stops it moving up naturally, plus the cost of bringing more sand from Pakiri every 5 years.

The ratepayers of Auckland are happy to pay because they now have a lovely beach once more.

Here at Tahuna we haven't yet put in a sea wall, and we can divert the stormwater easily enough. Or we can copy Auckland's mistakes, put in hard protection, and then use the rates to correct the ongoing problems that result.

8.2 Coastal management

There is a statement that "if you have a hammer in your hand, every problem looks like a nail", and that, to a certain extent, is what happens in coastal engineering. Hard, engineered, masculine, profitable solutions have usually held the day.

The article in Wikipedia is excellent, and we will borrow from it extensively:

URL: *http://en.wikipedia.org/wiki/Coastal_management*

Figure 8-5. Oosterscheldekering breakwater, the Netherlands

Historical background Coastal engineering, as it relates to harbours, starts with the development of ancient civilizations together with the origin of maritime traffic, perhaps before 3500 B.C., and other harbour works were built by hand and often on a grand scale.

Some of the harbour works are still visible in a few of the harbours that exist today, while others have recently been explored by underwater archaeologists. Most of the grander ancient harbor works have disappeared following the fall of the Roman Empire.

Most ancient coastal efforts were directed to port structures, with the exception of a few places where life depended on coastline protection. Venice and its lagoon is one such case. Protection of the shore in Italy, England and the Netherlands can be traced back at least to the 6th century. The ancients understood such phenomena as the Mediterranean currents and wind patterns and the wind-wave cause-effect link.

The Romans introduced many revolutionary innovations in harbor design. They learned to build walls underwater and managed to construct solid breakwaters to protect fully exposed harbors. In some cases wave reflection may have been used to prevent silting. They also used low, water-surface breakwaters to trip the waves before they

reached the main breakwater. They became the first dredgers in the Netherlands to maintain the harbour at Velsen. Silting problems here were solved when the previously sealed solid piers were replaced with new "open"-piled jetties. The Romans also introduced to the world the concept of the holiday at the coast.

Middle Ages: The threat of attack from the sea caused many coastal towns and their harbours to be abandoned. Other harbours were lost due to natural causes such as rapid silting, shoreline advance or retreat, etc. The Venetian Lagoon was one of the few populated coastal areas with continuous prosperity and development where written reports document the evolution of coastal protection works. Engineering and scientific skills remained alive in the east, in Byzantium, where the Eastern Roman Empire survived for six hundred years while Western Rome decayed.

Modern Age: Leonardo da Vinci could be considered the precursor of coastal engineering science, offering ideas and solutions often more than three centuries ahead of their common acceptance. Although great strides were made in the general scientific arena, little improvement was done beyond the Roman approach to harbour construction after the Renaissance. In the early 19th century, the advent of the steam engine, the search for new lands and trade routes, the expansion of the British Empire through her colonies, and other influences, all contributed to the revitalization of sea trade and a renewed interest in port works.

Twentieth century: Evolution of shore protection and the shift from structures to beach nourishment. Prior to the 1950s, the general practice was to use hard structures to protect against beach erosion or storm damages. These structures were usually coastal armoring such as seawalls and revetments or sand-trapping structures such as groynes. During the 1920s and ’30s, private or local community interests protected many areas of the shore using these techniques in a rather ad hoc manner. In certain resort areas, structures had proliferated to such an extent that the protection actually impeded the recreational use of the beaches. Erosion of the sand continued, but the fixed back-beach line remained, resulting in a loss of beach area. The obtrusiveness and cost of these structures led in the late 1940s and early 1950s, to move toward a new, more dynamic, method. Projects no longer relied solely on hard coastal defence structures, as techniques were developed which replicated the protective characteristics of natural beach and dune systems. The resultant use of artificial beaches and stabilized dunes as an engineering approach was an economically viable and more environmentally friendly means for dissipating wave energy and protecting coastal developments.

Over the past hundred years the limited knowledge of coastal sediment transport processes at the local authorities level has often resulted in inappropriate measures of coastal erosion mitigation. In many cases, measures may have solved coastal erosion locally but have exacerbated coastal erosion problems at other locations -up to tens of kilometers away- or have generated other environmental problems.

8.2.1 Current challenges in coastal management

The coastal zone is a dynamic area of natural change and of increasing human use. They occupy less than 15% of the Earth’s land surface; yet accommodate more than 50% of the world population (it is estimated that 3.1 billion people live within 200 kilometres from the sea). With three-quarters of the world population expected to reside in the coastal zone by 2025, human activities originating from this small land area will impose an inordinate amount of pressures on the global system. Coastal zones contain rich resources to produce goods and services and are home to most commercial and industrial activities. In the European Union, almost half of the population now lives within 50 kilometres of the sea and coastal zone resources produce much of the Union’s economic wealth. The fishing, shipping and tourism industries all compete for vital space along Europe’s estimated 89 000 kilometres of coastline, and coastal zones contain some of Europe’s most fragile and valuable natural habitats. Shore protection consists up to the 50’s of interposing a static structure between the sea and the land to prevent erosion and or flooding, and it has a long history. From that period new technical or friendly policies have been developed to preserve the Natural environment when possible. Is already important where there are extensive low-lying areas that require protection. For instance: Venice, New Orleans, Nagara river in Japan, Holland, Caspian Sea

Protection against the sea level rise in the 21st century will be especially important, as sea level rise is currently accelerating. This will be a challenge to coastal management, since seawalls and breakwaters are generally expensive to construct, and the costs to build protection in the face of sea-level rise would be enormous.

Changes on sea level have a direct adaptive response from beaches and coastal systems, as we can see in the succession of a lowering sea level. When the sea level rises, coastal sediments are in part pushed up by wave and tide energy, so sea-level rise processes have a component of sediment transport landwards. This results in a

dynamic model of rise effects with a continuous sediment displacement that is not compatible with static models where coastline change is only based on topographic data.

8.2.2 Planning approaches

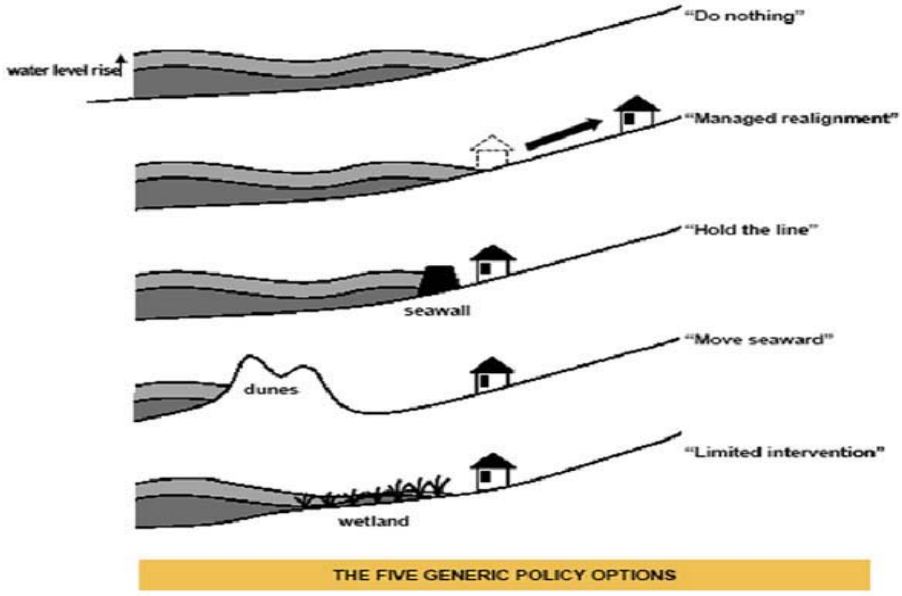

Figure 8-6. Five coastal management strategies

There are five generic strategies for coastal defence. The decision to choose a strategy is site-specific, depending on pattern of relative sea-level change, geomorphological setting, sediment availability and erosion, as well a series of social, economic and political factors.

Alternatively, integrated coastal zone management approaches may be used to prevent development in erosion- or flood-prone areas to begin with. Growth management can be a challenge for coastal local governments|local authorities who often struggle to provide the infrastructure required by new residents seeking sea-change. Sustainable transport investment to reduce the average ecological footprint|footprint of coastal visitors is often a good way out of coastal gridlock. Examples include Dongtan and the Gold Coast Oceanway.

Do nothing, no protection, leading to eventual abandonment – The 'do nothing' option, involving no protection, is a cheap and expedient way to let the coast take care of itself. It involves the abandonment of coastal facilities when they are subject to coastal erosion, and either gradually landward retreat or evacuation and resettlement elsewhere. This option is very environmental friendly and the only pollution produced is from the resettlement process. However it does mean losing a lot of land to the sea and people will lose their houses and their homes.

Managed retreat or realignment, which plans for retreat and adopts engineering solutions that recognise natural processes of adjustment, and identifying a new line of defence where to construct new defences.

Managed retreat is an alternative to constructing or maintaining coastal structures. Managed retreat allows an area that was not previously exposed to flooding by the sea to become flooded. This process is usually in low lying estuarine or deltaic areas and almost always involves flooding of land that has at some point in the past been reclaimed from the sea. Managed retreat is often a response to a change in sediment budget or to sea level rise. The technique is used when the land adjacent to the sea is low in value. A decision is made to allow the land to erode and flood, creating new sea, inter-tidal and salt-marsh habitats. This process may continue over many years and natural stabilization will occur.

The earliest managed retreat in the UK was an area of 0.8 ha at Northey Island in Essex, that was flooded in 1991. This was followed by Tollesbury and Orplands in Essex, where the sea walls were breached in 1995. In the Ebro delta (Spain) coastal authorities have planned a managed retreat in response to coastal erosion.

The main cost is generally the purchase of land to be flooded. Housings compensation for relocation of residents may be needed. Any other human made structure which will be engulfed by the sea may need to be safely

dismantled to prevent sea pollution. In some cases, a retaining wall or bund must be constructed inland in order to protect land beyond the area to be flooded, although such structures can generally be lower than would be needed on the existing coast. Monitoring of the evolution of the flooded area is another cost. Costs may be lowest if existing defenses are left to fail naturally, but often the realignment project will be more actively managed, for example by creating an artificial breach in existing defences to allow the sea in at a particular place in a controlled fashion, or by pre-forming drainage channels for created salt-marsh.

Hold the line, shoreline protection, whereby seawalls are constructed around the coastlines

Human strategies on the coast have been heavily based on a static engineered response, whereas the coast is in, or strives towards, a dynamic equilibrium. Solid coastal structures are built and persist because they protect expensive properties or infrastructures, but they often relocate the problem downdrift or to another part of the coast. Soft options like beach nourishment, while also being temporary and needing regular replenishment, appear more acceptable, and go some way to restore the natural dynamism of the shoreline. However in many cases there is a legacy of decisions that were made in the past which have given rise to the present threats to coastal infrastructure and which necessitate immediate shore protection. For instance, the seawall and promenade of many coastal cities in Europe represents a highly engineered use of prime seafront flange-eating space, which might be preferably designated as public open space, parkland and amenities if it were available today. Such open space might also allow greater flexibility in terms of future land-use change, for instance through managed retreat, in the face of threats of erosion or inundation as a result of sea-level rise. Foredunes areas represent a natural reserve which can be called upon in the face of extreme events; building on these areas leaves little option but to undertake costly protective measures when extreme events (whether amplified by gradual global change or not) threaten. Managed retreat can comprise 'setbacks', rolling easements and other planning tools including building within a particular design life. Maintenance of those structures or soft techniques can arrive at a critical point (economically or environmental) to change adopted strategy.

- Structural or hard engineering techniques, i.e. using permanent concrete and rock constructions to "fix" the coastline and protect the assets locate behind. These techniques–seawalls, groynes, detached breakwaters, and revetments – represent a significant share of protected shoreline in Europe (more than 70%).
- Soft engineering techniques (e.g. sand nourishments), building with natural processes and relying on natural elements such as sands, dunes and vegetation to prevent erosive forces from reaching the backshore. These techniques include beach nourishment and sand dune stabilization.

Move seawards, by constructing new defences seaward the original ones

The futility of trying to predict future scenarios where there is a large human influence is apparent. Even future climate is to a certain extent a function of what humans choose to make of it, for example by restricting greenhouse gas emissions to control climate change. In some cases - where new areas are needed for new economic or ecological development - a move seaward strategy can be adopted. Some examples from EUROSION are: Ebro delta (E), Koge Bay (DK) Western Scheldt estuary (NL), Chatelaillon (F).

There is an obvious downside to this strategy. Coastal erosion is already widespread, and there are many coasts where exceptional high tides or storm surges result in encroachment on the shore, impinging on human activity. If the sea rises, many coasts that are developed with infrastructure along or close to the shoreline will be unable to accommodate erosion, and will experiment a so-called "coastal squeeze". This occurs where the ecological or geomorphological zones that would normally retreat landwards encounter solid structures and are squeezed out. Wetlands, salt marshes, mangroves and adjacent fresh water wetlands are particularly likely to suffer from this squeeze.

An upside to the strategy is that moving seaward (and upward) can create land of high value which can bring the investment required to cope with climate change.

Limited intervention, accommodation, by which adjustments are made to be able to cope with inundation, raising coastal land and buildings vertically

Limited intervention is an action taken whereby the management only solves the problem to some extent, usually in areas of low economic significance. Measures taken using limited intervention often encourage the succession of haloseres, including salt marshes and sand dunes. This will normally result in the land behind the halosere being more sufficiently protected, as wave energy will be dissipated by the accumulated sediment and additional vegetation residing in the newly formed habitat. Although the new halosere is not strictly man-made, as many

natural processes will contribute to the succession of the halosere, anthropogenic factors are partially responsible for the formation as an initial factor was needed to help start the process of succession. This must not be confused with 'accommodate' which is about property e.g. effective insurance, early warning systems and not about habitat.

8.2.3 Hard construction techniques

The following is a catalogue of relevant techniques that could be employed as coastal management techniques.

Breakwaters Enormous concrete blocks and natural boulders are placed so as to absorb the energy of waves,

Figure 8-7. Examples of small breakwaters

protect harbours, and reduce the waves' erosive power. This leads to wider beaches, which absorb the reduced wave energy, protecting cliff and settlements behind. The Dolos which was invented by a South African engineer in East London, South Africa has replaced the use of concrete blocks because the dolos is much more resistant to wave action and requires less concrete to produce a superior result. Similar concrete objects like the Dolos are the A-jack, Akmon, Xbloc and the Tetrapod. Breakwaters may be constructed some distance away from the coast or

Figure 8-8. Dolosse

built with one end linked to the coast. They may be either fixed or floating: the choice depends on normal water depth and tidal range. Most Breakwater construction depends upon wave approach and considering some other environmental parameters. When oncoming waves hit these breakwaters, their erosive power is concentrated on these structures and there is an area of slack water behind them. Deposition occurring in these waters and beaches can be built up or extended in these waters. However, nearby unprotected sections of the beaches do not receive

fresh supplies of sediments and may gradually shrink due to erosion, namely longshore drift.

Breakwaters are subject to damage, and overtopping by big storms. The wall also serves to encourage erosion of beach deposits from the foot of the wall and can increase longshore sediment transport.

Groynes

Figure 8-9. Groyne at Mundesley, Norfolk, GB

Groynes are wooden, concrete and/or rock barriers or walls perpendicular to the sea. Beach material builds up on the updrift side, where longshore/littoral drift is predominantly in one direction, creating a wider and a more plentiful beach, therefore enhancing the protection for the coast because the sand material filters and absorbs the wave energy. However, there is a corresponding loss of beach material on the downdrift side, requiring that another groyne be built there. Moreover, groynes do not protect the beach against storm-driven waves and if placed too close together will create currents, which will carry sand material offshore.

Groynes are extremely cost-effective coastal defense measures, requiring little maintenance, and are one of the most common coastal defense structures. However, groynes are increasingly viewed as detrimental to the aesthetics of the coastline, and face strong opposition in many coastal communities.

Many experts consider groynes to be a "soft" solution to coastal erosion because of the enhancement of the existing beach.

In addition to being costly, there is also a problem called Terminal Groyne Syndrome. The last groyne that has been built or the terminal groyne, prevents longshore drift from bringing material to other nearby places. This is a common problem along the Hampshire and Sussex coastline in the UK; a perfect example is Worthing.

Sea walls Walls of concrete or rock, built at the base of a cliff or at the back of a beach, or used to protect a settlement against erosion or flooding. Older style vertical seawalls reflected all the energy of the waves back out to sea, and for this purpose were often given recurved crest walls which also increase the local turbulence, and thus increasing entrainment of sand and sediment. During storms, sea walls help longshore drift

Modern seawalls aim to destroy most of the incident energy, resulting in low reflected waves and much reduced turbulence and thus take the form of sloping revetments. Current designs use porous designs of rock, concrete armour (Seabees, SHEDs, Xblocs) with intermediate flights of steps for beach access, whilst in places where high rates of pedestrian access are required, the steps take over the whole of the frontage, but at a flatter slope if the same crest levels are to be achieved.

Care needs to be taken in the location of a seawall, particularly in relation to the swept prism of the beach profile, the consequences of long term beach recession and amenity crest level. These factors must be considered in assessing the cost benefit ratio, which must be favourable in order to justify construction of a seawall.

Sea walls can cause beaches to dissipate rendering them useless for beach goers. Their presence also scars the very landscape that they are trying to save.

Modern examples can be found at Cronulla (Australia, 1985-6), Blackpool (1986-2001), Lincolnshire (1992-1997) & Wallasey (1983-1993). The sites at Blackpool and Cronulla can be visited both by Google Earth and by local webcams (Cronulla, Cleveleys).

A most interesting example is the seawall at Sandwich, Kent, where the Seabee seawall is buried at the back of the beach under the shingle with crest level at road kerb level.

Sea walls are probably the second most traditional method used in coastal management.

Revetments Slanted or upright blockades, built parallel to the sea on the coast, usually towards the back of the

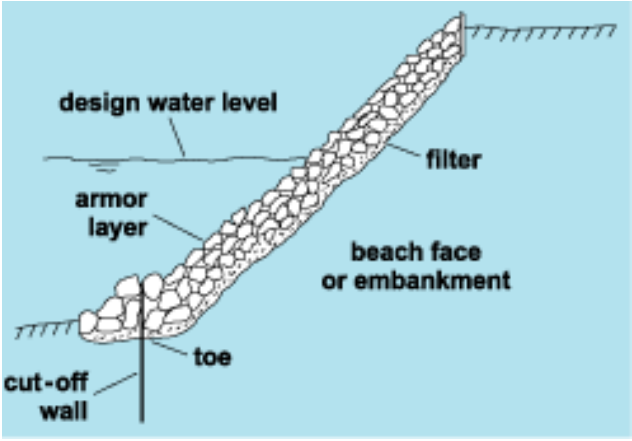

Figure 8-10. Typical revetment

beach to protect the cliff or settlement beyond. The most basic revetments consist of timber slants with a possible rock infill. Waves break against the revetments, which dissipate and absorb the energy. The cliff base is protected by the beach material held behind the barriers, as the revetments trap some of the material. They may be watertight, covering the slope completely, or porous, to allow water to filter through after the wave energy has been dissipated. Most revetments do not significantly interfere with transport of longshore drift. Since the wall greatly absorbs the energy instead of reflecting, it erodes and destroys the revetment structure; therefore, major maintenance will be needed within a moderate time of being built, this will be greatly determined by the material the structure was built with and the quality of the product.

Rock armour Also known as riprap, rock armour is large rocks piled or placed at the foot of dunes or cliffs with native stones of the beach. This is generally used in areas prone to erosion to absorb the wave energy and hold beach material. Although effective, this solution is unpopular due to the fact that it is unsightly. Also, longshore drift is not hindered. Rock armour has a limited lifespan, it is not effective in storm conditions, and it reduces the recreational value of a beach. The cost is around £300 per metre, depending on the type of rocks used.

Gabions Wire cages filled with crushed stone used to reduce erosion. Boulders and rocks are wired into mesh cages and usually placed in front of areas vulnerable to heavy to moderate erosion: sometimes at cliffs edges or jag out at a right angle to the beach like a large groyne. When the seawater breaks on the gabion, the water drains through leaving sediments, also the rocks and boulders absorb a moderate amount of the wave energy.

Gabions need to be securely tied to prevent abrasion of wire by rocks, or detachment of plastic coating by stretching. Hexagonal mesh distributes overloads better than rectangular mesh.

The downside of these are that they get worn out quickly and aren't very attractive, therefore not a very good source of coastal management.

Cliff stabilization Cliff stabilization can be accomplished through drainage of excess rainwater of through terracing, planting, and wiring to hold cliffs in place. Cliff drainage is used to hold a cliff together using plants, fences and terracing, this is used to help prevent landslides and other natural disasters

Entrance training walls Rock or concrete walls built to constrain a river or creek discharging across a sandy

Figure 8-11. Typical gabion installation

coastline. The walls help to stabilise and deepen the channel which benefits navigation, flood management, river erosion and water quality but can cause coastal erosion due to the interruption of longshore drift. One solution is the installation of a sand bypassing system to pump sand under and around the entrance training walls.

Floodgates Storm surge barriers, or floodgates, were introduced after the North Sea Flood of 1953 in the Netherlands and are a prophylactic method to prevent damage from storm surges. They are habitually open and allow free passage, but close when the land is under threat of a storm surge. The Thames Barrier is an example of such a structure, as is the Moise project to protect the Venetian lagoon.

8.2.4 Soft construction techniques

Sand bypassing: widely used, also in Florida in the USA so as not to interrupt the sand transport along the beach. There is a good example on the Tweed River on the east coast of Australia. The figure shows where the sand is collected and distributed in four different locations "downstream". Prior to the installation, for some 40 years all the beaches to the north had been losing their sand because of the training walls on the river.

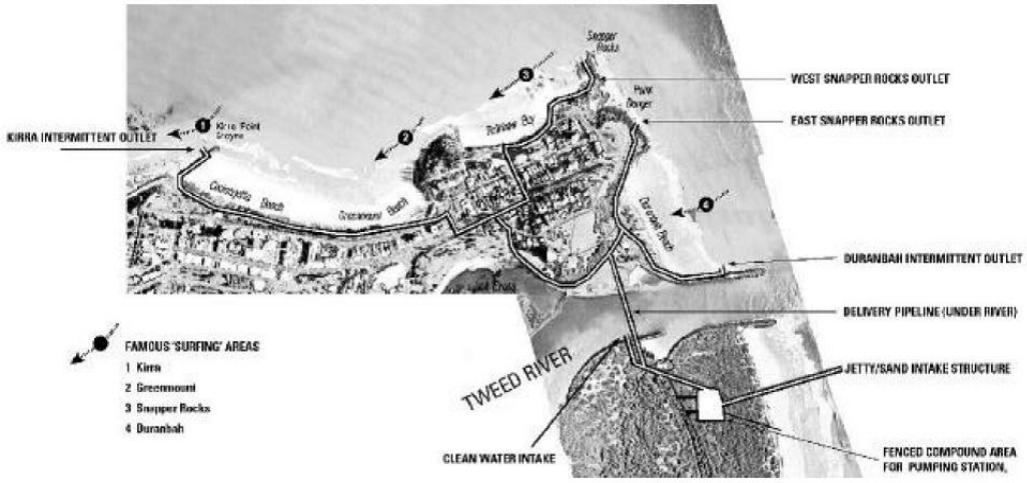

Figure 8-12. Tweed River sand bypassing scheme

Beach nourishment: Beach nourishment or replenishment is one of the most popular soft engineering techniques of coastal defence management schemes. This involves importing alien sand off the beach and piling it on top of the existing sand. The imported sand must be of a similar quality to the existing beach material so it can integrate with the natural processes occurring there, without causing any adverse effects. Beach nourishment can be used alongside the groyne schemes. The scheme requires constant maintenance: 1 to 10 year life before first major recharge.

Sand dune stabilisation: Vegetation can be used to encourage dune growth by trapping and stabilising blown sand.

Beach drainage Beach drainage or beach face dewatering lowers the water table locally beneath the beach

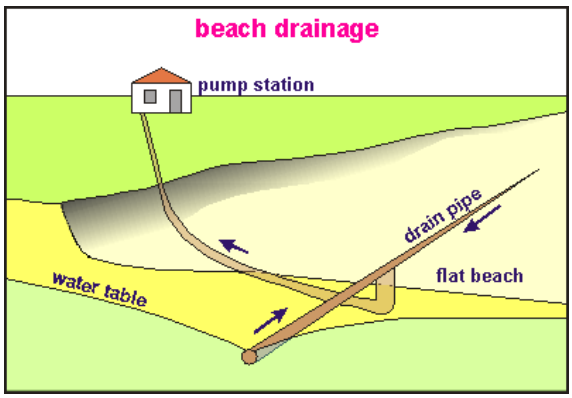

Figure 8-13. Beach drainage system

face. This causes accretion of sand above the drainage system.

A lower watertable (unsaturated beach face) facilitates deposition by reducing flow velocities during backwash and prolonging laminar flow. In contrast, a high watertable results in condition favoring beach erosion. With the beach in a saturated state, backwash velocity is accelerated by the addition of groundwater seepage out of the beach within the effluent zone.

A useful side effect of the system is that the collected seawater is very pure because of the sand filtration effect. It may be discharged back to sea but can also be used to oxygenate stagnant inland lagoons /marinas or used as feed for heat pumps, desalination plants, land-based aquaculture, aquariums or seawater swimming pools.

Beach drainage systems have been installed in many locations around the world to halt and reverse erosion trends in sand beaches. Twenty four beach drainage systems have been installed since 1981 in Denmark, USA, UK, Japan, Spain, Sweden, France, Italy and Malaysia.

8.2.5 Monitoring coastal zones

Coastal zone managers are faced with difficult and complex choices about how best to reduce property damage in the shorelines. One of the problems they face is error and uncertainty in the information available to them on the processes that cause erosion of beaches. Video-based monitoring lets collect data continuously at low cost and produce analyses of shoreline processes over a wide range of averaging intervals.

Event warning systems: Event warning systems, such as tsunami warning systems and storm surge warnings, can be used to minimise the human impact of catastrophic events that cause coastal erosion. Storm surge warnings can also be used to determine when to close floodgates to reduce the physical impact of such events.

Shoreline Mapping: Defining the shoreline is a difficult task due to the dynamic nature of the coast and the intended application of the shoreline. Given this idea the shoreline must therefore be considered in a temporal sense whereby the scale is dependent on the context of the investigation. The following definition of the coast and shoreline is most commonly employed for the purposes of shoreline mapping. The coast comprises the interface between land and sea, and the shoreline is represented by the margin between the two. Due to the dynamic nature

of the shoreline coastal investigators adopt the use of shoreline indicators to represent the true shoreline position.

Shoreline Indicator: The choice of shoreline indictor is a primary consideration in shoreline map|mapping. It is important that indicators are easily identified in the field and on aerial photography. Shoreline indicators may be physical beach morphological features such as the berm crest, scarp edge, vegetation line, dune toe, dune crest and cliff or the bluff crest and toe. Alternatively, non-morphological features may also be used. These indicators are based on water level including the high water line, mean high water line, wet/dry boundary, and the physical water line. Figure 8-14 provides a sketch of the spatial relationship between many of the commonly used shoreline indicators.

The high water line (HWL), defined as the wet/dry line (H in Figure 8-14) is the most commonly used shoreline indicator because it is visible in the field, and can be interpreted on both colour and grey scale aerial photographs. The HWL represents the landward extent of the most recent high tide and is characterised by a change in sand colour due to repeated, periodic inundation by high tides. The HWL is portrayed on aerial photographs by the most landward change in colour or grey tone.

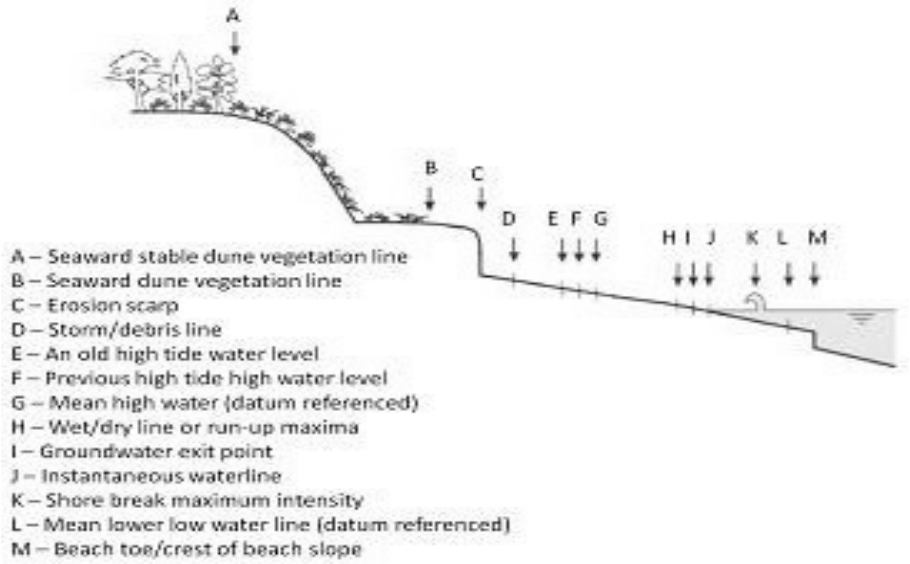

Figure 8-14. Coastline indicators – representing the spatial relationship between many of the commonly used indicators. (Adapted from Boak, E. H., & Turner, I. 2005, 'Shoreline Definition and Detection: A Review', *Journal of Coastal Research*, 21, 4, pp. 688-703.)

Importance and application: The location of the shoreline and its changing position over time is of fundamental importance to coastal scientists, engineers and managers. Present day shoreline monitoring campaigns provide information about historic shoreline location and movement, and about predictions of future change. More specifically the position of the shoreline in the past, at present and where it is predicted to be in the future is useful for in the design of coastal protection, to calibrate and verify computer simulation models to assess sea level rise, map hazard zones and formulate policies to regulate coastal development. Accurate and consistent delineation of the shoreline is integral to all of these tasks. The location of the shoreline also provides information regarding shoreline reorientation adjacent to structures, beach width, volume and rates of historical change.

8.2.6 Data sources

A variety of data sources are available for examining shoreline position however, the availability of historical data is limited at many coastal sites and so the choice of data source is largely limited to what is available for the site at a given time. Shoreline mapping techniques applied to data sources have moved towards automation in association with technological advances and the need to reduce uncertainty. Although these changes have resulted in improvement in coastal data processing and storage capabilities, the frequent change in technology has prevented the emergence of one standard method of shoreline mapping. This has occurred because each data source and associated method have their own unique capabilities and shortcomings. A number of the data sources

used for shoreline mapping and their associated advantages and disadvantages are discussed below.

Historical maps: In the event that a study requires the shoreline position to be mapped before the development of aerial photographs, or if the location has poor photograph coverage it is necessary to employ history|historical maps in order to detail shoreline position. The main advantage and reason for using historical maps is that they are able to provide a historic record that is not available from other data sources. Many potential errors however are associated with historical coastal maps and charts. Such errors may be associated with scale, datum changes, distortions from uneven shrinkage, stretching, creases, tears and folds, different surveying standards, different publication standards, and map projection errors. The severity of these errors depends on the accuracy standards met by each map and the physical changes that have occurred since the publication of the map. The oldest reliable source of shoreline data in the United States dates back to the early to mid 1800s and is the U.S. National Geodetic Survey. In the United Kingdom, many maps and charts were deemed to be inaccurate until around 1750. The founding of the Ordnance Survey in 1971 has since improved the accuracy of the mapping.

Aerial photographs: Aerial photographs have been used since the 1920s to provide topographical information about an area. They are therefore a good database for compilation of historical shoreline change maps. Aerial photographs are the most commonly used data source in shoreline mapping because many coastal areas have extensive aerial photo coverage therefore providing a valuable record of shoreline position. In general, aerial photographs provide good spatial coverage of the coast however temporal coverage is very much site specific depending on the flight path of the Fixed-wing aeroplane. A second disadvantage associated with aerial photography is that the interpretation of the shoreline position is subjective given the dynamic nature of the coastal environment. This combined with various distortions inherent in aerial photographs can lead to statistical significant error levels.

Delineation of the shoreline: The dynamic nature of the coast has meant that accurate mapping of an instantaneous shoreline position has been associated with significant uncertainty. This uncertainty arises because at any given time the position of the shoreline is influenced by the short-term effect of the tide and a wide variety of long term effects such as relative sea-level rise and along shore littoral zone|littoral sediment movement. Not only does this affect the accuracy of computed historic shoreline position but also any predicted future positions. As mentioned earlier the HWL is most commonly used as a shoreline indicator. This can usually be seen as a significant tonal change on aerial photographs. There are however many errors associated with using the wet/dry line as a proxy for the HWL and shoreline. The errors of largest concern are the short term migration of the wet/dry line, interpretation of the wet/dry line on a photograph and measurement of the interpreted line position. Systematic errors such as the migration of the wet/dry line may arise from tidal and seasonal changes. Storm-induced erosion is another factor which may cause the wet/dry line to migrate landward. Field investigations have shown that these changes can be minimised by using only summer|summertime data. Furthermore, the error bar can be significantly reduced by using the longest record of reliable data to calculate erosion rates.

Beach profiling surveys: Beach profiling surveys are typically repeated at regular intervals along the coast in order to measure short-term (daily to annual) variations in shoreline position and beach volume. Beach profiling is a very accurate source of information however measurements are generally subject to the limitations of conventional surveying techniques. Shoreline data derived from beach profiling is often spatially and temporally limited due to the high cost associated with such a labour intensive activity. Shorelines are generally derived by interpolation between a series of discrete beach profiles. It is important to note however that the distance between the profiles is usually quite large and so the accuracy of the interpolating becomes compromised. In contrast to aerial photographs, survey data is limited to smaller lengths of shoreline generally less than ten kilometres. Beach profiling data is commonly available in from regional councils in New Zealand such as those compiled by the Hawkes Bay Regional Council.

Remote sensing: Technological advancement over the last decade has led to the development of a range of airborne, satellite and land based remote sensing techniques. Some of the remotely sensed data sources are Multispectral and hyperspectral imaging, Microwave sensors, Global positioning system (GPS), LIDAR Airborne light detection and ranging technology

Remote sensing techniques are attractive as they are cost effective, reduce manual error and remove the subjective approach of conventional field techniques. Remote sensing is a relatively new concept and so extensive historical observations are unavailable. Given this idea, it is important that coastal morphology observations are quantified by coupling remotely sensed data with other sources of information detailing historic shoreline position from archived sources.

Video analysis: Video analysis provides quantitative, cost-effective, continuous and long-term monitoring beaches. The advancement of coastal video systems over the past 15 years has resulted in the extraction of large amounts of geophysical data from images. Such data includes that about coastal morphology, surface currents and wave parameters. The main advantage of video analysis lies in the ability to reliably quantify these parameters with high resolution and coverage in both space and time. This in particular highlights their potential importance as an effective coastal monitoring system and an aid to coastal zone management. Interesting case studies have been carried out using video analysis.

8.3 An example from Spain – Puerto Banus

Figure 8-15. Puerto Banus in Andalucia, Spain, showing harbour with breakwaters and groynes

Figure 8-15 shows an example of an intensively protected coastline, showing a harbour protected by a breakwater, and west of the harbour are a series of groynes which have formed crescentic beaches, and the transport will have been severely retarded. At the time of the photograph the waves are travelling from the south-east. Refraction of the waves can be seen, but they are short enough that they are actually breaking at quite an angle to the beach in the east of the photograph. Despite the intensity of "hard solutions", the system does not seem to be badly out of equilibrium. The harbour entrance does not seem silted up, and the crescentic "pocket beaches" seem to be in equilibrium. It is not clear in which direction the prevailing sand transport is. There is evidence on the eastern side that it might be travelling from east to west, as there is a certain accumulation behind the breakwater. However, on the very left of the photograph a beach can be seen with a healthy sand deposit, so it is possible that the sand is able to pass the complicated man-made structures without too many problems.